



NTNU

Norwegian University of
Science and Technology

Neural and Vascular Development in a Rat Model for Diseases of Prematurity

The Influence of Intermittent Hyperoxia-Hypoxia and Growth
Retardation on Brain Microstructure and Retinal Vasculature

Julia Anna Adrian

June 2016

MASTER THESIS IN NEUROSCIENCE

Norwegian University of Science and Technology

Department of Circulation and Medical Imaging

Supervisor 1: Assoc. Prof. Marius Widerøe, MD, PhD

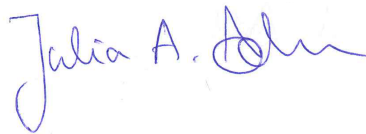
Supervisor 2: Assoc. Prof. Tora Sund Morken, MD, PhD

Preface

This master thesis is part of the *master of science in neuroscience* program at the Norwegian University of Science and Technology (NTNU) in Trondheim, Norway. It was carried out in the Department of Circulation and Medical Imaging at NTNU during the academic year 2015/2016. The project was funded by the university and the Olav Raagholt and Gerd Meidel Raagholt research foundation.

The experiments were executed and conducted in cooperation with my fellow neuroscience master student Jennifer Olsen. She analyzed brain volumes, whereas I focused on microstructural development of white and grey matter. Further, we analyzed different measures of abnormal retinal vasculature.

Trondheim, May 31, 2016

A handwritten signature in blue ink that reads "Julia A. Adrian". The signature is written in a cursive style with a large initial 'J' and a stylized 'A'.

Julia Anna Adrian

Acknowledgment

First, I thank **Marius Widerøe** for affiliating me to the Department of Circulation and Medical Imaging at NTNU and for giving me the opportunity to work out this thesis under his supervision. Thank you for your guidance and trust, and our inspiring discussions.

I thank **Tora Sund Morken** for her help with the experimental setup especially regarding the retinal experiments. Your advice was always valuable and encouraging, your point of view helped me to critically connect my experiments to the clinical setting.

I thank **Jennifer Olsen**, my fellow neuroscience master student, for her company and support during the whole year. All the nights scanning our rat pups made us a truly great team.

I thank **Bjørnar Sporsheim** from the Cellular and Molecular Imaging core facility for answering all my questions about fluorescence microscopy and for his practical support.

I thank the staff of the **AKM comparative medicine core facility** for their assistance and for sharing their knowledge regarding rat handling and maintenance.

Lastly, I thank **Madina Akan**, **Hester Berger** and **Kam Sripada** along with everyone else from the magnetic resonance center for warmly taking me in as new group member, for their kindness and our enlightning discussions.

J. A. A.

Abstract

Preterm born infants are at high risk of periventricular leukomalacia, a distinct form of white matter damage, and retinopathy of prematurity, a disease affecting the retinal vasculature. Further, they often suffer from breathing disorders and thus require supplemental oxygen therapy. In addition, preterm birth is often associated with poor postnatal weight gain.

The aim of this thesis was to investigate the influence of oxygen fluctuations, growth retardation and their combined effect on brain maturation and retinal vasculature by means of a neonatal rat model. Rat pups were held in intermittent hyperoxia-hypoxia (IHH, $n = 52$) or room air ($n = 32$) for the first 14 postnatal days. Litter size was manipulated to 8, 12 or 16 pups per litter to induce variations in weight gain. Diffusion tensor imaging (DTI) was performed on postnatal day 15 and 28 and fractional anisotropy, mean, axial and radial diffusivity were measured. Rat pups were euthanized after the second scan, the left retina dissected and its vasculature stained.

White matter structures were differentially affected by IHH exposure. The fractional anisotropy, a measure for white matter maturation, increased in all structures over time independent of oxygen condition. In limbic fibers, this increase was higher in the IHH compared to the room air group. Conversely, the fractional anisotropy of pups exposed to IHH increased less in commissural, projection and association fibers. Presumably, this was due to varying development time and maturation-dependent vulnerability of these regions. In grey matter, exposure to IHH led to a less increase in fractional anisotropy, and a less decrease in mean, axial and radial diffusivity over time than in room air controls. Weight gain was positively correlated with mean, axial and radial diffusivity at P28, possibly reflecting higher brain water content. Hence, these DTI parameters are poor measures of brain maturation *per se*, as they highly depend on weight.

Arteries and veins showed abnormal dilation in the mid-periphery of the retina after IHH exposure, but there was no difference in vessel tortuosity comparing oxygen groups. Interestingly, even though exposure to IHH affected both, the brain microstructure and retinal vasculature, DTI parameters were not associated with measures of abnormal retinal vascularization.

Concluding, exposure to IHH led to subtle microstructural alterations in white and grey matter, and dilated vessels in the retina. Consequently, supplemental oxygen treatment must be applied cautiously to avoid severe hyperoxic-hypoxic fluctuations in preterm born infants.

Contents

Preface	iii
Acknowledgment	v
Abstract	vii
1 Introduction	1
1.1 Preterm birth	1
1.2 Early Development in Human and Rat	3
1.2.1 Neural Development	3
1.2.2 Vascular Development	6
1.3 Vulnerability of the Premature Brain	7
1.4 Diseases of Prematurity	11
1.4.1 Periventricular Leucomalacia	11
1.4.2 Retinopathy of Prematurity	13
1.4.3 Link between Periventricular Leukomalacia and Retinopathy of Prematurity	15
2 Objectives	17
3 Magnetic Resonance Imaging	19
3.1 Principles of Magnetic Resonance	19
3.1.1 Excitation and Relaxation	20
3.1.2 Magnetic Resonance Image Acquisition	21
3.2 Diffusion Tensor Imaging	21
3.2.1 The Diffusion Tensor	22

4	Material and Methods	25
4.1	Animal Model	25
4.1.1	Animal Handling	25
4.1.2	Experiment Groups	26
4.1.3	Exposure to Intermittent Hyperoxia-Hypoxia	26
4.2	Magnetic Resonance Imaging	27
4.2.1	Diffusion Tensor Imaging	27
4.2.2	MRI Data Analysis	27
4.3	Tissue Processing	28
4.3.1	Retinal Dissection	28
4.3.2	Staining of Retinal Vasculature	29
4.3.3	Imaging and Image Analysis	29
4.4	Statistical Analysis	30
5	Results	33
5.1	DTI Parameters by Oxygen Condition	33
5.1.1	Fractional Anisotropy	34
5.1.2	Mean Diffusivity	34
5.1.3	Axial Diffusivity	37
5.1.4	Radial diffusivity	40
5.1.5	Summary	40
5.2	DTI Parameters by Weight	40
5.2.1	Fractional Anisotropy	41
5.2.2	Mean Diffusivity	42
5.2.3	Axial Diffusivity	44
5.2.4	Radial Diffusivity	45
5.3	Weight and Weight Gain	46
5.4	The Combined Effect of Oxygen and Weight	48
5.5	Retinal Vasculature	49

6 Discussion	51
6.1 Main Findings	51
6.2 Methodological Considerations	52
6.2.1 Strength and Limitations	52
6.2.2 Utility of Neonatal Rats to Model Diseases of Prematurity	53
6.2.3 Ethical Considerations	54
6.2.4 Confounding Factors of Development	55
6.2.5 Hemispheric Differences in Brain Structures	55
6.3 Weight Influenced by Litter Size and IHH Exposure	56
6.4 Maturation of White and Grey Matter	57
6.4.1 What Are the Physiological Correlates of these White Matter Findings? . . .	57
6.4.2 Why Is the White Matter Differentially Affected by IHH Exposure?	58
6.4.3 What Are the Physiological Correlates of these Grey Matter Findings?	60
6.4.4 Why Is Grey Matter Maturation Impaired by IHH Exposure?	61
6.4.5 How does Weight Influence White and Grey Matter Microstructure?	62
6.5 Retinal Vascularization	63
6.6 Is there a Link between Altered Brain Microstructure and Retinal Vasculature? . . .	65
7 Conclusions and Future Perspectives	67
A Acronyms	69
B Regions of Interest on FA Maps	71
C Raw Data	73
List of Figures	82
List of Tables	83
Bibliography	107

Chapter 1

Introduction

1.1 Preterm birth

Preterm birth is defined as birth below 37 completed weeks of gestation. Worldwide an estimated 15 million babies are born preterm every year, equaling a global average preterm birth rate of 11.1 %. However, across countries this rate ranges from 5 % to 18 %. Preterm birth is the leading cause of neonatal death and the second most common cause of death among children under 5 years of age. Of all children born below 37 completed weeks of gestation, around 84 % are born moderate or late preterm (32-36 weeks), 10 % are born very preterm (28-31 weeks), and 5 % are born extremely preterm (<28 weeks) (Blencowe et al., 2012).

Recently, novel classification models have been developed to identify the causes of preterm birth. It was found that infection/inflammation, decidual hemorrhage and cervical insufficiency were significantly more prevalent than other conditions in births before 28 weeks of gestation and often occurred collectively (Manuck et al., 2015). Further, genetic factors such as single nucleotide polymorphisms in the insulin gene and in genes associated with inflammatory pathways were identified to be predisposing factors for preterm birth (Esplin et al., 2015). Other risk factors include high maternal age, use of assisted reproductive technologies, and multiple gestations (Chang et al., 2013). Additionally, socio-economic inequalities like individual and neighborhood poverty are related to a higher risk for preterm birth (Kaufman et al., 2003; O'Campo et al., 2008).

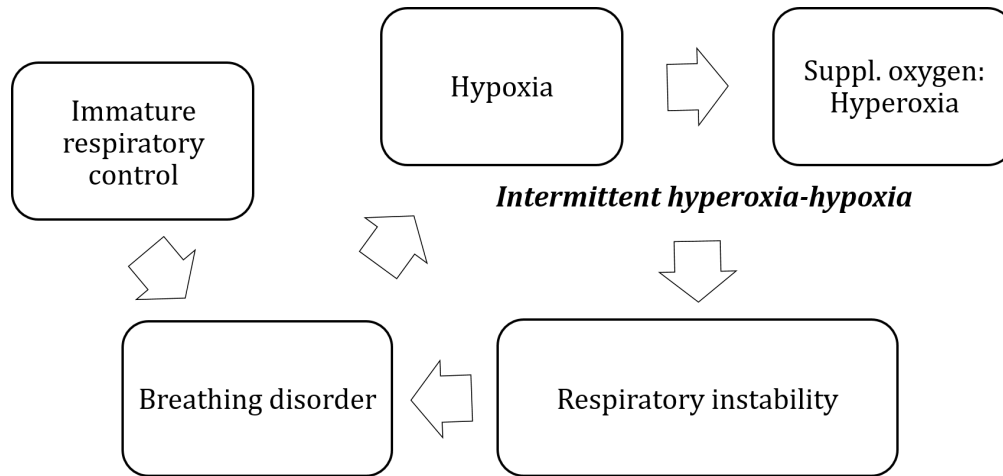


Figure 1.1: Vicious cycle of breathing disorder, oxygen fluctuations and respiratory instability, induced by immature respiratory control of the preterm neonate.

The respiratory control of preterm born children is immature, which often leads to breathing disorders such as apnea (see figure 1.1, Martin et al. (2015)). These may subsequently cause tissue hypoxia. To counteract this, preterm born infants receive supplemental oxygen therapy (Sola et al., 2007). In combination, this leads to fluctuations in oxygen level. Concretely, preterm born infants are exposed to long episodes of hyperoxia, which are intermittent by short episodes of hypoxia due to apnoeic attacks. This in turn may cause respiratory instability leading to or worsening breathing disorders (Martin et al., 2015).

Preterm born infants are often born small for gestational age and/or with low birth weight due to fetal growth restriction (Manuck et al., 2015). In addition, preterm birth is associated with poor postnatal weight gain, thus leading to growth retardation (Cooke et al., 2004). This in turn influences their neurodevelopmental outcome (Latal-Hajnal et al., 2003).

Among the potential secondary consequences of preterm birth are periventricular leukomalacia (PVL) and retinopathy of prematurity (ROP). These two diseases are discussed in more detail in sections 1.4.1 and 1.4.2. Further, of all infants born with very low birth weight (< 1500 g), 25 % to 50 % suffer from cognitive, behavioural and/or attentional deficits (Allin et al., 2008; Larroque et al., 2008; Wolke et al., 2008). In addition, 5 % to 10 % suffer from cerebral palsy or other forms of motor deficits (Platt et al., 2007). There is an inverse relationship between gestational age at birth and the severity of consequences after birth such as mortality, disability, and intensity of neonatal care required (Frey and Klebanoff, 2016).

1.2 Early Development in Human and Rat

In general, the sequence of developmental processes are remarkably conserved across (especially mammalian) species. While the order of these events is mostly the same, the time scales show considerable differences (Rice and Barone, 2000). The gestational period in humans is about 40 weeks, in rats approximately 21 days. Table 1.1 summarizes the time wise comparison of brain development for different animal models usually used to investigate prematurity. When comparing different species there are always limitations and mostly only one developmental aspect can be compared. In the following sections, the early development in humans and rats is discussed in more detail.

Table 1.1: Comparative time schedule for brain development in animals and humans, adapted from Hagberg et al. (2002). P is for postnatal day, E is for embryonic day.

Model animal	Human preterm 23-36 weeks of gestation	Human term 37-42 weeks of gestation
Mouse	P3 - P7	P8 - P12
Rat	P3 - P7	P8 - P12
Rabbit	E20 - E28 (70 % - 85 %)	Birth
Dog	Birth	> 2 weeks postnatal
Sheep	E93 - E99 (65 %)	E119 - E133 (90 %)

1.2.1 Neural Development

All neural tissue, such as brain and retina develop from the ectodermal germ layer (Gilbert, 2014). Temporarily during neural development, a distinct structure called subplate zone serves as source for new neurons. The subplate is located between the cerebral cortex and white matter and contains excitatory as well as inhibitory neurons (Semple et al., 2013). While it is a single cell layer in rodents, in humans the subplate is a more dispersed structure (Semple et al., 2013). Neurogenesis occurs approximately between day 9 of gestation (E9) and postnatal day 15 (P15) in rats, with slight regional differences (Babikian et al., 2010; Rice and Barone, 2000). In humans most of neurogenesis is completed during gestation, but may continue until 2,5 years postnatally (Prins and Hovda, 2003).

An example for a considerable difference between the rat and human brain development is gyrification, which only occurs in humans (Semple et al., 2013). Gyrification describes the pro-

cess of cortical folding thereby increasing the cortical surface. It starts around gestational week 15 and is essentially completed at birth (Dubois et al., 2008). However, the gyri and sulci increase in complexity postnatally due to maturation of subcortical fibers (Armstrong et al., 1995; Levine and Barnes, 1999).

Generally, the neural tissue can be divided into white and grey matter. White matter contains foremost neuronal axons and glia cells, therefore transmitting information and maintaining homeostasis in the brain. Conversely, grey matter comprises the soma and terminals of neuron, hence plays a role in information integration (Kandel et al., 2013).

White matter

White matter comprises the axonal part of neurons and a variety of glial cells, particularly oligodendrocytes. Glial cells arise from the subventricular zone of the lateral ventricles, a process called gliogenesis (Sanai et al., 2011). Gliogenesis occurs relatively late during development, that is during the last trimester of gestation in humans and within the first two postnatal weeks in rodents (Salmaso et al., 2014). The developmental stage of oligodendrocytes, astrocytes and microglia is crucial regarding the vulnerability of the white matter and thus the susceptibility to injury (see section 1.3). Since the neonatal rat resembles the preterm infant in respect to gliogenesis, it can be used to model diseases like PVL (see section 1.4.1). Table 1.2 shows a comparative time schedule for oligodendrocyte precursor prevalence. Premyelinating oligodendrocytes predominate in the first postnatal days in rats and between 23 and 32 weeks of gestation in humans. Axons develop extensively in the last trimester of gestation and in the early postnatal period. Thereafter, the next precursor form, called immature oligodendrocytes are abundant. Finally, in the weeks just before birth, there is the peak of gliogenesis in humans, which can be seen between P8 and P14 in rodents (Semple et al., 2013). Giedd et al. (1999) found that there is a linear increase in white matter volume, and thus a steady ongoing myelination, until adulthood.

Notably, there are regional differences in white matter development and maturation. In general, the myelination pattern follows a rostro-caudal gradient (Dubois et al., 2014). Limbic fibers mature earliest during development (Huang et al., 2006). The *hippocampal fimbria* is part of the subiculum and thus the limbic system. It lies medial of the hippocampus, starts from the hippocampal alveus and merges with the fornix (Lövblad et al., 2014).

Table 1.2: Comparative time schedule for axonal maturation in humans and rats, adapted from Semple et al. (2013).

Human	Rat	Developmental event
23 - 32 gest. wks	P1 - P3	Predominance of premyelinating oligodendrocytes
33 - 36 gest. wks	P4 - P7	Predominance of immature oligodendrocytes
37 - 40 gest. wks	P8 - P14	Peak in gliogenesis Increasing axonal and dendritic density Ongoing myelination
2 - 3 years of age	P20 - P21	Peak in synaptic density Peak in myelination rate

Thereafter, commissural fibers and projection fibers get myelinated (Huang et al., 2006). The *corpus callosum* is a commissural fiber, forming the connection between the two hemispheres. It is one of the largest white matter structures in humans and facilitates independent information processing as well as communication between the hemispheres (van der Knaap and van der Ham, 2011). The *internal capsule* is a projection fiber and borders the lentiform nucleus laterally, and the caudate nucleus and thalamus medially. It contains ascending and descending tracts and comprises the corticospinal tract conveying information from the primary motor cortex (Rea, 2015). Conversely, association fibers mature late during development (Dubois et al., 2014; Huang et al., 2006). The *external capsule* is a thin sheet of white matter comprising frontoparietal association fibers. It runs between the claustrum and lentiform nucleus of each hemisphere (Moeller et al., 2015). In human, it has been shown to play a role in language processing (Axer et al., 2013).

Grey matter

There are several important regions of interest in the grey matter. The *hippocampus* is especially prominent in rats. Like the hippocampal fimbria, it is part of the limbic system and plays a crucial role in spatial learning and memory (Strange et al., 2014).

The cerebral *cortex* is not a pure grey matter structure as it contains cortico-cortical fibers connecting different layers with each other. While there are many gyri and sulci enlarging the cortical surface in humans, the rat cortex is barely folded and less thick (Peters and Jones, 2013; Zilles, 2012).

The *thalamus* is a major relay station. It includes the first synapses of afferent fibers from

the spino-thalamic tract. Further, it contains connections to other major information processing regions like the cortex via the cortico-thalamo-cortical tracts and the hippocampus via the mammillo-thalamic tract (Jones, 2012).

The dorsal *striatum* comprises the putamen and caudate nucleus. It integrates sensorimotor and cognitive information via corticostriatal circuits and plays a role in action selection and initiation (Balleine et al., 2007).

1.2.2 Vascular Development

Vascular development involves two distinct processes, vasculogenesis and angiogenesis. Vasculogenesis describes the *de novo* vessel formation through differentiation of angioblasts (vascular precursor cells) into endothelial cells. Conversely, angiogenesis describes the formation of new capillaries from already existing vessels (Vailhé et al., 2001; Vallon et al., 2014).

Cerebral vascularization

In humans the first cerebral blood vessels appear around the 7th week of gestation (Korzhevskii and Otellin, 2000), but it is not until gestational week 36 that cortical regions are vascularized (Volpe, 2008). As expected, the vascular density in a certain tissue is positively correlated with its metabolic demand (Miyawaki et al., 1998). Consequently, there is a higher vascular density in grey matter than in white matter structures throughout development (Ballabh et al., 2004).

Furthermore, certain brain regions are supplied by distal parts of the major cerebral arteries. These so called watershed areas are particularly susceptible to hypotension, and thus prone to infarcts (Ringelstein et al., 2001; Sarnat, 2004).

Retinal vascularization

Like the brain, the retina is part of the central nervous system. Hence, the vascularization follows a similar pattern. However, retinal vascularization occurs relatively late during development, in both humans and rats (Provis, 2001; Semple et al., 2013). Initially, retinal neurons are supplied by hyaloid arteries. These are later replaced by an intraretinal vascular system that derives from them (Ruhrberg and Bautch, 2013). Therefore, vessel formation in the retina occurs only by an-

giogenesis and not vasculogenesis (Fruttiger, 2002). Retinal vascularization starts at the optic discs and expands radially until the arteries and veins reach the periphery. At birth, retinal vascularization in human infants is usually complete, while rat retinas still contain large avascular areas. It is not until postnatal day 15 that the rat retina is fully vascularized (Barnett et al., 2010). Therefore, in respect to vascularization, the neonatal rat retina resembles the retina of preterm born children. For this reason, rats are commonly used as laboratory animals to model diseases like retinopathy of prematurity (see 1.4.2).

Hypoxia-induced angiogenesis

To counteract insufficient blood oxygen supply, angiogenesis is induced by hypoxia. This occurs naturally during gestational development, such as during retinal vascularization (Stone et al., 1995), but also in the adult, for example during tumor growth (Harris, 2002). Especially vascular endothelial growth factor (VEGF) plays an important role during angiogenesis (Rezzola et al., 2014). VEGF expression is induced by hypoxia, mediated by HIF-1 (hypoxia inducible factor-1) (Kurihara et al., 2014) or PGC-1 α (peroxisome-proliferator-activated receptor-gamma coactivator-1 α) (Thom et al., 2014). Hypoxia-induced angiogenesis is beneficial under physiologic conditions in normal development. However, the vascular control in preterm infants is not fully developed. Thus the blood supply of a certain tissue may not always be sufficient for its metabolic demand (Fyfe et al., 2014). This may subsequently causes abnormal neovascularization or vessel destabilization and thus edema formation and mechanical rupture (Baburamani et al., 2012) as it is seen in ROP (Joyal et al., 2012).

1.3 Vulnerability of the Premature Brain

Neuronal abnormalities, especially white matter injury, are often caused by cerebral ischemia and/or systemic fetal inflammation. The brain of preterm born neonates is more susceptible to these processes than the term-born brain. Excitotoxicity and free radical attack are the consequences, further injuring the neonatal brain (Khwaja and Volpe, 2008). In the following the most important factors contributing to this increased vulnerability are discussed in more detail.

Premyelinating, Immature Oligodendrocytes

Oligodendrocytes are a type of glia found in the central nervous system. They produce myelin sheaths to insulate neurons and facilitate information transmission (Kandel et al., 2013). Oligodendrocyte progenitor cells develop via premyelinating oligodendrocytes and immature oligodendrocytes into mature myelinating oligodendrocytes (Back et al., 2007). The human brain is especially susceptible for PVL between 23 to 32 weeks of gestation, the same time at which premyelinating and immature oligodendrocytes are most abundant. Consistently, the decline of white matter damage occurs simultaneously with the presence of mature oligodendrocytes, and thus the onset of myelination (Back et al., 2001, 2007). Furthermore, Billiards et al. (2008) found evidence for maturational arrest of premyelinating oligodendrocyte, damage to oligodendrocyte processes and impaired axonal-oligodendrocyte signaling in patients with PVL. In rat oligodendrocytes, it has been shown *in vitro* and *in vivo* that hyperoxic exposure leads to apoptosis of oligodendrocyte precursors but not mature oligodendrocytes (Gerstner et al., 2006, 2008).

Activated Microglia

Microglia are cells of the innate immune system and thus responsible for inflammatory response (Ginhoux et al., 2015; Wake et al., 2011). They play a crucial role throughout ontogenesis as they contribute to plasticity by pruning of overabundant synapses (Hong et al., 2016). Further, microglia are thought to guide axons (Squarzoni et al., 2015) and maintain homeostasis (Michell-Robinson et al., 2015). Microglia belong to the earliest glial cells appearing already at four weeks of gestation. They develop rapidly until approximately week 25 of gestation when they have their highest density, and decline in abundance afterwards (Monier et al., 2006, 2007; Verney et al., 2010). Further, since they appear throughout the cerebral white matter, they are in close contact with premyelinating oligodendrocytes. This in combination with their abundance around midgestation, the peak period of vulnerability for white matter damage, points towards microglia as key effectors of injury (Verney et al., 2012; Volpe, 2009). As with chronic inflammatory diseases, long-lasting and severe immune responses often cause more damage than benefit.

Glutamate Receptors and Transporters

N-methyl-D-aspartate (NMDA) and α -amino-3-hydroxy-5-methyl-4-isoxazole-propionic acid (AMPA) glutamate receptors are widely expressed ligand-gated ion channels (Traynelis et al., 2010). Both are expressed in premyelinating and mature oligodendrocytes and in neurons (Jantzie et al., 2015). Depending on subunit constellation, NMDA and AMPA receptors may be permeable for Ca^{2+} -ions. Influx of Ca^{2+} into brain cells plays a crucial role in excitotoxicity and free radical generation (Görlach et al., 2015; Johnston, 2005; Szydłowska and Tymianski, 2010). Due to developmental expression of the receptors or specific subunits, excitotoxicity is maturation-dependent, with a peak vulnerability at around week 30 of gestation in humans (Talos et al., 2006).

In addition, excitatory amino acid transporters in the membrane of astrocytes that are responsible for the reuptake of extracellular glutamate are less expressed in the neonatal compared to the adult brain (Danbolt, 2001). It has been shown that hypoxia causes maturational arrest and impaired function of these glutamate transporters. This subsequently contributes to the excitotoxic effect of hypoxic-ischemic brain injury (Raymond et al., 2011).

Subplate and Subventricular Neurons

Subplate neurons and neurons of the subventricular zone are crucial populations during brain development. Subplate neurons provide axonal guidance for afferents targeting the cerebral cortex and cortical projection neurons targeting subcortical structures, thereby facilitating cortical organisation. They are most abundant and show their highest developmental impact at 24 to 32 weeks of gestation, the window of vulnerability for white matter injury (Kostović and Jovanov-Milošević, 2006; Pogledic et al., 2014). Further, cell death of subplate neurons is seen after hypoxic-ischemic injury in the neonatal rat (McQuillen et al., 2003).

The subventricular zone is a cell layer containing neuronal and glial progenitor cells. From week 20 until at least week 27 of gestation, the subplate extensively generates neurons, especially GABAergic interneurons that subsequently migrate to upper cortical layers (Bystron et al., 2008; Xu et al., 2011). Since both subplate and subventricular zone neurons are maximally active in the preterm period, they may be especially susceptible to injury at that time.

Less Resistance to Oxidative Stress

Oxidative stress in form of reactive oxygen species occurs naturally as a side product of cell metabolism. Enzymatic antioxidants such as superoxid dismutase convert reactive oxygen species to less toxic products. Further, antioxidants like vitamine C and vitamine E reduce and thus neutralize oxygen radicals. Under pathologic conditions the detoxifying cascade is disrupted thus causing cell death (mainly via apoptosis) (Dixon and Stockwell, 2014). The developing compared to the adult brain differs in composition of cellular components. High concentrations of unsaturated fatty acids, low concentration of antioxidants and higher availability of redox-active iron result in a environment of high susceptibility to oxidative stress. In addition, the oxygen consumption and hence production of reactive oxygen species is higher in the developing brain (McQuillen and Ferriero, 2004).

During the last 6 weeks of gestation, the antioxidant enzyme system is upregulated, presumably as protection against the relative hyperoxic extrauterine environment. Preterm born infants lack these elevated levels of antioxidant enzymes and thus are more susceptible to oxidative stress (Davis and Auten, 2010; Georgeson et al., 2002).

Cerebral blood flow

The cerebral blood flow in preterm born infants, even when they are healthy with normal neurological outcomes, is much lower than the threshold for viability in adults (Munro et al., 2004; Brew et al., 2014). Further, it has been shown that the cerebrovascular autoregulation of sick preterm infants is impaired and cerebral circulation is foremost pressure-passive in the early postnatal period (Soul et al., 2007; Tsuji et al., 2000). Hence, even a slight reduction in systemic blood pressure can lead to impaired cerebral perfusion and thus ischemia (Boylan et al., 2000; Van Os et al., 2006).

Tissue around vascular end zones, also known as watershed areas, are prone to infarcts (Momjian-Mayor and Baron, 2005) in adults (Juergenson et al., 2011) as in neonates (Groenendaal and de Vries, 2005). Internal watershed infarcts occur in the periventricular white matter. These areas lie in between and are supplied by the borders of deep and superficial middle cerebral artery or superficial parts of middle and anterior cerebral artery (Momjian-Mayor and

Baron, 2005). Especially during episodes of low blood pressure, the oxygen supply through the blood may be insufficient and eventually lead to necrosis (Børch et al., 2010).

In addition, cerebral and retinal vascularization might be abnormal. This is because vasculogenesis occurs at the same time and location as neurogenesis (Stubbs et al., 2009). Among others, VEGF has been shown to promote vascularization (Kajdaniuk et al., 2011; Patel-Hett and D'Amore, 2011) and neurodevelopment (Carmeliet and de Almodovar, 2013; Thau-Zuchman et al., 2012). Further, its expression is hypoxia-induced in the retina (Bache et al., 2015; Watkins et al., 2013) and brain (Baburamani et al., 2012). Therefore, in preterm born infants the relative hyperoxia experienced at birth (Perrone et al., 2015) and respiratory impairments may cause abnormal vascularization by imbalanced expression of hypoxia-induced growth factors like VEGF (Asikainen et al., 2005).

1.4 Diseases of Prematurity

Prematurely born infants have a higher chance to suffer from a variety of conditions. In this study, we focus on periventricular leukomalacia (PVL) and retinopathy of prematurity (ROP) because these two diseases of the premature may have the same underlying pathology.

1.4.1 Periventricular Leucomalacia

White matter disease of the premature has been named PVL (Banker and Larroche, 1962) despite the fact that the damage is mostly not limited to the periventricular area. Instead, the injury is more widespread including lesions in the callosal and subcortical white matter (Volpe, 2009). Furthermore, PVL often appears in combination with neuronal injury in grey matter structures such as the thalamus and basal ganglia (Pierson et al., 2007). Hence, Volpe (2005) suggested the term *encephalopathy of prematurity* to describe the complex pattern of white and grey matter damage distinctly affecting preterm born infants. In addition to the primary lesions it comprises secondary maturational deficits and cognitive impairment.

PVL has a focal component in the deep white matter and a diffuse component affecting the central cerebral white matter. Depending on the amount and characteristic of these two components, three major forms of PVL are distinguished. Cystic PVL is defined by macroscopic focal

necroses that evolve into cysts (Volpe, 2003, 2009). Albeit rare, it appears to be the severest form of the disease and is, as well as non-cystic PVL, associated with cognitive deficits (Choi et al., 2015). Non-cystic PVL is the most common form and is characterized by focal necroses that are of microscopic size and evolve to glial scars. Conversely, the mildest form of this disease is called diffuse white matter necrosis and comprises solely the diffuse components, characterized by loss of premyelinating oligodendrocytes (Dyet et al., 2006; Khwaja and Volpe, 2008; Volpe, 2009).

Preterm born infants are exposed to the extrauterine milieu in a more immature state than term born children (Back et al., 2007). Among others, the low cerebral blood flow in preterm neonates seems to be crucial, as first signs of PVL occur in watershed areas (Volpe, 2009). These are prone to infarcts since they are only supplied by vascular end zones (Momjian-Mayor and Baron, 2005). Furthermore, preterm born infants are more susceptible to oxygen fluctuations, inflammation and excitotoxicity. Consequently, these are the three factors used to induce symptoms of PVL in animal models.

First, white matter damage can be induced by hypoxic-ischemic insults. Thereby it is common to ligate the carotid artery uni- or bilaterally and expose the animals to hypoxia for 1 - 3 hours. This protocol was first established by Rice et al. (1981) and is still used in similar form to date (Widerøe et al., 2008; Yao et al., 2016). Exposure to intermittent hypoxia-hyperoxia as it is done in this study relates to this category of animal models for PVL. However, our approach addresses slightly different aspects of preterm birth.

Second, white matter damage can be induced through systemic inflammation either by injection of living bacteria like *E. coli* (Yuan et al., 2005; Shen et al., 2009) or bacterial endotoxins like lipopolysaccharide (LPS) (Bell and Hallenbeck, 2002; Mathai et al., 2013) into the pregnant or neonatal animal. In addition to systemic inflammation, administration of LPS induces hypotension and reduced cerebral blood flow especially in white matter regions (Recoquillon et al., 2015; Yilmaz et al., 2008; Young RS, 1982).

Third, administration of NMDA or AMPA receptor agonists, such as ibonate, leads to excitotoxicity injuring the immature white matter. Injection of ibotenate into the early postnatal rodent brain has been shown to cause white matter damage and lesions in the striatum, hippocampus and cerebral cortex (McDonald et al., 1988; Silverstein et al., 1997; Marret et al., 1995).

The model animals range from rodents to rabbits, dog, cats and sheep. Generally, the pattern of white matter injury is more similar to humans in gyrencephalic species than in rodents (Back et al., 2012). This may be due to the more similar intrauterine maturation processes and the white to gray matter ratio. The lower white to gray matter ratio in rodents might make their brain more resistant to oxygen fluctuations (Rice and Barone, 2000).

1.4.2 Retinopathy of Prematurity

ROP is a biphasic disease affecting the retinal vasculature of prematurely born infants. The first phase is dominated by vessel growth retardation due to the relative hyperoxic environment extrauterine compared to intrauterine and the supplemental oxygen that is given to sick preterm born infants. The intrauterine environment stimulates the production of vascular endothelial growth factor (VEGF) and thus leads to normal angiogenesis. In contrast to term born children, retina of preterm born infants is not fully vascularized by the time they are born. Instead, the retina possesses an avascular peripheral zone whose size is inversely related to the gestational age at birth (Gole et al., 2005). The second phase of ROP is induced when the retarded vessel growth causes tissue hypoxia in the retina. This subsequently leads to an overproduction of VEGF and thus to abnormal neovascularization (Chen et al., 2011; Shah et al., 2016).

The international classification system divides ROP into five stages. The first two stages are characterized by mild and moderate abnormal blood vessel growth, respectively, and do not require treatment. Stage three is defined by severely abnormal blood vessel growth. It is associated with so-called *plus disease*, where the retinal arteries and veins are abnormally dilated and more tortuous. The last two stages are characterized by partially and completely detached retina, respectively. This requires treatment and may lead to visual impairment and blindness (Gole et al., 2005).

Even though it is still one of the leading causes of childhood blindness, today only very few individuals suffer from ROP. Further, in most of these cases the retarded angiogenesis catches up without any intervention. Only less than 10 % of ROP patients need treatment and even less have irreversible consequences (NEI, 2014).

Retinopathy of prematurity, formerly named retrolental fibroplasia, was first described by Terry (1942). Already in 1951, the disease was connected with the administration of supple-

mental oxygen to newborns with respiratory disabilities (Campbell, 1951). This insight led to reduced use of supplemental oxygen and consequently a decline in ROP cases in the following decade (Hatfield, 1972).

Nevertheless, most animal models used to investigate ROP still use exposure to hyperoxia and/or hypoxia to induce abnormal retinal vascularization. This is called oxygen-induced retinopathy. Hyperoxia mimics the supplemental oxygen preterm born infants receive when suffering from breathing disorders such as apnea (Fairchild et al., 2016; Martin et al., 2015). Conversely, hypoxia mirrors the reduced oxygen supply in the newborn due to these conditions (York et al., 2004). In the early models rats are exposed to severe hyperoxia for long periods without (Patz, 1954) or with recovery in room air (Brands et al., 1958). Penn et al. (1993, 1994) demonstrated that hyperoxic-hypoxic fluctuations are an important factor in the induction of ROP. Subsequently, they established a paradigm of fluctuations between hyperoxia (50 %) and hypoxia (10 %) every 24 hours (Penn et al., 1995; Werdich et al., 2004).

However, oxygen levels that fluctuate only every 24 hours poorly reflect the newborns' experience of minute-by-minute changes. Consistently, Coleman et al. (2008) found more severe retinopathy (leaky vessels, retinal hemorrhage, vascular overgrowth) and higher serum VEGF and lower serum IGF-1 (insulin-like growth factor-1) levels in rats exposed to clustered versus dispersed hypoxic episodes at P21. Furthermore, they found an inverse correlation between body weight and severity of vessel anomalies. This is in agreement with the finding of larger avascular areas in large compared to small litters at P6 and P21 (Holmes and Duffner, 1995, 1996). Furthermore, in preterm born infants, too, poor postnatal weight gain has been associated with severity of ROP (Wallace et al., 2000).

In the last years other methods have been used to induce retinopathy in the rat. Wang et al. (2013) knocked down VEGF by subretinal injections of short hairpin RNA at P8 and found reduced neovascularization. McCloskey et al. (2013) showed retarded angiogenesis in the retina after intravitreal injection of anti-VEGF antibodies on P12. Both studies used their methods in addition to the 24 hours cycle of 50 % and 10 % oxygen established by Penn et al. (1994).

1.4.3 Link between Periventricular Leukomalacia and Retinopathy of Prematurity

PVL and ROP are two diseases extensively modeled in neonatal animals. There are several methods to induce either disease. However, both, symptoms of PVL and ROP occur after exposure to hyperoxia and/or hypoxia. PVL is presumably caused by oxygen-susceptibility of the brain because first signs of necrosis or diffuse white matter damage are seen in watershed areas where insufficient blood supply can be caused by even a slight reduction in blood flow (Momjian-Mayor and Baron, 2005; Volpe, 2009). ROP on the other hand is a disease directly affecting the retinal vasculature. Since angiogenesis is induced by hypoxia, fluctuations in oxygen level severely influence the development of the retinal blood vessels, specifically the hypoxia-induced expression of VEGF (Stone et al., 1995). VEGF is expressed by a variety of cell types, including astrocytes (Baburamani et al., 2012). They are in close contact with endothelial cells surrounding blood vessels in the central nervous system, together forming the blood brain barrier (Abbott et al., 2006). Astrocytic expression of VEGF is essential for the stabilization of both, cerebral (Ogunshola et al., 2000) and retinal (Scott et al., 2010) blood vessels. This leads to the assumptions that astrocytic cell death or malfunction affects the vascular development in both, brain and retina. Bucher et al. (2013) has shown that the density of retinal astrocytes decreases after hyperoxic exposure. Presumably, this may also be the case in the cerebrum.

Interestingly, Steck et al. (2015) induced retinal vascular abnormalities in an established rat model for PVL (unilateral artery ligation), thereby making a connection between the two diseases. Conversely, in this study we investigate the effect of an established model for ROP on the white and grey matter microstructural development. A previous study by Morken et al. (2013) had a similar objective. Rat pups were exposed to hyperoxia with intermittent hypoxic episodes from birth until P14. At P28 after two weeks of room air recovery, this caused abnormal retinal neovascularization beyond the ora serrata. Furthermore, this exposure led to increased mean, axial and radial diffusivity in several white matter structures at P14. With a similar experimental setting but in a more comprehensive study, we want to confirm (or falsify) the findings by Morken et al. (2013).

Chapter 2

Objectives

The overall aim of this thesis is to investigate the influence of oxygen fluctuations and growth retardation on the brain microstructural development and retinal vascularization in the neonatal rat. We hypothesize that the maturation of white and grey matter will be altered by exposure to hyperoxia with intermittent hypoxic episodes, and that growth retardation potentiates this effect. Further, we expect to see abnormal retinal vascularization in pups exposed to intermittent hyperoxia-hypoxia (IHH). These vascular abnormalities may be worse in pups with low weight. Lastly, we assume there might be an association between DTI parameters and measures of abnormal retinal vascularization. Figure 2.1 illustrates the context of these hypotheses and the approaches used to answer the following more specific questions:

1. What effect does exposure to IHH have on the fractional anisotropy, mean, axial and radial diffusivity? How does it affect their development over time?
2. Does early postnatal weight gain influence DTI parameters? Is this influence different between rat pups exposed to IHH and those exposed to room air?
3. Does exposure to IHH influence retinal vascularization? Does early postnatal weight gain have an effect?
4. Is there a connection between DTI measures of white and grey matter maturation and (abnormal) retinal vascularization?

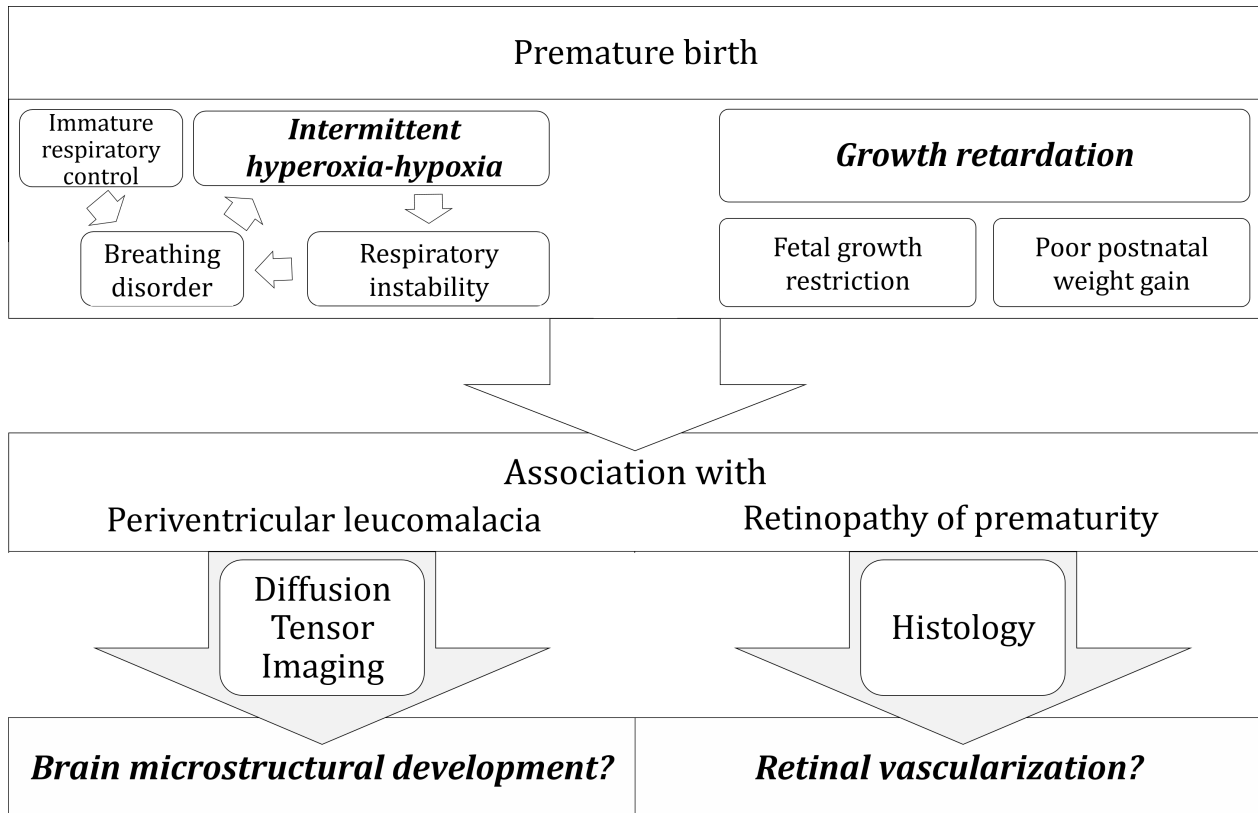


Figure 2.1: Research question of this thesis: How do intermittent hyperoxia-hypoxia and growth retardation influence white and grey matter maturation and retinal vascularization? For a detailed view of the upper left diagram, see figure 1.1. Periventricular leukomalacia is a distinct white matter disease, retinopathy of prematurity affects the retinal vasculature. Both diseases are associated with preterm birth.

Chapter 3

Magnetic Resonance Imaging

3.1 Principles of Magnetic Resonance

Magnetic Resonance Imaging (MRI) is based upon the law of electromagnetic induction expressed by Micheal Faraday in 1833. It discusses motion, magnetism and charge and states that if two of these forces are present, the third will be automatically induced. This phenomenon occurs in specific nuclei which have an odd mass number. These MR active nuclei possess a net charge and are spinning around their own axis. Consequently, they acquire a magnetic moment and can align in the presence of an external magnetic field. The one being most abundant in biological tissues and hence most commonly used is the hydrogen nucleus ^1H , consisting solely of a proton. The magnetic moment of these nuclei possess vector properties. In the resting state and in absence of an external magentic field the magnetic moments are randomly oriented, that is, the vectors point in random directions. However, they align when a strong static external magnetic field B_0 is applied. The magnetic moment of low-energy, spin-up nuclei align parallel, while that of high-energy, spin-down nuclei align antiparallel. At the thermal equilibrium, the ratio between these two populations of nuclei is given by the following equation:

$$\frac{N_\alpha}{N_\beta} = e^{\frac{\Delta E}{k_B T}} \quad (3.1)$$

where N_α , N_β is the number of parallel and antiparallel spins, respectively, e is Euler's number, k_B is the Boltzman's constant, and T is the temperature in Kelvin.

ΔE describes the energy difference between N_α and N_β and is defined as:

$$\Delta E = \hbar\gamma B_0 \quad (3.2)$$

where \hbar is the reduced Planck's constant, γ is the nuclei specific gyromagnetic ratio, and B_0 is the external magnetic field.

As a consequence from the equations 3.1 and 3.2, it follows that with increasing magnitude of the external magnetic field B_0 the surplus of low-energy state nuclei ($N_\alpha - N_\beta$) increases. The sum of all magnetic moments forms the net magnetization vector M_0 which is parallel to B_0 due to the aforementioned surplus of parallel aligned spins. The second process occurring in the presence of an external magnetic field is precession. The nuclei's magnetic moments precess around their axis at the so called Larmor frequency ω_0 , defined as:

$$\omega_0 = \gamma B_0 \quad (3.3)$$

3.1.1 Excitation and Relaxation

If a nucleus receives energy with the same frequency as its unique Larmor frequency, it gains this energy and resonates. This process is called excitation and leads to the transition of spin-up nuclei to spin-down nuclei. In MRI this energy is applied by means of a radio frequency (RF) pulse. The RF pulse causes M_0 to move out of alignment with a certain angle: a 90° RF pulse flips the M_0 into the transversal plane perpendicular to B_0 . Further, it moves the nuclei into phase with each other, meaning that all magnetic moments are on the same position on the precessional path.

After the RF pulse is turned off, the nuclei release the gained energy into the surrounding tissue and thus return to the low-energy, spin-up state until thermal equilibrium (see equation 3.1) is reestablished. This process is called longitudinal relaxation or T_1 recovery. It is an inversely exponential process and biological tissue has a specific inherent T_1 relaxation time. Simultaneously, the magnetic moments of the population of nuclei dephase, that is they are at different positions along the precessional path, since they precess at slightly different Larmor frequencies. Two magnetic moments pointing at opposite directions balance each other out thereby

reducing the length of M_0 . This process is called transverse relaxation or T_2 decay. As with the longitudinal relaxation, it is an exponential process and its speed depends on inherent chemical features of the surrounding tissue (Westbrook and Roth, 2011).

3.1.2 Magnetic Resonance Image Acquisition

Faraday's law of electromagnetic induction states that voltage is induced in a conductive loop if placed in the area of a changing magnetic field. Hence, the sum of the magnetic moments (M_0) precessing in phase in the transversal plane can be detected by placing a receiver coil into that plane. The induced voltage forms the MR signal, its magnitude depends on the magnitude of the component of M_0 in the transversal plane. It is reduced by both longitudinal (T_1) and transversal (T_2) relaxation.

The receiver coil detects the amplitude of induced voltage over time. Then, the signal has to be spatially encoded. By means of gradient coils the external magnetic field can be applied in three different directions perpendicular to each other and at different time points. Thereby each nuclei has a certain Larmor frequency depending on its position along the gradient axis. Through Fourier transformation the signal can be timely decoded and spatially encoded and hence the image created (Westbrook and Roth, 2011).

3.2 Diffusion Tensor Imaging

Diffusion is random translational motion along a density gradient due to thermal energy. Diffusion Tensor Imaging (DTI) is a form of functional MRI whereby the image contrast is based on the diffusion of water molecules. This form of contrast is commonly generated by using the Stejskal-Tanner sequence. Thereby, two gradients are applied after another: a dephasing and a rephasing gradient. First, the dephasing gradient dephases the protons dependent on their position within the tissue. Second, after some time, the rephasing gradient shifts the stationary protons back to their initial phase. This is possible because the rephasing and dephasing gradients have the same slope, just inverted. Protons (water molecules) diffusing in the time between the first and the second gradient are not fully rephased since they experience two different phase-shifts. These incompletely rephased protons are detectable by a signal loss which

is described by the following equation:

$$S_b = S_0 e^{-bD} \quad (3.4)$$

where S_b is the diffusion weighted signal, S_0 is the signal without diffusion-weighting, b is the diffusion weighting factor and D is the tissue-specific diffusion coefficient. The diffusion-weighting factor b can be controlled and is dependent on the gyromagnetic ratio γ , the strength and duration of the two gradients as well as the time between them. The more the water molecules diffuse, the higher is the detected signal loss (Mori and Zhang, 2006).

3.2.1 The Diffusion Tensor

The diffusion tensor describes the diffusion probability distribution of a water molecule in a certain tissue. In the three-dimensional space it is defined by three eigenvalues (λ_1 , λ_2 and λ_3) that scale the length of three eigenvectors (e_1 , e_2 and e_3). Therefore measurements in six directions are sufficient to describe the diffusion tensor. If the diffusion is isotropic, that is the diffusion has the same probability in all directions, the diffusion tensor describes a sphere (see figure 3.1). However, if the diffusion is anisotropic, that is the probability of diffusion in at least one directions differs from the ones for the other directions, the diffusion tensor describes an ellipsoid. Per definition, λ_1 describes the magnitude of diffusion along the longest axis of the diffusion tensor.

Generally, the diffusion in white matter is more directional, anisotropic, than in grey matter. Even though there are the boundaries in grey matter as well, they are more randomly oriented and thus diffusion is more isotropic. To be able to quantitatively assess diffusion anisotropy, the measure *fractional anisotropy* (FA, eq. 3.5) was established by Basser and Pierpaoli (1996). It is very useful owing to its scale from 0 (isotropic) to 1 (anisotropic) and since it provides a single measure of the degree of overall diffusion directionality.

$$FA = \sqrt{\frac{1}{2} \frac{\sqrt{(\lambda_1 - \lambda_2)^2 + (\lambda_2 - \lambda_3)^2 + (\lambda_3 - \lambda_1)^2}}{\sqrt{\lambda_1^2 + \lambda_2^2 + \lambda_3^2}}} \quad (3.5)$$

In this thesis, aside from fractional anisotropy, three other indices of diffusion in tissue are used.

Mean diffusivity (MD, eq. 3.6) describes the average diffusion in all directions. *Axial diffusivity* (AD, eq. 3.7) equals the first eigenvalue (λ_1) and thus describes the magnitude of diffusion along the first eigenvector (e_1). *Radial diffusivity* (RD, eq. 3.8) describes the average diffusivity along the remaining two eigenvectors (e_2, e_3) (see Figure 3.1).

$$\text{MD} = \frac{\lambda_1 + \lambda_2 + \lambda_3}{3} \quad (3.6)$$

$$\text{AD} = \lambda_1 \quad (3.7)$$

$$\text{RD} = \frac{\lambda_2 + \lambda_3}{2} \quad (3.8)$$

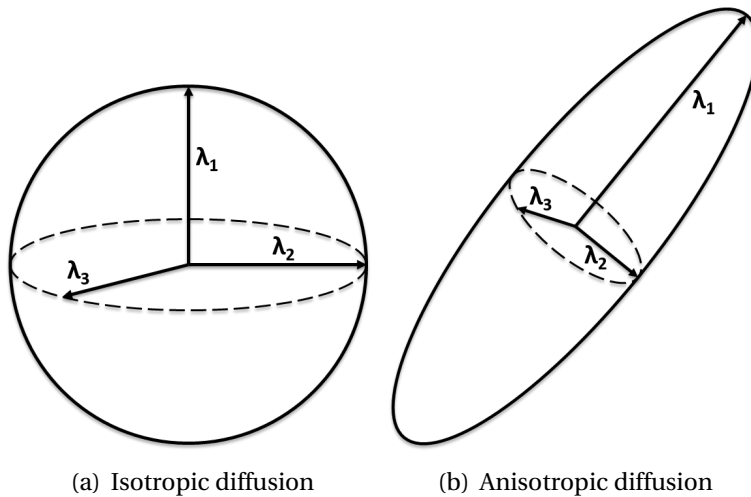


Figure 3.1: Diffusion tensor for isotropic and anisotropic diffusion If the diffusion probability is the same in all directions, the eigenvalues are equal and the diffusion tensor is a sphere. If the probability for diffusion is different in at least one direction, the diffusion tensor is an ellipsoid.

Chapter 4

Material and Methods

4.1 Animal Model

The animal experiments were approved by the local authority on animal welfare (Forsøksdyruttvalget) and conducted in accordance with the Norwegian Ethics Committee for Animal Research. Testing subjects are the pups of time-mated Sprague-Dawley rats (Taconic Biosciences).

4.1.1 Animal Handling

The animals and their offspring were handled either in the comparative medicine core facility (Avdeling for Komparativ Medisin, AKM) or in a designated animal room in the MR Center at NTNU. They were moved in their cage between the two facilities by means of a special transportation box. The rats were kept on a 12:12 hours light:dark cycle with one hour of dusk. They were held in rat cages (IVC class 3, Innovive) and had access to water and food (RM1, Scanbur BK) *ad libitum* at all times. The rooms were kept at $(22.8 \pm 0.22)^{\circ}\text{C}$ and $(48 \pm 12.4)\%$ humidity. Bedding was changed after each MRI scan, that is at postnatal day 15 (P15) and P28. To allow acclimatization, the pregnant rats arrived at the AKM at least one week before giving birth. From two days before scheduled birth until birth they were checked every four hours between 7 am and 11 pm each day to narrow down the time frame in which the pups were born. When two births occurred within 12 hours, the pups from both litters were put together, mixed and redistributed to both mother rats (culling).

4.1.2 Experiment Groups

Within 12 hours after birth, the pups were weighted and the litters culled to litter sizes of 8, 12, or 16 pups, respectively. When more pups than needed were born, the ones with the weights closest to the median of the population were chosen to be excluded from the litter. Excluded pups were euthanized by first anesthesia with 4 % isoflurane in O₂ and then decapitation. In total eight litters were included (see figure 4.1). Five litters contained 8 pups per litter, three of these were exposed to intermittent hyperoxia-hypoxia (IHH). One litter comprised 12 pups, it was exposed to IHH. Two litters contained 16 pups per litter, one was exposed to IHH the other one to room air (21 % O₂, RA). In the 16 pups litter exposed to IHH, one pup died shortly after culling. In one of the 8 pups litter exposed to IHH, one pup died during the first MRI scan.

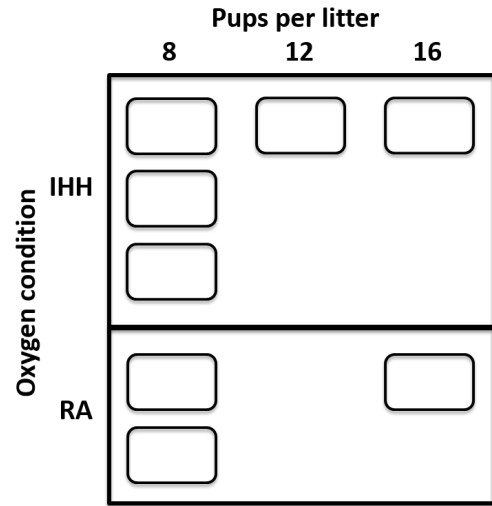


Figure 4.1: Testing subjects by litter. In total, eight litters are included in the study: five with 8 pups, one with 12 pups, two with 16 pups per litter. Five litters are exposed to IHH, three to RA. IHH: Intermittent hypoxia-hyperoxia, RA: Room air

4.1.3 Exposure to Intermittent Hyperoxia-Hypoxia

Five of eight litters ($n_{\text{IHH}} = 52$, $n_{\text{RA}} = 32$) were exposed to fluctuating oxygen levels for 14 days starting within 12 hours after birth. The oxygen profile is called intermittent hyperoxia-hypoxia (IHH). Concretely, long episodes of hyperoxia (50 % O₂) are intermitted by three consecutive, short 5 min episodes of hypoxia (12 % O₂) every third hour (see figure 4.2). The application of the IHH profile was executed by means of the OxyCycler A84XOV (BioSpherix, 2013) and the respective software and oxygen chambers, into which the whole cages were set. The oxycycler has an accuracy of $\pm 1\%$ (BioSpherix, 2013) and has had a ramp time of 3 minutes going from 12 % to 50 %, and of 8 minutes vice versa. The O₂ and CO₂ ($(11194 \pm 857)\text{ppm CO}_2$) levels as well as temperature ($(22.8 \pm 0.22)^\circ\text{C}$) and relative humidity ($(48 \pm 12.4)\%$) were continuously monitored. The concentration of oxygen within the chamber was controlled via influx of N₂ or O₂,

respectively. Once a day, during the hyperoxic episode, the cage was taken out of the oxygen chamber for health monitoring of the pups. This took less than four minutes.

4.2 Magnetic Resonance Imaging

MRI was performed on a 7 T magnet with water-cooled gradients (660 mT/m). For radio frequency (RF) transmission a 86 mm volume resonator was used. For RF reception on the first scan (at P15) an actively decoupled phased array mouse head surface coil was used and on the second scan (P28) an actively decoupled phased array rat head surface coil. Anesthesia was induced shortly before scanning with 4 % isoflurane in room air with added O₂ and kept with 2 % isoflurane during scanning. The animals were placed prone onto a water-heated animal bed and their head was fixated by means of a tooth-bar, nose-mask and polystyrene, as well as earplugs on P28. Furthermore, cotton wool was placed on top of the animals to insulate the pup and thus limit heat loss. The respiratory rate and body temperature were monitored and kept stable by adjustment of anesthesia and animal bed heating.

4.2.1 Diffusion Tensor Imaging

After a initial localizer scan with optimization of global shims, local field homogeneity of an ellipsoid volume covering the entire brain was optimized based on an acquired b_0 -map using the inbuilt MAPSHIM procedure in Paravision 6.0 (Bruker Biospin). Subsequently DTI was performed using a spin echo sequence with Tjeskal-Tanner diffusion preparation and single shot echo planar signal read-out. 5 images without diffusion weighting ($b = 0$ ms) and 30 images diffusion weighting ($b = 800$ ms) were acquired in different non-collinear directions. The number of averages was 16 at P15 and 24 at P28 resulting in scan times of 23.3 minutes and 35 minutes, respectively. The remaining parameters are given in table 4.1.

4.2.2 MRI Data Analysis

DTI analysis was performed with FMRIB software library (FSL) tools (Jenkinson et al., 2012). To reduce motion artifacts and eddy current distortions, images were pre-processed by affine

Table 4.1: Scan parameters of DTI sequences at P15 and P28

Repetition time	2500 ms
Echo time	22 ms
Field of view	(20.48 × 15.36) mm
Acquisition matrix	128 × 96
Number of slices	18
Slice thickness	0.8 mm with 0.2 mm gaps
Resolution	(160 × 160 × 800) μm^3

transformation and co-registration of the diffusion-encoded images to the first b_0 image. Images with severe motion artifacts were excluded, resulting in 43 and 30 images suitably for analysis of the IHH and room air group at P15, respectively. At P28, 45 and 30 images of the IHH and room air group, respectively, could be used for analysis. Brains were automatically selected and extracted from the b_0 images using the Brain Extraction Tool. Then a diffusion tensor model was fitted voxelwise using FMRIB's Diffusion Toolbox. Maps for fractional anisotropy, as well as mean, axial and radial diffusivity were created according to equations 3.5-3.8. On all relevant slices, regions of interest were manually drawn in the centre of the corpus callosum, internal capsule, hippocampal fibria, external capsule, hippocampus, cortex, thalamus and striatum (see figure 4.3 and B.1). For all structures except the corpus callosum masks were drawn separately for each side. The fractional anisotropy, mean, axial and radial diffusivity was calculated for each region of interest accordingly.

4.3 Tissue Processing

4.3.1 Retinal Dissection

The rats were euthanized after the MRI scan at P28 by an overdose of pentobarbital (300 mg/kg, Vetoquinol GmbH). Subsequently, the tissue was perfusion-fixed by an intracardial injection of approximately 20 ml of 4 % paraformaldehyde (PFA, Fluka Chemie AG) in phosphate-buffered saline (PBS, Oxoid Limited).

The left retina of all animals was dissected according to the protocol described in Tual-Chalot et al. (2013). First, the eye was enucleated, fixated in PFA and transferred to a petri dish containing cold PBS. Then, the cornea and iris were cut out. By inserting forceps between retina

and sclera the two layers were separated. Further, the lens, vitreous humour and hyaloid vessels were removed. Then, the retina was rinsed with PBS and transferred to a clean petri dish. By making radial incisions, the cup shaped retina was flattened. The PBS was removed from the petri dish and the retina was covered with and then stored in ice-cold 70 % ethanol to facilitate permeabilization.

4.3.2 Staining of Retinal Vasculature

The dissected retinas were stored in 2 ml-ependorf tubes filled with 70 % ethanol at -20°C . They were stored between 24 and 72 hours prior to staining and pilot experiments showed no difference for these storage periods. The staining protocol described by Dhaliwal et al. (2011) was used. The ethanol was removed and the retinas washed three times in PBS for 5 min, 1 % triton X. They were incubated in blocking buffer (5 % swine serum, 0.1 % bovine serum albumin, 0.3 % triton X in PBS) for 2 h at room temperature to block unspecific binding sites. The primary antibody is biotinylated griffonia and simplicifolia lectin I isolectin B4 diluted 1:40 in PBS 0.1 % triton X, which is commonly used for endothelial staining. The retinas were covered with 100 μl of the primary antibody and incubated overnight at 4°C . The primary antibody was then removed and the retinas were washed three times for 5 min in PBS 0.1 % triton X before incubation with the secondary antibody, fluorescein streptavidin diluted 1:100 in PBS 0.1 % triton X, for 2 h at room temperature with gentle shaking. Lastly, the retinas were washed three times for 5 min in PBS 0.1 % triton X and once for 5 min in pure PBS. Then they were mounted onto glass slides with VectaShield as mounting media. During and after incubation with the secondary antibody the retinas were continuously covered.

4.3.3 Imaging and Image Analysis

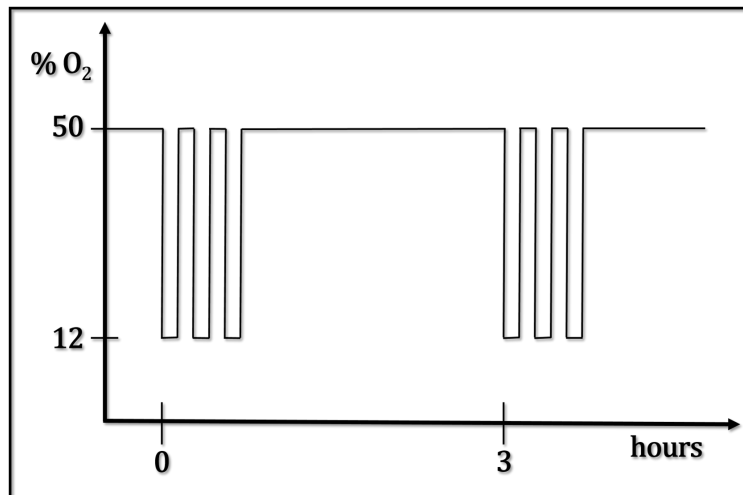
The stained and mounted retinas were imaged the same day with the EVOS FL Auto (ThermoFisher Scientific) microscope and images were created. The images are put together from several single images with 4x magnification. 38 retinas (23 in IHH, 15 in room air group) were suitable for analysis, the remaining had to be excluded because they were severely disrupted or parts were missing.

Using Fiji (Schindelin et al., 2012), for each sample the diameters of three arteries and three veins in the center (close to the optic nerve) and just before the first major bifurcation (in the midperiphery) were measured blindly (see figure 4.4a). Subsequently the ratio between the vessel diameter in the center and in the midperiphery (before the first bifurcation) were calculated.

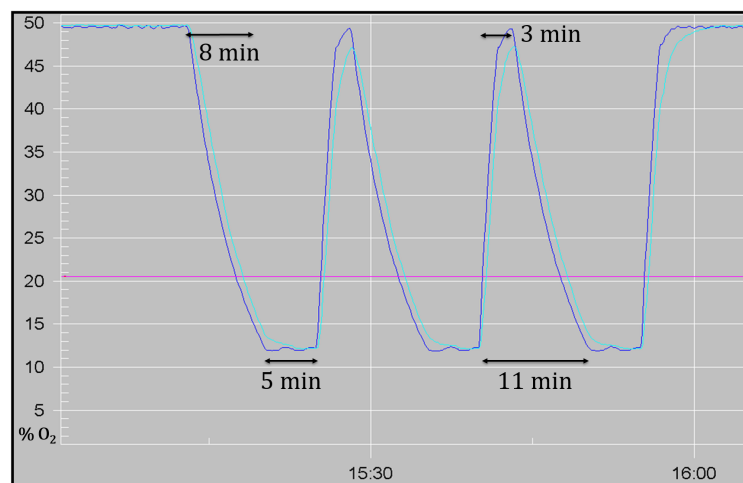
Furthermore, the tortuosity of three arteries and three veins from the center to the first major bifurcation was determined. The length between the starting and end point was measured (yellow line in figure 4.4b), and by drawing manually the absolute length of the blood vessel identified (red line in figure 4.4b). The quotient of latter and first equals the vessel tortuosity.

4.4 Statistical Analysis

Statistical analyses were performed using IBM SPSS Statistics 23. Statistical significance was defined as $p < 0.05$. Since only few subgroups of the data were normally distributed, non-parametric tests were used for all analysis. Concretely, for comparison between two groups the Mann-Whitney U test was performed, for comparison between more than two groups the Kruskal-Wallis test. Correlations between different parameters were quantified using Pearson's r correlation coefficient. Results are displayed as mean \pm standard deviation, unless indicated otherwise. In the boxplot, mild outliers ($< 25\text{-percentile} - 1.5 * \text{interquartile range (IQR)}$ or $> 75\text{-percentile} + 1.5 * \text{IQR}$) are marked with a circle. Extreme outliers ($< 25\text{-percentile} - 3 * \text{IQR}$ or $> 75\text{-percentile} + 3 * \text{IQR}$) are marked with an asterisk.



(a) IHH profile



(b) 3 hypoxic episodes



(c) Oxycycler

Figure 4.2: IHH profile and oxycycler. Every three hours 50% O_2 hyperoxia is intermitted by a cluster of three consecutive, short episodes of 12% O_2 hypoxia. The IHH study group received this treatment within the first 12 hours after birth until P14.



Figure 4.3: White matter regions of interest. Manually drawn mask of corpus callosum (red), internal capsule (pink), hippocampal fimbria (blue) and external capsule (green) on a center slice of a rat brain at P28.

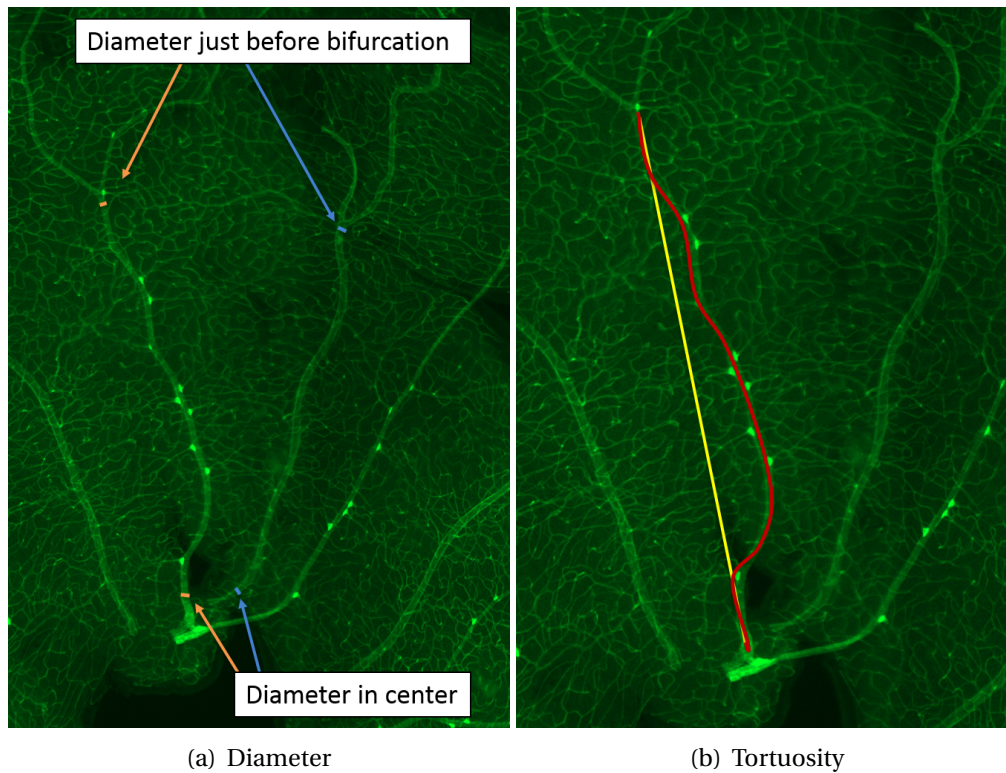


Figure 4.4: Measures for retinal vasculature. The vessel diameter and tortuosity were measured at three arteries and three veins in each sample.

Chapter 5

Results

In this chapter, first the diffusion tensor imaging (DTI) findings are displayed and explained according to oxygen condition, then the influence of weight and weight gain is addressed. Thereafter, the interaction between oxygen exposure and weight (gain) are shown. Lastly, measures of abnormal retinal vascularization are compared between groups of different oxygen exposure. Throughout the chapter, red and orange bars indicate $p < 0.01$ and $p < 0.05$, respectively. The respective raw data can be found in the appendix.

5.1 DTI Parameters by Oxygen Condition

This section compares the values for fractional anisotropy, mean, axial and radial diffusivity over time between the IHH and the room air group. In total, four white matter and four grey matter structures were analyzed (see table 5.1). In general, in all structures the fractional anisotropy increased over time, while the mean and radial diffusivity decreased. Axial diffusivity increased over time in white matter structures, but decreased in grey matter.

Table 5.1: Acronyms for brain structures analyzed in this study

White matter		Grey matter	
cc	corpus callosum	h	hippocampus
ic	internal capsule	c	cortex
hf	hippocampal fibria	t	thalamus
ec	external capsule	st	striatum

5.1.1 Fractional Anisotropy

There was a clear difference in fractional anisotropy between white and grey matter structures, both at P15 and at P28 (see figure 5.1). White matter structures such as the right internal capsule had a relatively high fractional anisotropy of 0.564 ± 0.035 and 0.683 ± 0.036 at P15 and P28, respectively. In contrast, grey matter structures have a lower fractional anisotropy, for example 0.138 ± 0.028 and 0.161 ± 0.030 in right thalamus at P15 and P28, respectively.

At P15, the fractional anisotropy was higher in the corpus callosum and left internal capsule in IHH exposed pups. The mean fractional anisotropy in the corpus callosum was 3.40 % higher in the IHH compared to the room air group, in the internal capsule the difference was 2.33 %. In all other structures, no difference between groups of different oxygen condition could be observed.

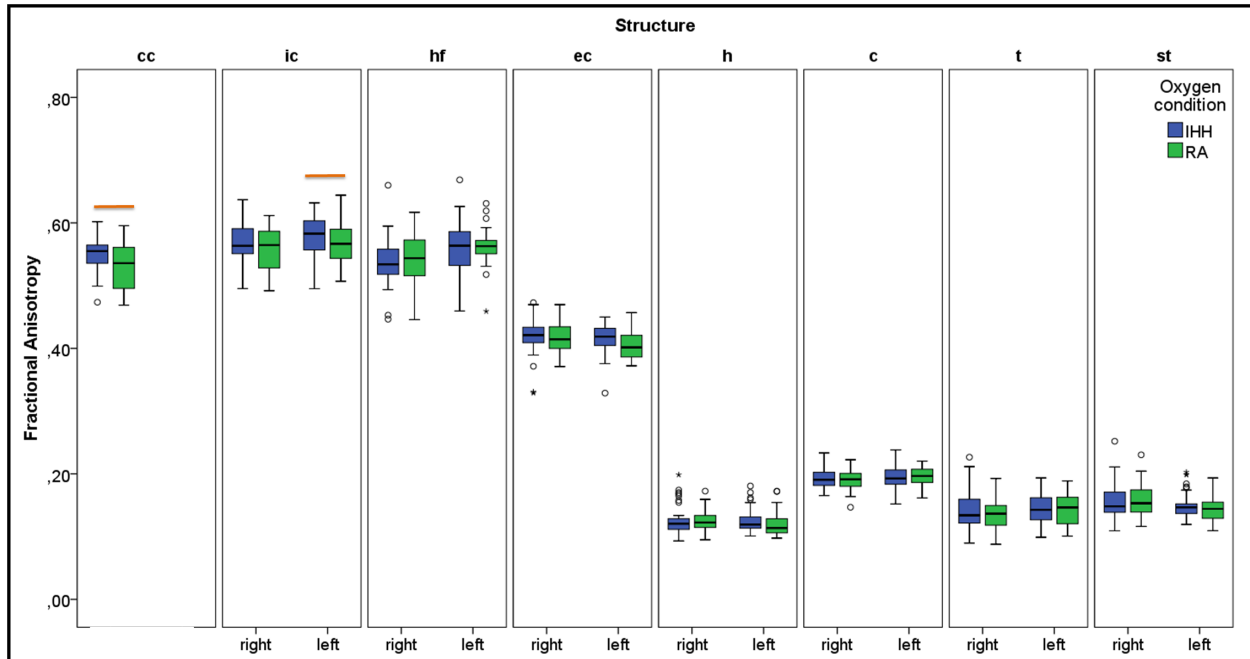
At P28, IHH exposed pups had a higher fractional anisotropy in the right hippocampal fimbria, while it was lower in the right external capsule. This is especially interesting, since both are white matter structures, but IHH exposure had an opposite effect on their fractional anisotropy. Furthermore, right cortex and left thalamus had a higher fractional anisotropy in the IHH compared to the room air group. The remaining structures did not show a significant difference between IHH and room air group.

5.1.2 Mean Diffusivity

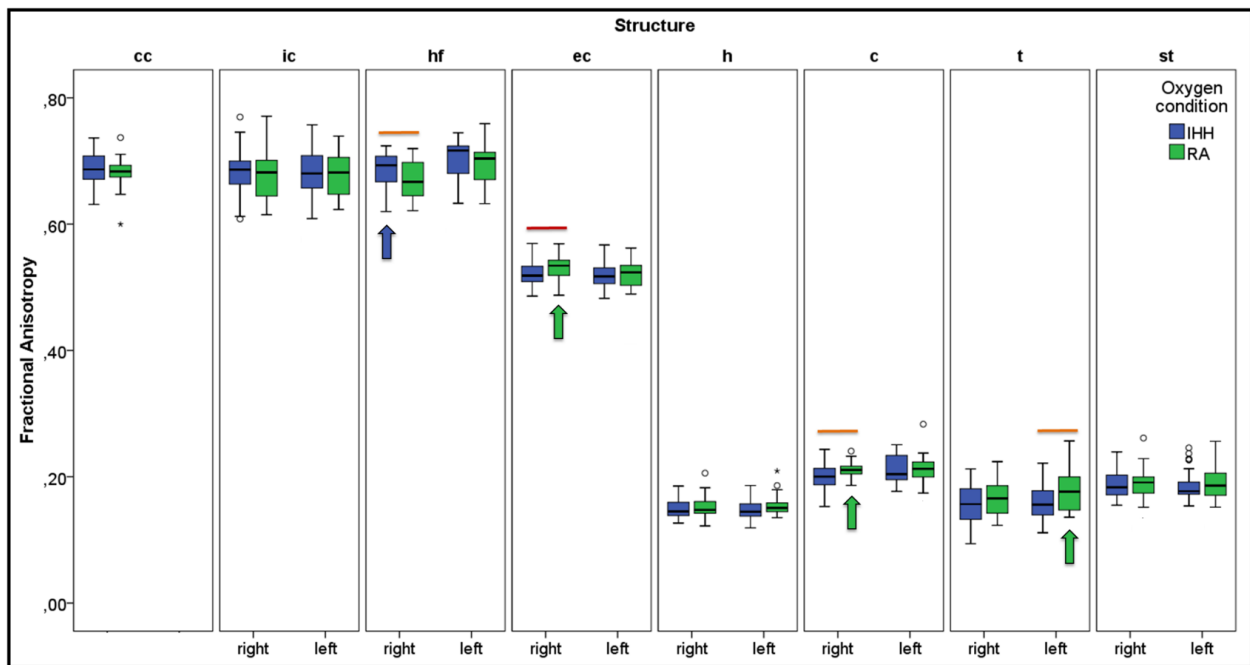
The mean diffusivity is displayed in figure 5.2. In general, white and grey matter structures were not as distinctly different regarding mean diffusivity as they were regarding fractional anisotropy.

At P15, none of the structures showed a significant difference in mean diffusivity across groups of different oxygen exposure. Conversely, at P28, pups exposed to IHH had higher values of mean diffusivity compared to pups kept in room air in all structures. The difference in mean diffusivity ranged across structures from 3.5 % in the left internal capsule to 4.8 % in the right thalamus.

Since the mean diffusivity in both groups decreased from P15 to P28, the higher values detected in the IHH group at P28 indicate a less decrease compared to the room air group.

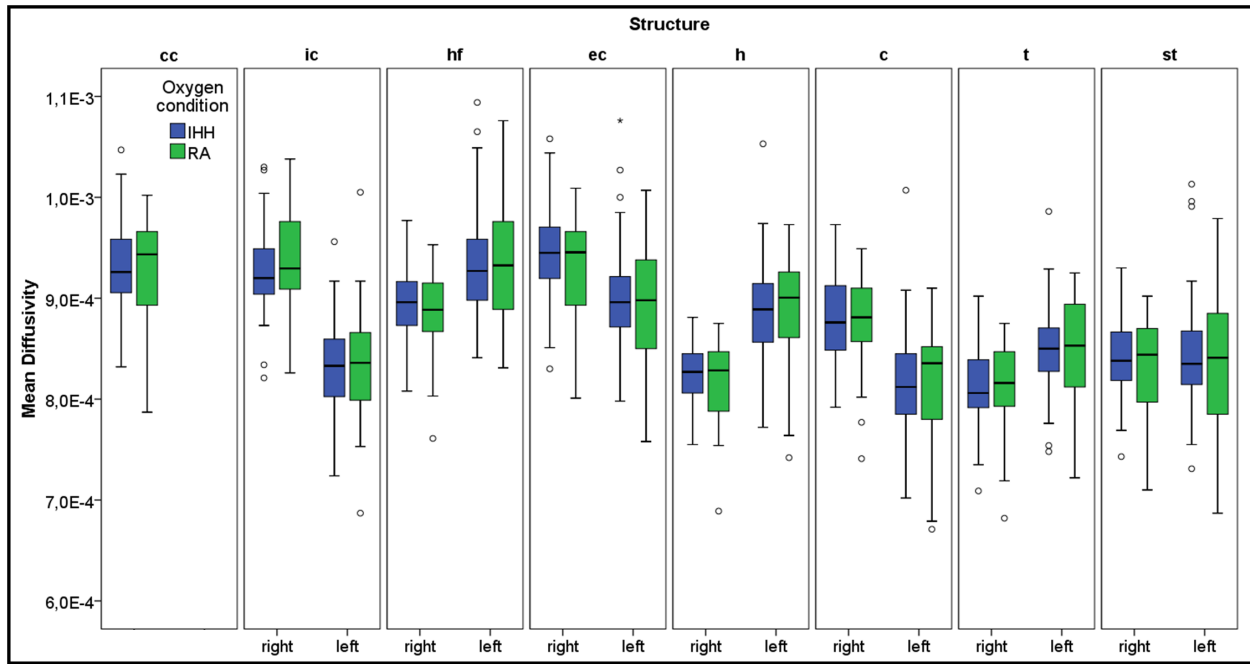


(a) P15

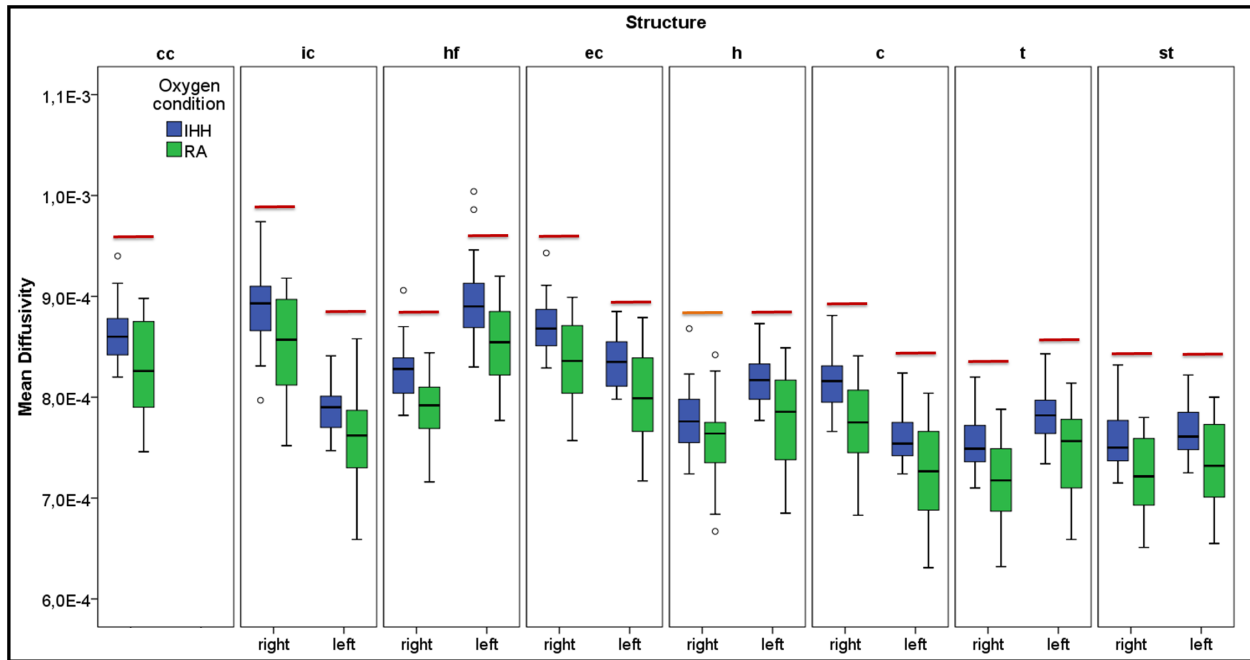


(b) P28

Figure 5.1: Fractional anisotropy by oxygen condition At P15, the FA of cc and left ic were higher in IHH compared to RA group. At P28, the FA of right hippocampal fimbria was higher in the IHH (blue arrow), while the FA of right external capsule, right cortex and left thalamus was higher in the room air group (green arrow). Red and orange bars indicate $p < 0.01$ and $p < 0.05$, respectively.



(a) P15



(b) P28

Figure 5.2: Mean diffusivity by oxygen condition. MD in mm^2/s . At P15, there was no difference between IHH and RA group in any structure. Contrarily, at P28, in all structures the MD was higher in pups exposed to IHH compared to room air. Red and orange bars indicate $p < 0.01$ and $p < 0.05$, respectively.

5.1.3 Axial Diffusivity

Figure 5.4 shows boxplots of axial diffusivity. The pattern of axial diffusivity resembles that of the fractional anisotropy. The axial diffusivity in white matter structures was higher than it was in grey matter, at both time points and in both, the IHH and the room air group. While the hemispheric differences in cortex, thalamus and striatum were small and partially insignificant, there were prominent side differences in internal and external capsule, hippocampal fimbria, and hippocampus.

Aside the right external capsule, there was no difference in axial diffusivity across categories of oxygen condition at P15. At P28, on the other hand, the axial diffusivity in pups exposed to IHH was higher compared to the room air group in all structures.

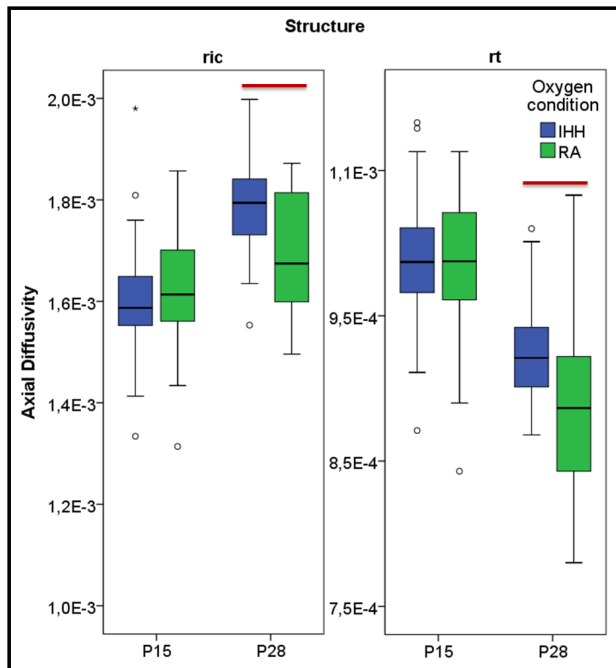
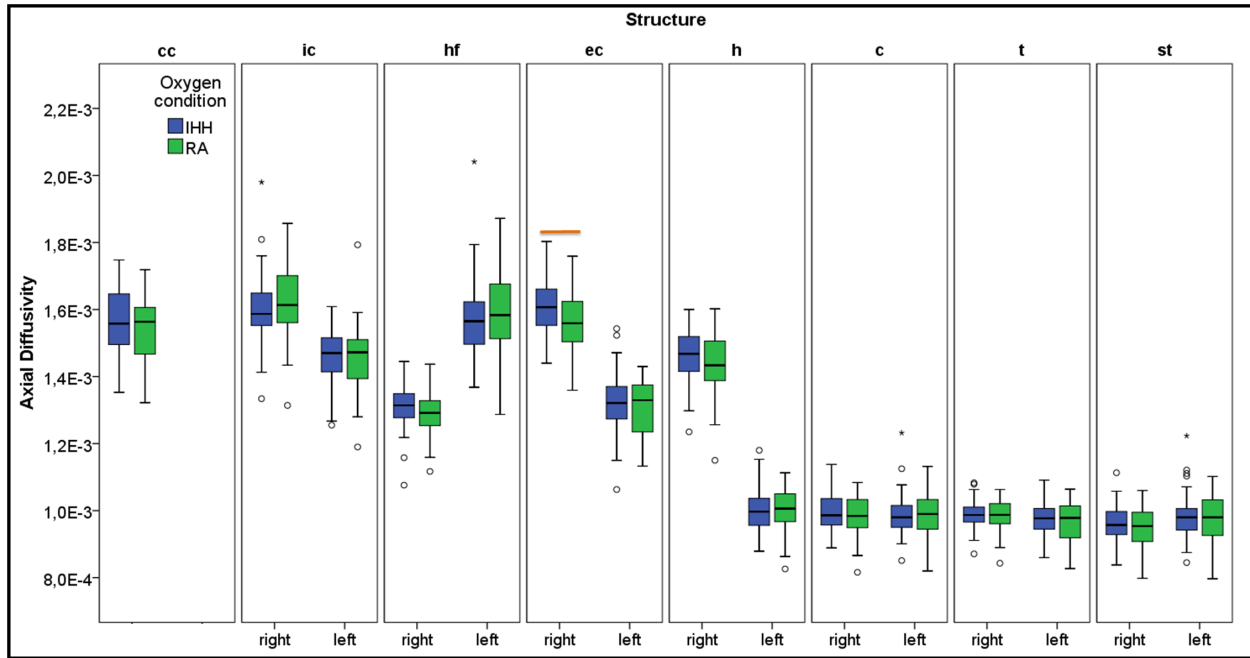


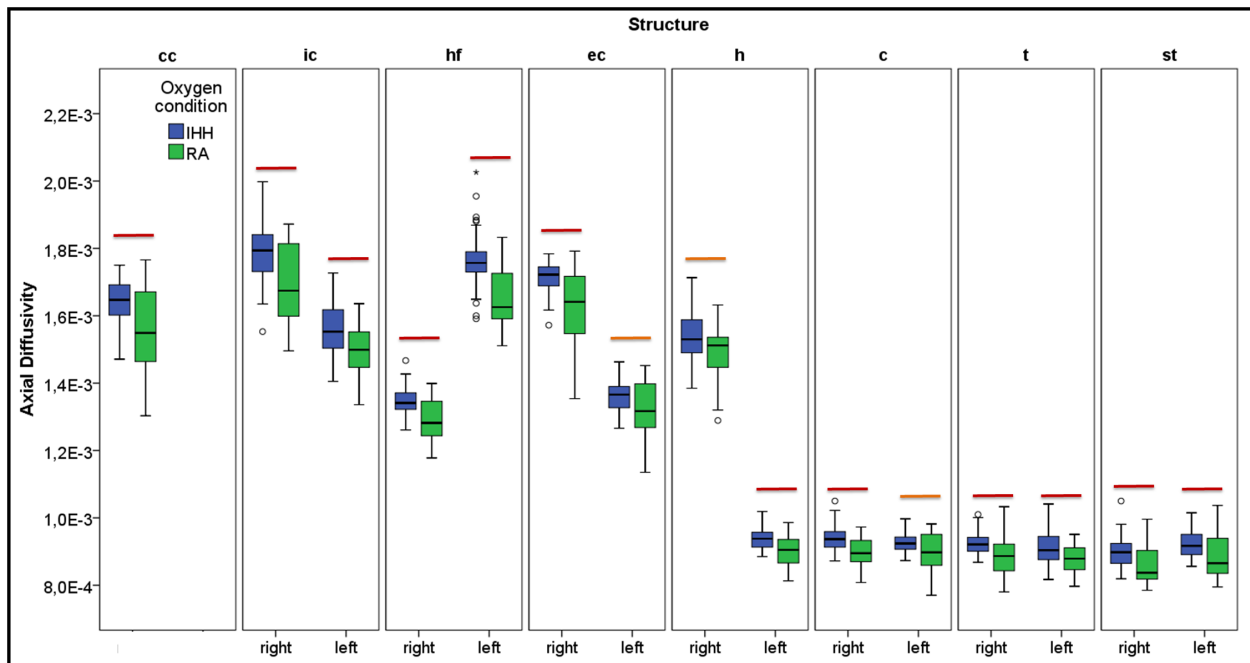
Figure 5.3: Axial diffusivity increased in white matter and decreased in grey matter. AD in mm^2/s . The increase of axial diffusivity in white matter was stronger, while the decrease in grey matter was weaker in the IHH versus the room air group. Right internal capsule (ric) and right thalamus (rt) serve as example for white and grey matter, respectively. Red bars indicate $p < 0.01$.

Interestingly, the development of axial diffusivity differed in white and grey matter. Exemplarily, values for right internal capsule and right thalamus over time are shown in figure 5.3. Albeit the axial diffusivity increased in the white matter of both groups, the increase was stronger in IHH exposed pups. For example, the right internal capsule had a mean increase in axial diffusivity of 11.25 % in the IHH group, compared to only 4.94 % in the room air group.

However, the reverse applied for grey matter. The axial diffusivity in grey matter decreased overall, but the decrease was weaker in the IHH group. In the right thalamus, there was a mean decrease of 6.12 % in IHH exposed pups, while the axial diffusivity in the control group decreased by 9.55 % between P15 and P28.

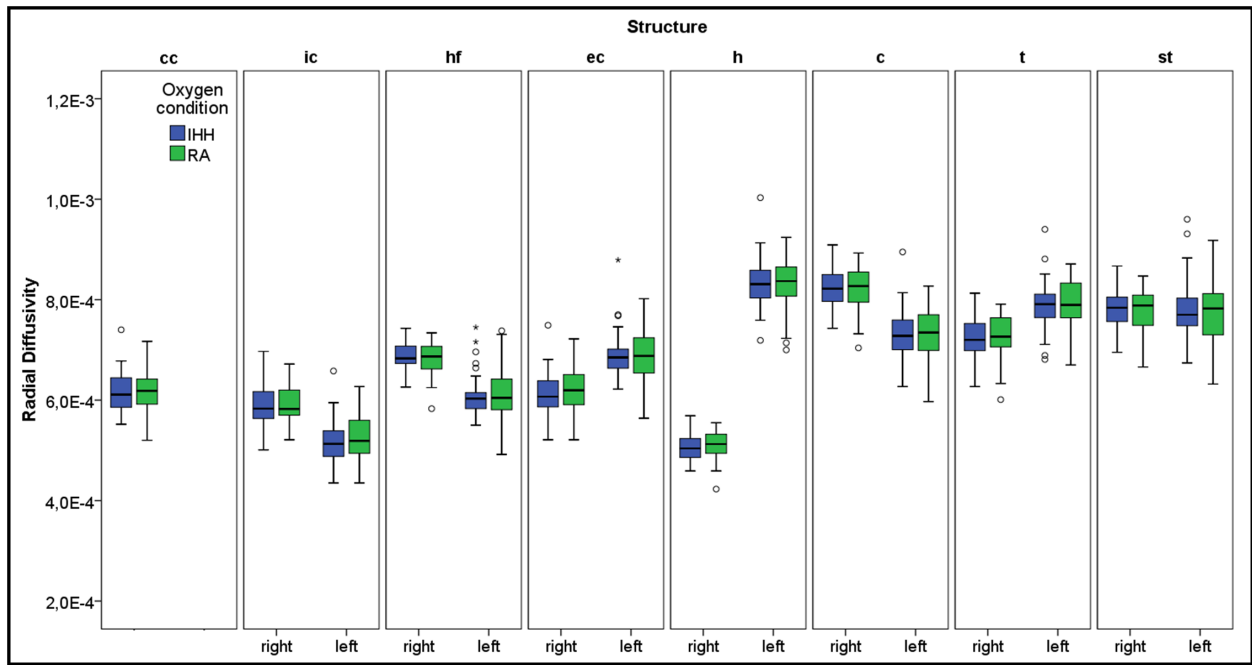


(a) P15

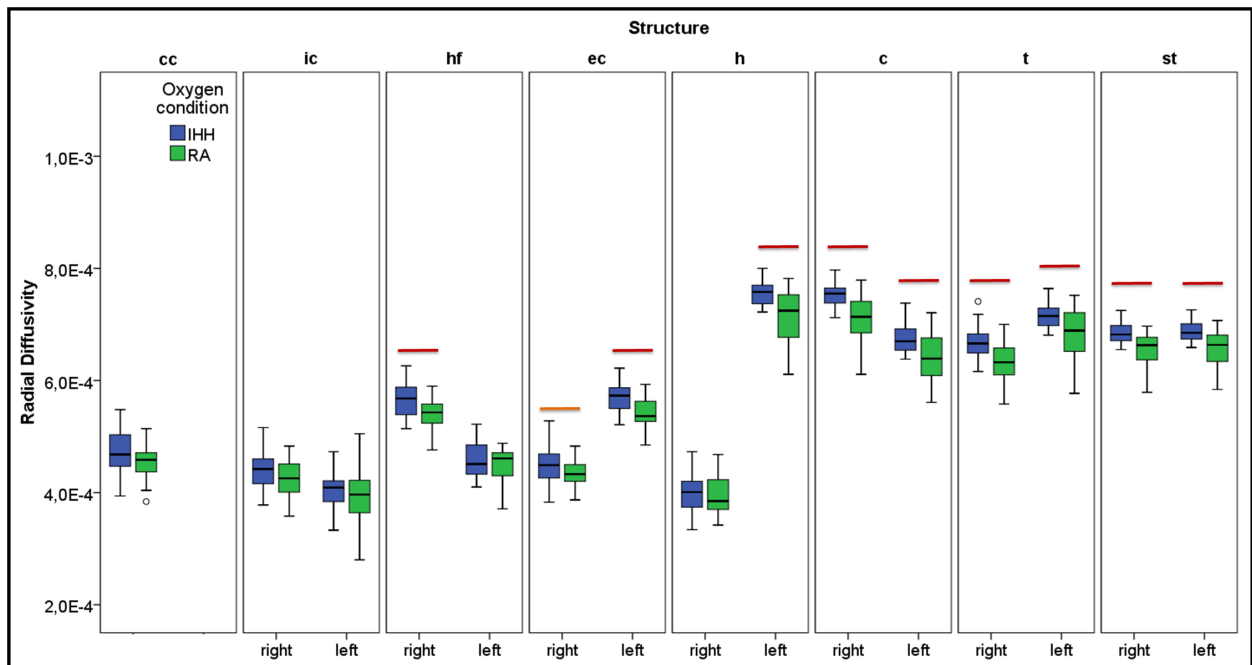


(b) P28

Figure 5.4: Axial diffusivity by oxygen condition AD in mm^2/s . Similar to MD, at P15 the AD in all structures was approximately the same, except for the right ec. At P28, however, the IHH group had a higher AD in all structures. Red bars and orange bars indicate $p < 0.01$ and $p < 0.05$, respectively.



(a) P15



(b) P28

Figure 5.5: Radial diffusivity by oxygen condition RD in mm²/s. Similar to MD and AD, the RD in all structures was approximately the same comparing groups of oxygen condition. At P28, the RD was significantly higher in right hf, left h, and both sides of ec, c, t, and st. Red and orange bars indicate $p < 0.01$ and $p < 0.05$, respectively.

5.1.4 Radial diffusivity

Generally, the radial diffusivity showed a reverse pattern as the axial diffusivity (figure 5.5). Highest values were found in grey matter structures, while lower values for radial diffusivity were present in white matter. As it was the case for mean diffusivity, the radial diffusivity did not show any significant difference between groups of different oxygen condition at P15.

At P28, however, all grey matter structures except right hippocampus showed a significantly higher radial diffusivity in the IHH compared to the room air group. Regarding the white matter, the right hippocampal fimbria and both sides of the external capsule were higher after IHH exposure. Likewise in corpus callosum and internal capsule, even though the difference was not significant, the radial diffusivity was higher in IHH exposed rat pups. Since the radial diffusivity was generally decreasing over time both in white and grey matter, the higher values in the IHH group indicate a less decrease.

5.1.5 Summary

In general, differences between IHH exposed pups and pups kept in room air were only rarely present at P15. At P28, however, all DTI parameters showed significant differences in almost all structures between the IHH and room air group. Both groups showed the same general development. In white matter, the IHH exposed pups had a stronger increase in fractional anisotropy and axial diffusivity, but a weaker decrease in mean and radial diffusivity than the pups kept in room air. In grey matter on the other hand, all DTI parameters changed less in the IHH group.

5.2 DTI Parameters by Weight

In the following figures 5.6-5.10, highlight tables of Pearson's correlation coefficient r are shown. While the correlation between fractional anisotropy and weight (gain) was generally stronger at P15, mean, axial, and radial diffusivity had stronger correlations with weight (gain) at P28. Aside from relative weight gain between P15 and P28, Pearson's r had similar values for all parameters of weight in the same structure. In tables C.3-C.6 of the appendix, the raw data of both Pearson's r and Spearman's ρ correlation coefficients with the respective p-values are displayed.

5.2.1 Fractional Anisotropy

The strongest correlation between fractional anisotropy and weight was seen at P15 in the corpus callosum, internal and external capsule and striatum, which all had correlation coefficients >0.5 in at least one side. Conversely, the correlation coefficient of hippocampal fimbria, hippocampus, cortex and thalamus was only weakly correlated with nearly all $r < 0.4$. At P28, the weight (gain) was generally less correlated with fractional anisotropy. Furthermore, all correlation coefficients at P28 were ≤ 0.421 , that is relatively weak. Interestingly, both at P15 and P28 the cortex was the only brain structure that shows a negative correlation with weight. However, the correlation was very weak with $r < 0.3$ in all combinations.

Fractional Anisotropy	cc		ic		hf		ec		h		c		t		st	
	right	left	right	left	right	left	right	left	right	left	right	left	right	left		
Weight at P15	.545	.383	.520	.242	.346	.475	.629	.237	.412	-.249	-.286	.299	.290	.260	.513	
Absolute weight gain P0 - P15	.538	.374	.513	.237	.337	.467	.621	.238	.409	-.239	-.280	.302	.290	.262	.508	
Relative weight gain P0 - P15	.507	.340	.487	.221	.304	.440	.590	.246	.397	-.195	-.255	.310	.283	.267	.483	

(a) Correlation with fractional anisotropy at P15

Fractional Anisotropy	cc		ic		hf		ec		h		c		t		st	
	right	left	right	left	right	left	right	left	right	left	right	left	right	left		
Weight at P15	.290		.308	.372							-.278			.292		
Weight at P28	.363		.326	.421										.352	.280	
Absolute weight gain P0 - P15	.280		.300	.365							-.279			.287		
Absolute weight gain P15 - P28	.383		.313	.421										.364	.310	
Relative weight gain P0 - P15	.235		.269	.338							-.288			.269		
Relative weight gain P15 - P28						.387					.243					

(b) Correlation with fractional anisotropy at P28

Figure 5.6: Highlight table of correlation coefficients between fractional anisotropy and weight (gain) Pearson's r between fractional anisotropy and weight (gain), blank space indicates non-significant correlation. While the fractional anisotropy at P15 showed a correlation in all structures, at P28 only the corpus callosum, hippocampal fimbria, cortex and striatum were correlated.

Absolute weight gain PX - PY := weight at PY - weight at PX

Relative weight gain PX - PY := (weight at PY - weight at PX)/weight at PX

5.2.2 Mean Diffusivity

The mean diffusivity in all structures was significantly correlated with weight (gain). The correlation was particularly strong at P28, with correlation coefficients up to 0.689 for left external capsule and relative weight gain between P0 and P15. At P15, on the other hand, the correlation was rather weak with all $r < 0.5$. Relative weight gain between P15 and P28 showed a special behavior as it has no significant correlation with almost any structure.

Mean Diffusivity	cc		ic		hf		ec		h		c		t		st	
	right	left	right	left	right	left	right	left	right	left	right	left	right	left		
Weight at P15	.385	.322		.441		.413	.255		.334	.424	.343	.487		.407	.232	
Absolute weight gain P0 - P15	.382	.313		.434		.410	.254		.331	.418	.341	.480		.403	.232	
Relative weight gain P0 - P15	.371	.280		.408		.399	.253		.318	.392	.330	.448		.384	.233	

(a) Correlation with mean diffusivity at P15

Mean Diffusivity	cc		ic		hf		ec		h		c		t		st	
	right	left	right	left	right	left	right	left	right	left	right	left	right	left		
Weight at P15	.635	.684	.544	.628	.610	.632	.680	.542	.668	.665	.689	.669	.641	.662	.659	
Weight at P28	.636	.669	.491	.581	.604	.612	.656	.541	.647	.637	.687	.652	.601	.632	.641	
Absolute weight gain P0 - P15	.629	.682	.542	.629	.611	.630	.679	.542	.665	.662	.685	.667	.640	.662	.658	
Absolute weight gain P15 - P28	.590	.609	.420	.507	.555	.554	.592	.500	.586	.571	.634	.592	.531	.566	.582	
Relative weight gain P0 - P15	.603	.666	.526	.627	.607	.614	.671	.537	.650	.647	.667	.653	.632	.655	.649	
Relative weight gain P15 - P28			-.256													

(b) Correlation with mean diffusivity values at P28

Figure 5.7: Highlight table of correlation coefficients between mean diffusivity and weight (gain) Pearson's r between mean diffusivity and weight (gain), blank space indicates non-significant correlation. Mean diffusivity of all structures at P28 strongly correlated with weight, and absolute and relative weight gain. Contrarily, at P15 the correlations between mean diffusivity and weight (gain) were weaker and less.

Absolute weight gain PX - PY := weight at PY - weight at PX

Relative weight gain PX - PY := (weight at PY - weight at PX)/weight at PX

Figure 5.8 shows scatter plots of mean diffusivity and weight at P15 (orange) and P28 (purple) for right internal capsule and right thalamus. Over time, the mean diffusivity generally decreased in both structures. However, regarding only the values for one time point, it is apparent that mean diffusivity and weight are positively correlated, meaning the higher the weight at one given time point, the higher the mean diffusivity. Comparing the Pearson's r between P15 and P28, as it is done in figure 5.7, it can be observed that the correlation was stronger at the later time point. Furthermore, both white and grey matter show a similar pattern of correlation with weight. Notably, the scatter plots of axial and radial diffusivity in structures correlating with weight are similar to the one displayed.

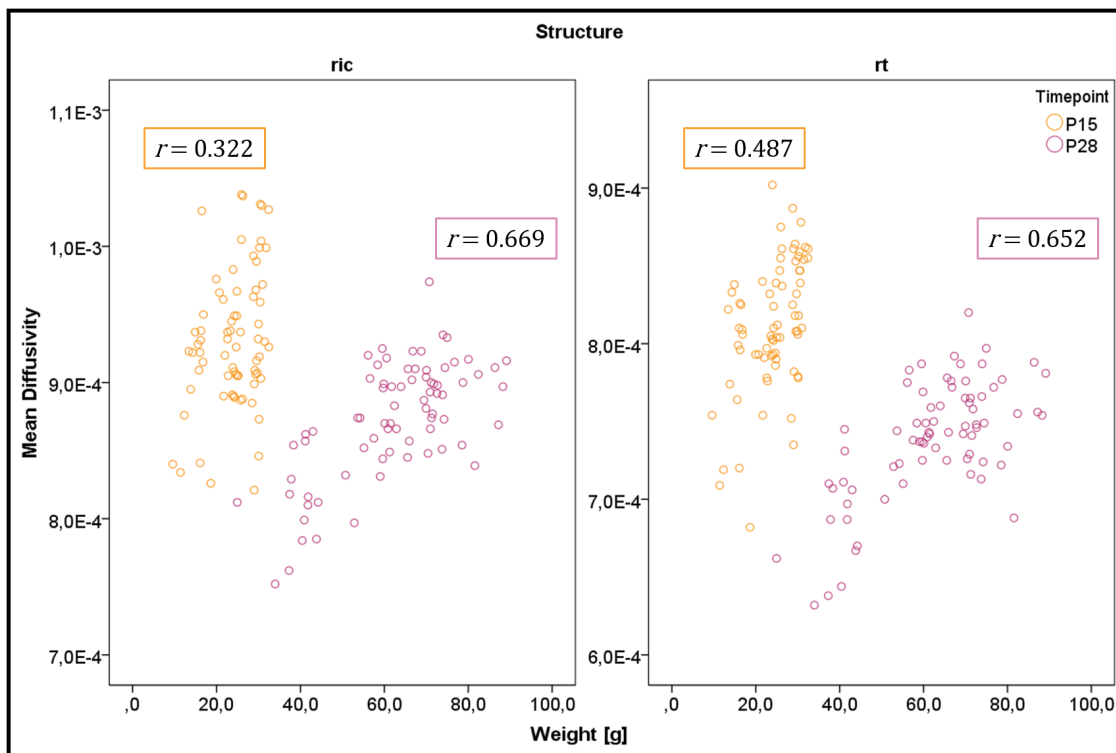


Figure 5.8: Mean diffusivity against weight at P15 and P28 This scatter plot illustrates the influence of weight and age on mean diffusivity. The respective Pearson's r correlation coefficients are displayed in the boxes. Right internal capsule (ric) and right thalamus (rt) are used as example for white and grey matter. The scatter plots for other DTI parameters show a similar pattern.

5.2.3 Axial Diffusivity

The axial diffusivity had the most and strongest correlation with weight (gain) of all DTI parameters. As with mean diffusivity, the correlations were generally stronger at P28, with $r > 0.5$ in at least one side of each structure and $r > 0.7$ in right internal and external capsule. Unexpectedly, even though axial diffusivity showed a disparate development in white and grey matter over time, the correlation with weight was positive in all structures.

As it is the case regarding mean diffusivity, the correlation between axial diffusivity and relative weight gain between P15 and P28 was generally non-significant.

Axial Diffusivity	cc		ic		hf		ec		h		c		t		st		1 0 -1
	right	left	right	left	right	left	right	left	right	left	right	left	right	left			
Weight at P15	.517	.430	.321	.589	.258	.623	.421	.430	.382	.493	.258	.425	.330	.485	.286		
Absolute weight gain P0 - P15	.512	.419	.313	.580	.255	.616	.417	.422	.380	.487	.259	.419	.326	.479	.287		
Relative weight gain P0 - P15	.491	.377	.282	.546	.244	.591	.406	.394	.372	.461	.258	.393	.309	.452	.291		

(a) Correlation with axial diffusivity at P15

Axial Diffusivity	cc		ic		hf		ec		h		c		t		st		1 0 -1
	right	left	right	left	right	left	right	left	right	left	right	left	right	left			
Weight at P15	.642	.706	.446	.613	.613	.677	.616	.428	.628	.594	.614	.556	.546	.626	.621		
Weight at P28	.683	.718	.420	.620	.615	.703	.655	.453	.610	.559	.650	.574	.459	.630	.638		
Absolute weight gain P0 - P15	.633	.701	.444	.609	.610	.669	.611	.425	.627	.594	.609	.553	.551	.624	.617		
Absolute weight gain P15 - P28	.658	.673	.372	.578	.570	.668	.631	.435	.552	.496	.624	.543	.369	.586	.601		
Relative weight gain P0 - P15	.589	.676	.425	.588	.591	.633	.586	.407	.617	.588	.583	.535	.566	.613	.599		
Relative weight gain P15 - P28													-.269				

(b) Correlation with axial diffusivity at P28

Figure 5.9: Highlight table of correlation coefficients between axial diffusivity and weight (gain) Pearson's r between axial diffusivity and weight (gain), blank space indicates non-significant correlation. The axial diffusivity at both timepoints is significantly correlated with weight and weight gain. There are strong correlations particularly at P28, with correlation coefficient r up to 0.718 between axial diffusivity in right internal capsule and weight at P28.

Absolute weight gain PX - PY := weight at PY - weight at PX

Relative weight gain PX - PY := (weight at PY - weight at PX)/weight at PX

5.2.4 Radial Diffusivity

The correlation between radial diffusivity and weight (gain) was different for white and grey matter structures, even though IHH exposure seemed to have the same effect on radial diffusivity in white and grey matter. At P15, only grey matter structures showed a correlation with weight (gain), even though $r \leq 0.5$ in all cases. At P28, some white matter structures also showed correlation. However, the correlation coefficients found in grey matter structures were higher overall.

Radial Diffusivity	cc		ic		hf		ec		h		c		t		st	
	right	left	right	left	right	left	right	left	right	left	right	left	right	left	right	left
Weight at P15									-.273	.286	.350	.380	.500			.315
Absolute weight gain P0 - P15									-.272	.282	.344	.376	.492			.312
Relative weight gain P0 - P15									-.270	.266	.319	.359	.459			.301

(a) Correlation with radial diffusivity at P15

Radial Diffusivity	cc		ic		hf		ec		h		c		t		st	
	right	left	right	left	right	left	right	left	right	left	right	left	right	left	right	left
Weight at P15			.323	.488			.601	.335	.668	.677	.685	.674	.582	.598	.620	
Weight at P28			.272	.401			.511	.302	.647	.654	.661	.631	.581	.543	.572	
Absolute weight gain P0 - P15			.323	.493			.606	.339	.664	.673	.683	.673	.578	.599	.621	
Absolute weight gain P15 - P28				.315			.415	.259	.585	.590	.596	.557	.538	.467	.498	
Relative weight gain P0 - P15			.235	.320	.510	.249	.619	.353	.646	.652	.670	.664	.555	.596	.620	
Relative weight gain P15 - P28					-.262		-.310									

(b) Correlation with radial diffusivity at P28

Figure 5.10: Highlight table of correlation coefficients between radial diffusivity and weight (gain) Pearson's r between radial diffusivity and weight (gain), blank space indicates non-significant correlation. At P15, grey matter but not white matter structures showed a correlation between radial diffusivity and weight (gain). The correlations at P28 were generally stronger and additionally present in some white matter structures. Interestingly, the correlation between right hippocampus and weight was negative at P15 and positive at P28, albeit weak in all cases. Absolute weight gain PX - PY := weight at PY - weight at PX
Relative weight gain PX - PY := (weight at PY - weight at PX)/weight at PX

5.3 Weight and Weight Gain

The birth weight was approximately the same in all categories of litter size. However, both at P15 and P28, pups in larger compared to smaller litters had significantly lower weight, see figure 5.11. Further, the weight differed between male and female rats. At P28, male rats had a higher weight than female rats. This trend was already apparent at P15, albeit not significant ($p = 0.102$).

The relative weight gain differed strongly between birth and P15, but not between P15 and P28 between litters of 8, 12 and 16 (see figure 5.12). The absolute weight gain, however, followed an approximately linear pattern and differed significantly across groups of different litter size at all times.

Comparing groups according to oxygen condition, the IHH group had a significantly higher weight at P15 than the room air group both, in litters of 8 and 16. At P28, the weight of the 16 pups litter in IHH was still higher than in the room air group, whereas in the 8 pups litter the room air group had higher weight at P28. In combination, this led to a non-significant difference in absolute weight gain from P15 to P28 (see figure 5.14).

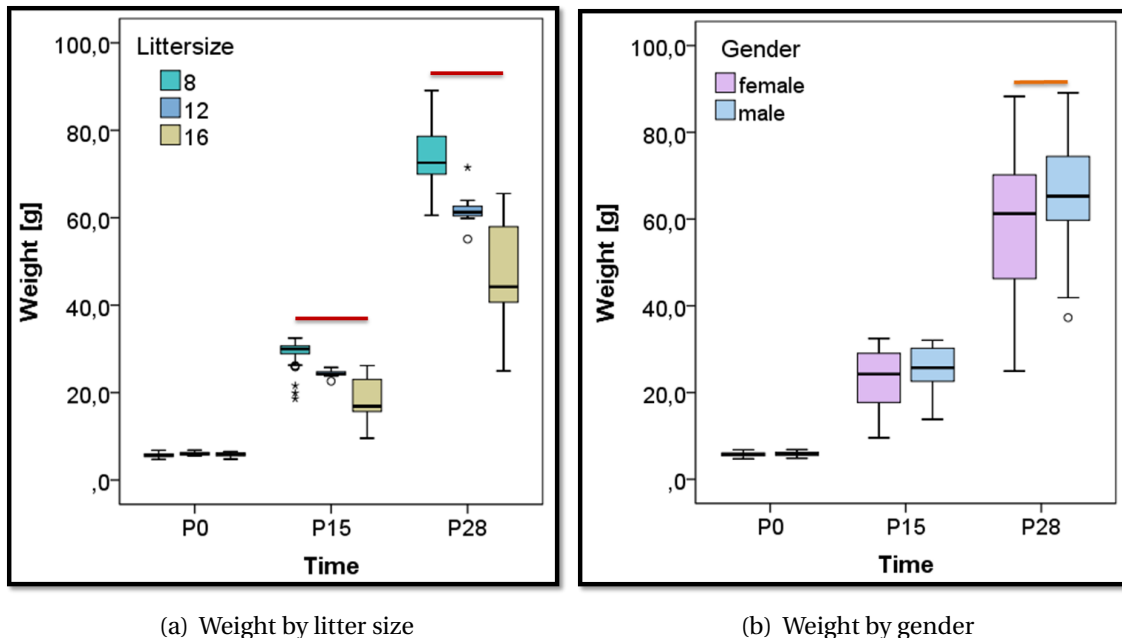
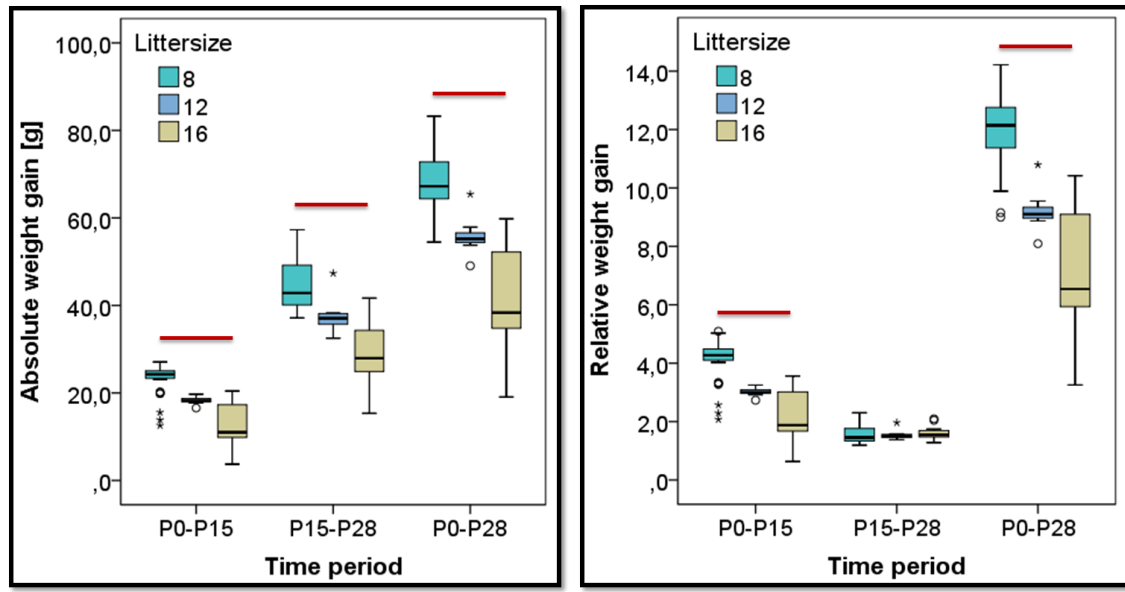


Figure 5.11: Weight at P0, P15 and P28 by litter size and gender. While the birth weight (P0) was the same, the weight at P15 and P28, respectively, was significantly different across categories of litter size and gender. Red and orange bars indicate $p < 0.01$ and $p < 0.05$, respectively.



(a) Absolute weight gain

(b) Relative weight gain

Figure 5.12: Absolute and relative weight gain by litter size. Across categories of litter sizes the absolute weight gain differed significantly at all time periods. Regarding the relative weight gain, there was no difference between P15 and P28. Red bars indicate $p < 0.01$.

Absolute weight gain PX - PY := weight at PY - weight at PX

Relative weight gain PX - PY := (weight at PY - weight at PX)/weight at PX

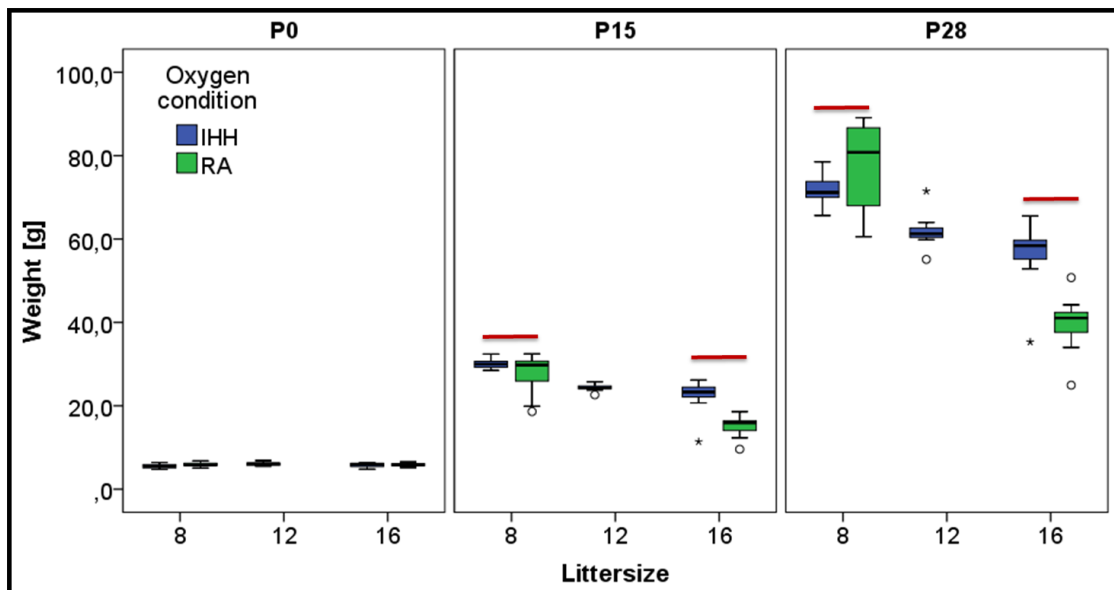
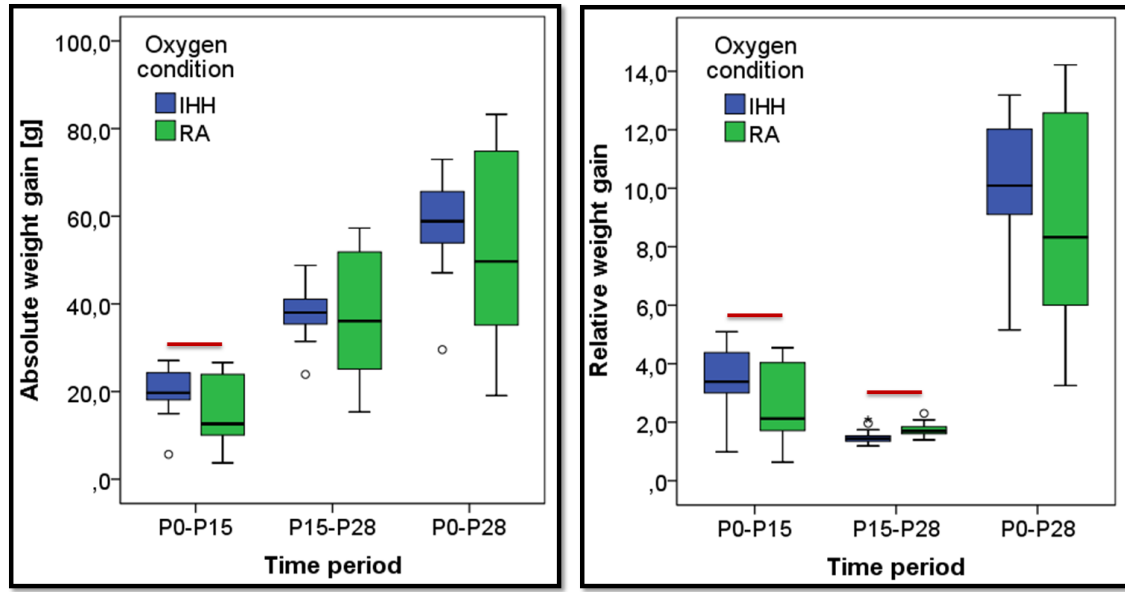


Figure 5.13: Weight at P0 (birth), P15 and P28 by litter size and oxygen condition. Independent of litter size, the weight between IHH and room air exposed pups differed significantly at both, P15 and P28, but not at P0. Red bars indicate $p < 0.01$.



(a) Absolute weight gain

(b) Relative weight gain

Figure 5.14: Absolute and relative weight gain by oxygen condition. The absolute weight gain between birth and P15 was higher in the IHH compared to the room air group. In IHH exposed pups, the relative weight gain was higher between birth and P15, but lower between P15 and P28 in comparison to the room air group. Red and orange bars indicate $p < 0.01$ and $p < 0.05$, respectively.

Absolute weight gain $PX - PY := \text{weight at } PY - \text{weight at } PX$

Relative weight gain $PX - PY := (\text{weight at } PY - \text{weight at } PX) / \text{weight at } PX$

5.4 The Combined Effect of Oxygen and Weight

One of the aims of this thesis was to investigate if low weight (gain) potentiates the effect of IHH exposure on white and grey matter maturation. One way to examine this is to compare the correlation between weight (gain) and DTI parameters across groups of oxygen condition. In this case, however, the comparison was inconclusive. This is due to the fact that the weight range of both groups differed strongly. While the weight in the room air group ranged between 24.94 g and 89.11 g at P28, IHH exposed animals have a weight range of only 52.84 g to 78.52 g. However, only six room air animals were included in the weight range of IHH exposed animals (see figure 5.15).

For analysis, a linear regression model with mean diffusivity at P28 as dependent variable, and oxygen condition and weight at P28 as independent variables, has been used. The right internal capsule and right thalamus have been analyzed exemplarily for white and grey matter,

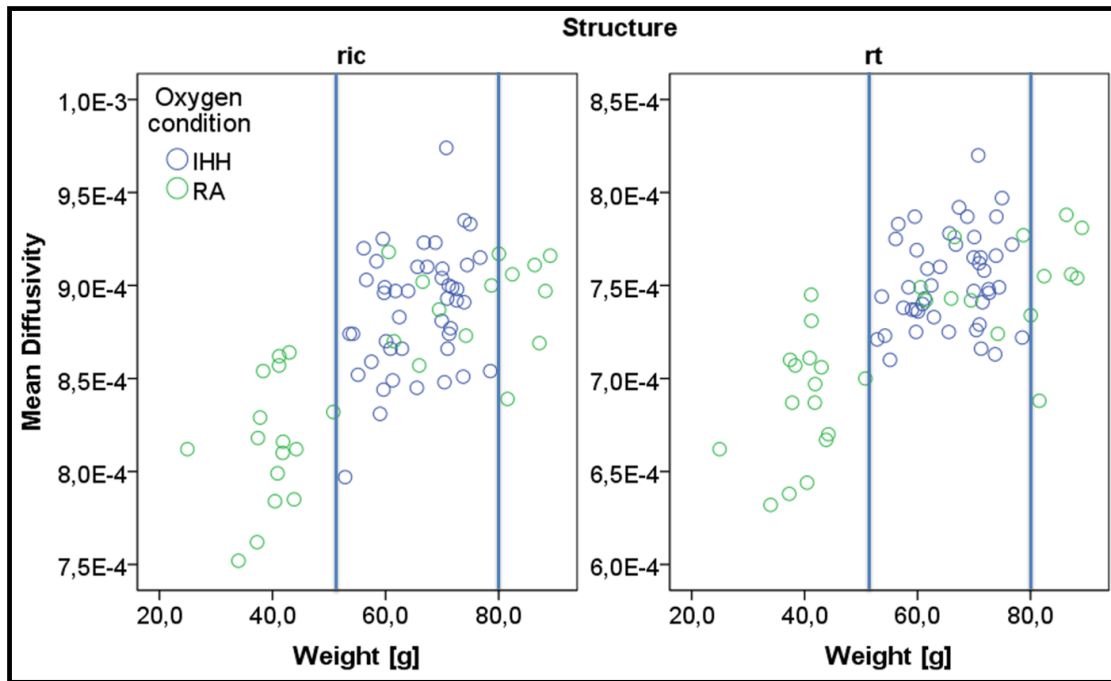


Figure 5.15: Scatterplot of mean diffusivity against weight at P28 Right internal capsule (ric) and right thalamus (rt) are displayed exemplarily for white and grey matter. Only six pups of the room air group lie within the weight range of IHH animals (blue borders).

respectively. For pups within the weight range of the IHH group, neither in IHH nor in room air group a linear correlation between weight and mean diffusivity could be found. However, if all cases were included, there was a significant linear correlation with $r^2 = 0.424$ and $r^2 = 0.417$, for right internal capsule and right thalamus, respectively.

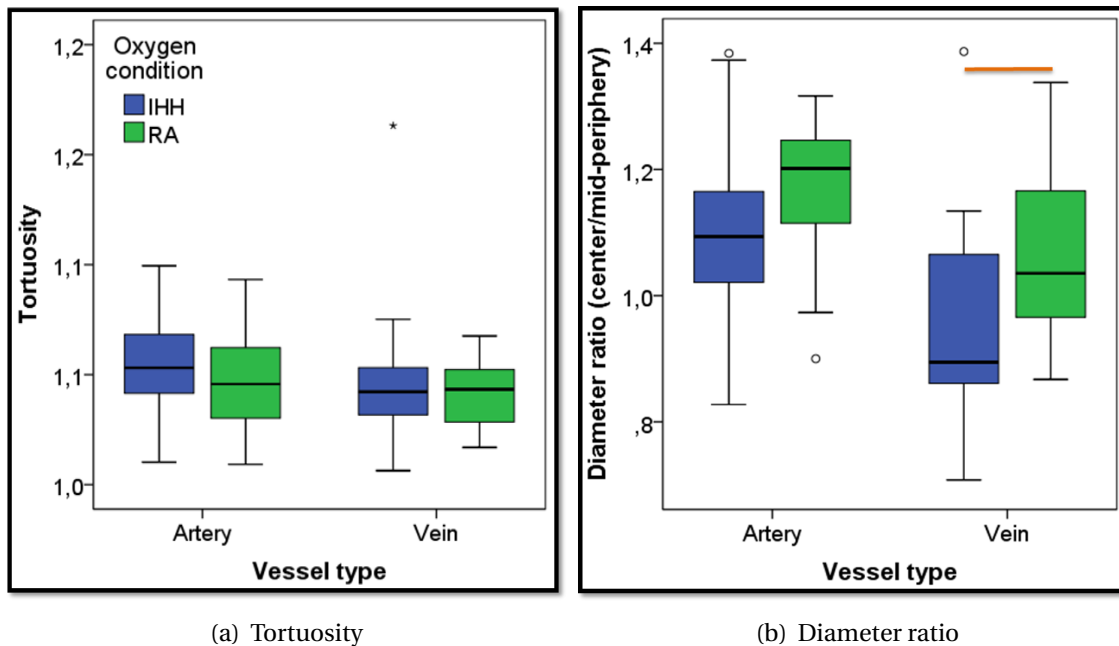
To summarize, while there most definitely is an influence of oxygen on weight, it can not be determined if the correlation between weight and DTI parameters differs between IHH and room air exposed pups.

5.5 Retinal Vasculature

Exposure to IHH for the first 14 postnatal days did not result in more tortuous arteries and veins at P28 (see figure 5.16). Furthermore, the absolute vessel diameter was not significantly different between IHH and room air group, independent of location (center/mid-periphery) and vessel type. However, there was a trend towards smaller vessel diameter in the center and larger vessel diameter in the mid-periphery in the IHH group (not shown). Both are included in the diameter

ratio, defined as the quotient of central and mid-peripheral diameter. Therefore, there was a significantly lower vein diameter ratio in the IHH compared to the room air group. A similar but not significant ($p = 0.068$) pattern is seen in arteries.

Interestingly, neither tortuosity nor diameter rate had significant correlation with weight, relative or absolute weight gain. Further, there was no correlation between measures of abnormal retinal vasculature and fractional anisotropy, or mean, axial and radial diffusivity in any of the regions of interest.



(a) Tortuosity

(b) Diameter ratio

Figure 5.16: Tortuosity and diameter ratio in arteries and veins by oxygen condition Neither in arteries nor in veins was a difference in tortuosity comparing IHH and RA group. The diameter ratio, that is the quotient of diameter in center and in mid-periphery, was significantly ($p < 0.05$, orange bar) lower in veins. The same trend was seen in arteries ($p = 0.068$).

Chapter 6

Discussion

6.1 Main Findings

A major aim of this thesis was to investigate the effect of exposure to intermittent hyperoxia-hypoxia (IHH) on the white and grey matter maturation measured by DTI in the neonatal rat. In both, the IHH and the room air group, the fractional anisotropy increased while mean and radial diffusivity decreased from P15 to P28 in all analyzed structures. Axial diffusivity showed a dichotome behavior with an increase in white, and a decrease in grey matter.

Exposure to IHH led to less change of DTI parameters in grey matter. Concretely, the fractional anisotropy increased less over time in pups exposed to IHH, while mean, axial and radial diffusivity decreased less. In white matter, however, IHH exposure led to a stronger increase of axial diffusivity while the decrease in mean and radial diffusivity was less apparent. The fractional anisotropy of white matter structures was differentially affected by IHH exposure. Table 6.1 summarizes these changes.

Table 6.1: Summary of longitudinal development of DTI parameters by oxygen condition between P15 and P28. Wider compared to less wide arrows indicate a higher change.

Parameter	White matter		Grey matter	
	IHH	RA	IHH	RA
Fractional anisotropy	↑↑	↑↑	↑	↑
Mean diffusivity	↓	↓	↓	↓
Axial diffusivity	↑	↑	↓	↓
Radial diffusivity	↓	↓	↓	↓

Weight and weight gain have significant, mainly positive, correlations with all DTI parameters. While fractional anisotropy was particularly correlated with weight at P15, mean, axial and radial diffusivity had stronger correlations with weight at P28.

There was no difference in tortuosity between groups of different oxygen condition, whereas the vein diameter ratio was higher in IHH exposed animals. Further, measures of abnormal vascularization did not correlate with weight (gain) or DTI parameters.

6.2 Methodological Considerations

6.2.1 Strength and Limitations

One of the major strengths of this study is its scope. It is not only comprehensive in number of testing subjects but also in structures that are analyzed, each at two different time points. Thus the longitudinal development could be observed and the long-term effect of IHH exposure examined. This gives valuable insight in comparison to measurement at only one single time point. Furthermore, the fractional anisotropy, mean, axial and radial diffusivity were calculated from the acquired DTI data. The combined analysis of these four parameters gives further information and thus allows additional insight on the underlying developmental processes and/or the type of injury.

The only interventions the rat pups were subjected to are exposure to the IHH profile and alteration of litter size. Conversely, other models for diseases of prematurity interfere in the gene expression of growth factors, such as vascular endothelial growth factor (VEGF) (for example Wang et al. (2013)). The IHH model is favorable in that regard that it merely adjusts the environment to mimic the condition of preterm birth. Hence, the interventions in these experiments are less specific but more globally affect the animal as a whole.

DTI is used in the clinic to assess (abnormal) brain development, especially of white matter structures, in preterm infants (Qiu et al., 2015). Further, the tortuosity and dilation of arteries and veins is measured to determine severity of ROP, or more specifically of plus disease (Heneghan et al., 2002). In our study, these exact same methods were used to analyze the white and grey matter maturation and the retinal vascularization, respectively. Therefore, the results

obtained from this study are highly translatable to the clinical setting.

Furthermore, the combination of non-invasive methods and histological studies provides a comprehensive illustration of the underlying processes. A drawback of this study, however, is the tissue sample at P28 only. It would have been interesting to see if there are alterations in retinal vasculature at P15 for example, that are reversible and thus not seen at P28. In addition, it would be intriguing to know when the abnormalities in vessel diameter become apparent.

DTI is a valuable tool to investigate the maturation of white matter tracts, and the directionality of water diffusion within the brain. However, in each voxel only one dominant fiber orientation can be determined (Johansen-Berg and Behrens, 2013). This does not necessarily reflect reality, as multiple fibers can be contained in one voxel, especially at regions of fiber crossings or grey matter structures like the thalamus. To counteract this effect, the resolution can be enhanced and thus the voxel size decreased. However, this prolongs the image acquisition time which should be kept short not to harm the animal. In this study we tried to find a compromise with a resolution of $(160 \times 160 \times 800) \mu\text{m}^3$.

6.2.2 Utility of Neonatal Rats to Model Diseases of Prematurity

Animal models are useful to investigate underlying mechanisms of diseases by targeted intervention. There are several advantages to use the rat as laboratory animal over other animals, especially in research on diseases of prematurity.

Rat pups are naturally born premature, which is reflected in many aspects including an avascular retina at birth. The maturational status of a human at birth can be compared to a rat at around P10 (Rice and Barone, 2000). Further, by manipulating the litter size and thus limiting the amount of nutrition per pup, growth restriction was successfully induced in this study. Therefore, a subgroup of our testing subjects experienced the conditions of sick prematurely born infants with low birth weight.

Further, the pathological pattern of diseases of prematurity could successfully be reproduced as seen in patients. In preterm infants suffering from ROP, dilated veins are the first sign of plus disease (Wallace et al., 2000). This was recreated by exposure of rat pups to IHH. Even though there are many ways to characterize the severity of ROP, the methods are well-defined and highly correlated to the methods used in the clinical setting (Heneghan et al., 2002). On

the other hand, rats are not as closely related to humans as are higher order mammals. This is especially reflected in the development of the central nervous system. Since rats have a higher grey to white matter ratio, they are less susceptible to fluctuations in oxygen (Rice and Barone, 2000).

Rats are relatively inexpensive to purchase and maintain compared to higher order mammals. One of the reasons is that they have a short pregnancy and many pups per litter, even compared to other rodents. Furthermore, since rats have been used as laboratory animal for decades, many methods have been developed and extensively tested in the rat. This allows valuable comparison in between studies.

However, there are strain- and even vendor-related differences in rats (Barnett et al., 2010; Floyd et al., 2005). Sprague Dawley rats, that were used in our study, have an intermediate susceptibility to vessel abnormalities after hyperoxic and/or hypoxic exposure compared to other rat strains (van Wijngaarden et al., 2005). Accordingly, it can be assumed that there are also strain-related differences regarding white and grey matter injury. Therefore, other rat strains may show more or less effects of IHH exposure on white and grey matter maturation in comparison to our study.

6.2.3 Ethical Considerations

The purpose of this animal experiment was to investigate the influence of exposure to hyperoxia with intermittent episodes of hypoxia on brain microstructure and retinal vasculature. A similar previous study by Morken et al. (2013) found impaired white matter maturation and abnormal retinal neovascularization after this kind of oxygen exposure but with small sample size. Hence, there was the need for a comprehensive study to confirm these results and to reveal additional information.

The principle of the “three R’s” (Russel and Burch, 1959) was applied to ensure welfare of the rats. The number of animals was *reduced* as far as possible without compromising the research. Several samples in addition to those needed for our study were taken from the animals, including the pancreas, heart, lungs, blood serum and urine sample. These will be investigated in different projects. The methods were *refined* by previous studies and self-conducted pilot studies. Further, the animals were handled with care, and factors such as body temperature and breath-

ing monitored thoroughly while in the MR scanner. In this case the experiments on laboratory rats could not be *replaced* by *in vitro* research as it was important to investigate the influence of IHH in combination with interaction occurring between cells and during development in a living being. *In vitro* studies only reflect certain aspects of a disease and can not encompass the complexity of impaired brain maturation due to IHH exposure.

6.2.4 Confounding Factors of Development

The adjustment of oxygen levels from 50 % to 12 % oxygen and vice versa in the oxycycler was associated with noise. Loud noise has been shown to induce stress (Manikandan and Devi, 2005). Even though the room air control rats were held in the same room with the IHH group the sound they experienced was less loud. Furthermore, during the MRI scan, the whole litter was kept in a designated room in the MR Center. Still, especially the fast gradient changes during DTI acquisition were audible and might again have led to noise-induced stress. Additionally, the transport from the animal facility to the MR center and the stay in an unfamiliar environment most likely induced stress. Notably, both groups were exposed to these stressors. Even though we cannot rule out interactions, we assume a significant effect of these factors is unlikely.

6.2.5 Hemispheric Differences in Brain Structures

At both, P15 and P28, hemispheric differences in DTI parameters were found in a variety of structures. These differences are especially large regarding radial diffusivity. While Bockhorst et al. (2008) did not find lateral differences, they used a different rat strain, indicating that this lateralization may be particular to Sprague Dawley rats.

Side differences can also be found in various brain structures in humans. This is especially apparent in the arcuate fasciculus, a white matter structure associated with language processing (Lebel and Beaulieu, 2009). Others have found hemispheric differences in fractional anisotropy in structures involved in auditory spatial attention (Barrick et al., 2007). Since the lateralization in our study is consistent in both, IHH and room air group, and occurs at both time points, we assume it is a true physiological feature. Consequently, we investigated the difference in DTI parameter in between groups for each side separately.

6.3 Weight Influenced by Litter Size and IHH Exposure

The weight at P15 and P28 differed significantly across categories of litter size, with the lowest mean weight in the litters of 16. Hence, growth retardation was successfully induced by manipulation of number of siblings shortly after birth. Accordingly, the absolute weight gain from birth to P15 and from P15 to P28 differed significantly between groups of different litter size. This was supposedly mainly due to the higher competition for food. Social aspects dependent on the number of individuals per cage might also have had an influence (Mendi, 1988). Interestingly, while the relative weight gain from birth until P15 differed across categories of litter size, it was approximately the same from P15 to P28. Thus no catch up growth had occurred. Notably, there was a high variation of weight within the litters, especially in the 16 pups litters. One possible reason may be that some pups could assert themselves over others and thus got a larger share of food (milk from the mother). This may have been reinforced by the fact that pups with more food got stronger and subsequently received more food in the future (Mendi, 1988).

Furthermore, weight was influenced by exposure to IHH. This is especially visualized in figure 5.13. At both time points there were significant differences between IHH and room air group. The 16 pups litter exposed to IHH had a higher mean weight compared to the room air litter, both at P15 and P28. A confounding factor might have been that one pup of the IHH litter died shortly after birth, thus effectively making it a litter of 15 instead of 16. However, this effect was most probably marginal. Further, since only two litters are compared to each other, differences in weight may just reflect litter differences and not necessarily an effect of IHH exposure. However, an increased mean weight of litters exposed to IHH could also be seen in the 8 pups litter at P15. In contrast, at P28, pups in litters of 8 exposed to IHH had lower weight compared to pups kept in room air. This could be explained by the withdrawal of chronic hyperoxic exposure, leading to the experience of a relative hypoxia. In humans, it has been shown that exposure to hypoxic environment (such as in high altitude), causes weight loss (Quintero et al., 2010; Westerterp et al., 1994; Westerterp-Plantenga et al., 1999). This is associated with loss of appetite (Shukla et al., 2005) and metabolic changes such as insulin resistance (Netzer and Breitenbach, 2010).

6.4 Maturation of White and Grey Matter

6.4.1 What Are the Physiological Correlates of these White Matter Findings?

During development, many maturational processes occur simultaneously and may affect the same parameter, either in the same or in contradictory ways. Further, different brain structures mature at different times (Huang et al., 2006). Therefore, it is difficult to ascribe a definite physiological correlate to the change in a certain DTI parameter.

Within the first postnatal weeks, the white matter of neonatal rats develops and matures extensively. In this study, we found that already at P15 the fractional anisotropy was substantially higher in white compared to grey matter. At the same time, the axial diffusivity was higher and the radial diffusivity lower compared to grey matter structures, together resulting in approximately similar mean diffusivity in all structures. A similar DTI parameters of white matter structures were observed by others (Bockhorst et al., 2008). This pattern of DTI parameters presumably reflects the axonal organization into parallel tracts, a process exclusively occurring in white matter (Dubois et al., 2008).

Between P15 and P28, the fractional anisotropy and axial diffusivity of white matter structures increased, while the mean and radial diffusivity decreased. This may have been due to ongoing generation and growth of glial cells (Semple et al., 2013). Especially the asymmetrical expansion of oligodendrocyte processes has been shown to contribute to anisotropy (Nossin-Manor et al., 2013; Zanin et al., 2011). Further, myelination by mature oligodendrocytes starts around P15 and peaks around P20 (Cuzner et al., 1965). Hence this maturational process is likely to be the main cause for the change in DTI parameters between P15 and P28 that was detected in our study. Further, this supports the hypothesis by Wimberger et al. (1995) that anisotropic diffusion before P15 precedes fiber myelination.

Note that in white matter in contrast to grey matter, the water that leads to the DTI signal is mainly located intracellularly, while the extracellular space is relatively small due to high axonal density. Collectively, the glial cell growth and myelination of axons further contributes to reduced extracellular space (Johansen-Berg and Behrens, 2013).

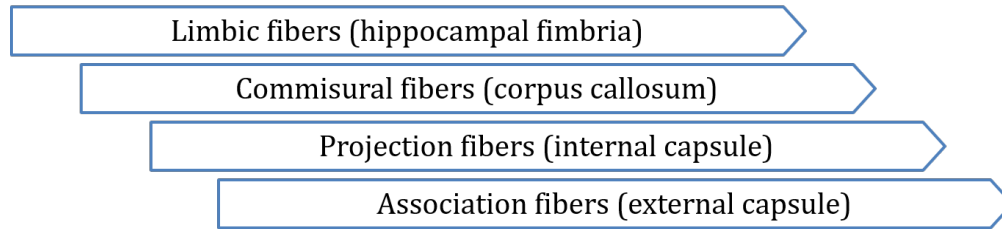


Figure 6.1: Time line of white matter development and maturation. Limbic fibers develop and mature first, thereafter commissural and projection fibers and lastly association fibers. Brackets display examples for these fibers that were analyzed in this study.

6.4.2 Why Is the White Matter Differentially Affected by IHH Exposure?

Interestingly, white matter structures were differentially affected by IHH exposure. At P15, the corpus callosum and right internal capsule showed higher fractional anisotropy in the IHH compared to the room air group. However, at P28 no significant difference could be detected between the IHH and room air exposed pups in these structures. Thus, the fractional anisotropy of corpus callosum and right internal capsule increased less from P15 to P28 after IHH exposure. Furthermore, at P28, in IHH exposed pups, the fractional anisotropy is higher in the right hippocampal fimbria, but lower in the right external capsule compared to pups kept in room air.

The differential influence of IHH exposure could be explained by the different maturational time line of white matter structures (see figure 6.1). The hippocampal fimbria is a part of the limbic system. Limbic fibers are among the first white matter structures to develop and mature during ontogenesis. Thereafter, commissural fibers such as the corpus callosum, and projection fibers such as the internal capsule evolve. Conversely, association fibers such as the external capsule develop and mature relatively late (Huang et al., 2006; Judaš et al., 2005).

At P28, the differences in fractional anisotropy between pups exposed to IHH and pups kept in room air were most likely due to variations in myelination. Myelination is the process of ensheathment of axons by myelin-containing oligodendrocyte extensions. Oligodendrocytes develop from oligodendrocyte precursors via pre-oligodendrocytes and immature oligodendrocytes into mature myelinating oligodendrocytes (Back et al., 2007). Immature oligodendrocytes have a much higher susceptibility to oxygen exposure than mature oligodendrocytes (Gerstner et al., 2006, 2008). Accordingly, Vottier et al. (2011) found decreased myelin content (–31 %)

in the developing white matter of the rat after early postnatal exposure to hyperoxia. Since the external capsule is less mature than the other white matter structures at the same time (Huang et al., 2006), there is most likely an increased portion of immature oligodendrocytes in this region thus making it more vulnerable to injury. This is in line with lower values of fractional anisotropy in the right external capsule in the IHH group. The less increase in fractional anisotropy from P15 to P28 in corpus callosum and right internal capsule may have had the same cause.

The hippocampal fimbria on the other hand is more matured than external capsule, corpus callosum and internal capsule at the same time (Huang et al., 2006). Thus there may have been less or no immature, but instead more mature oligodendrocytes in this region during our experimental period. Accordingly, the increase in fractional anisotropy between P15 and P28 was not impaired, but even higher in the IHH compared to the room air group. Further, the IHH exposed pups had a higher axial diffusivity in all white matter structures. This confirms findings of increased axial diffusivity in white matter structures after IHH exposure at P14 (Morken et al., 2013). This is in contrast to our expectations of reduced or retarded development due to IHH exposure. Consequently, it needs to be discussed if there is a potential effect towards higher maturation instead, especially since others have found similar results. Studies in preterm infants found increased fractional anisotropy and axial diffusivity in several white matter tracts at 12 month corrected age (Padilla et al., 2014) and in adulthood (Eikenes et al., 2011).

It is, however, unknown if higher levels of fractional anisotropy represent more matured white matter, or if it has other structural correlates which may be pathologically. Increased fractional anisotropy has been shown to be correlated with neurodevelopmental disorders such as autism (Cheng et al., 2010) and Williams syndrom (Hoeft et al., 2007). Notably, however, it has to be considered that the difference in fractional anisotropy of the right hippocampal fimbria was, albeit significant, only 2.2 %. This is about the same magnitude as the difference that could be detected between the two sides of the hippocampal fimbria.

6.4.3 What Are the Physiological Correlates of these Grey Matter Findings?

Both at P15 and P28 the axial diffusivity of grey matter compared to white matter was lower, while the radial diffusivity was higher. This is due to the inherent microstructure of the tissue

(Westbrook and Roth, 2011). Per definition, grey matter predominantly contains cell bodies and synapses, where the water diffusivity is less directional than in white matter tracts (Johansen-Berg and Behrens, 2013).

The DTI parameters at P15 mainly mirror neurogenesis, which is finished at approximately that time (Babikian et al., 2010; Rice and Barone, 2000). Further, glial cells are generated, with a peak astrogliosis between P11 and P16 in the hippocampus (Catalani et al., 2002). Coinciding, synaptogenesis increases abruptly at about P10 in rats (Crain et al., 1973). While these three processes may restrict water diffusion, this restriction is not anisotropic (fractional anisotropy < 0.2 in all grey matter structures).

Between P15 and P28, an increase in fractional anisotropy with a decrease in mean, axial and radial diffusivity was found. This is consistent with a longitudinal rat DTI study by Bockhorst et al. (2008). Our findings most likely reflect a decrease in extracellular space, which was found to be reduced by more than half within the first three postnatal weeks in rats (Lehmenkühler et al., 1993). This is due growth of neurons and astrocytes, as well as ongoing gliogenesis until P30 (Catalani et al., 2002). Furthermore, the intracellular diffusivity decreases due to proliferation of membranes and thus compartmentalization, both in neurons and astrocytes. In addition, synaptogenesis reaches adult levels between P25 and P30, dependent on brain region (Rice and Barone, 2000).

To summarize, the development of DTI parameters between P15 and P28 was presumably due to neuronal and glial maturation, including changes in morphology, connectivity and functional properties (Zhou et al., 2006; Zhang, 2006). Notably, only recently DTI is used as method to investigate grey matter structures. However, earlier studies analyzed T_2 -relaxation times to examine its tissue composition and found a reduction over time (Thornton et al., 1999; Morken et al., 2013). They too conclude that the extracellular water content decreases with maturation.

6.4.4 Why Is Grey Matter Maturation Impaired by IHH Exposure?

At P15, no difference between IHH and room air group could be detected in any of the grey matter structures. However, at P28, the fractional anisotropy of the right cortex and left thalamus was lower, while mean, axial and radial diffusivity of all structures were higher in IHH exposed pups. One possible reason therefore might be that the IHH exposure has had rather long-term

instead of immediate effects on grey matter maturation. On the other hand, the hyperoxia withdrawal may have been the noxious stimulus causing the maturational deficits in this case.

IHH exposure in the grey matter may have primarily affected astrocytes, as they have previously been shown to be vulnerable to hypoxic and hyperoxic exposure (Danilov and Fiskum, 2008; Raymond et al., 2011). Astrocytes are in close contact with neuronal cell bodies. They express glutamate transporters and thus play an important role in maintaining homeostasis by removing glutamate from the extracellular space (Kandel et al., 2013). The fact that differences in DTI parameters could be found at P28 but not at P15 led to the assumption that the relative hypoxia after the IHH paradigm caused the maturational retardation. Raymond et al. (2011) found impaired expression and function of glutamate transporters in mice astrocytes after chronic exposure to hypoxia *in vivo* and *in vitro*. Further, chronic hyperoxic exposure prior to oxygen deprivation was found to cause apoptosis of astrocytes *in vitro* (Danilov and Fiskum, 2008). It can be speculated that the exposure to hyperoxia with intermittent episodes of hypoxia has an even more severe impact. This effect might be increased in the preterm brain since the expression of these glutamate transporters is maturation-dependent (Danbolt, 2001).

Interestingly, while we could not observe differences at P15, Morken et al. (2013) found increased T_2 relaxation times at P14 in the thalamus after IHH exposure. Their findings indicate higher brain water content, which can also be reflected by increased mean, axial and radial diffusivity, as seen in our study. One explanation for higher water content is neuronal and astrocytic cell death. Topçu et al. (2014) found apoptosis of rat hippocampal cells after hyperoxic exposure *in vivo*. Consistently, lower hippocampal volumes and poor neurobehavioural outcome was found in hyperoxia-exposed neonatal mice (Ramani et al., 2013). In contrast, we only found differences between IHH and room air group at P28, and not at P15.

Our results are consistent with findings in sick preterm born infants, as it has been shown that injury to grey matter structures is associated with PVL (Pierson et al., 2007; Volpe, 2009). A study in preterm infants with very low birth weight found the thalamic microstructure to be especially vulnerable to neonatal risk factors (Rose et al., 2014). In our study, too, the thalamus was particularly affected as it not only showed less decrease of mean, axial and radial diffusivity but also less increase of fractional anisotropy from P15 to P28.

6.4.5 How does Weight Influence White and Grey Matter Microstructure?

Generally, in all structures a positive correlation was found between all DTI parameters and weight, absolute, and relative weight gain (see figures 5.6-5.10). Interestingly, even though mean and radial diffusivity decrease over time in all structures, and axial diffusivity decreases in grey matter, the correlation with weight was positive at both time points (see figure 5.8). This means that at the same age, the mean, axial and radial diffusivity are higher in individuals with higher weight. These findings are supported by DTI studies associating high body mass index (BMI) to low structural integrity of several white matter structures in healthy adults (Bolzenius et al., 2013; Verstynen et al., 2012). The higher values for mean, axial and radial diffusivity may predominantly reflect the higher extracellular water content in the brains of pups with higher weight gain.

The reason for this theory is that the water content does not influence the fractional anisotropy strongly, which was less and only weakly correlated with weight at P28. Conversely, mean and axial diffusivity, and radial diffusivity in grey matter structures, highly reflect the overall brain water content (Neil et al., 1998). Due to the dense myelin sheaths in white matter, the extracellular water content is low in these structures (Johansen-Berg and Behrens, 2013). This might be one reason why radial diffusivity was not (strongly) correlated with weight in white matter structures. However, with higher extracellular water content the overall diffusivity is higher which would explain the positive correlation between weight and diffusivity parameters. Supporting this theory are findings by Jennifer Olsen, who analyzed the T₂ weighted images also acquired in our experiments. She found a positive correlation between body weight and volume in several grey matter structures, including hippocampus, thalamus, cortex and striatum.

Nevertheless, the correlation between fractional anisotropy and weight (gain) might in deed reflect the microstructural brain development. The fact that fractional anisotropy showed strong correlations with weight (gain) at P15, but not at P28, indicates a (stronger) influence of weight gain from birth to P15 regarding white and grey matter maturation. This is in line with findings in preterm born children. Individuals with appropriately high postnatal weight gain show better neurodevelopmental outcome compared to those suffering from poor postnatal weight gain (Latal-Hajnal et al., 2003).

Notably, there was a high correlation between weight (gain) at P15 and weight (gain) at P28.

This explains why structure-wise the correlation coefficients for all weight parameters are relatively similar. The correlation between weight measures at P15 with DTI parameters at P28 indicates a predictive value of early weight (gain). IHH exposure affects the correlation between weight (gain) and DTI measures by influencing the weight itself. In our study, no differences between the IHH and room air group could be found when comparing pups within the same (narrow) weight range. However, from these experiments we cannot rule out that there is a potentiating effect of poor postnatal weight gain and IHH exposure.

Summarizing, we hypothesize that early postnatal weight gain until P15 strongly correlates with brain microstructural development, but later weight gain (from P15 to P28) predominantly correlates with brain water content. This leads to the conclusion that the mean, axial and radial diffusivity have to be used cautiously as measures for brain maturation. Higher diffusivity does not necessarily reflect an impaired maturation in pups with higher weight. Future measurements of T_2 relaxation times would give further information of the validity of this theory.

6.5 Retinal Vascularization

Plus disease is associated with ROP of stage 3 or higher. In this study, clinical measures for the severity for plus disease are applied. Neither exposure to IHH nor weight (gain) had an effect on vessel tortuosity. However, the vessel diameter was influenced by oxygen condition, as seen in a significantly lower vessel diameter ratio in IHH exposed compared to room air pups. Similar to humans suffering from ROP, veins were more affected than arteries (Wallace et al., 2000). Notably, the differences in vessel diameter were so subtle, that only the quotient of central and mid-peripheral diameter showed significant differences and not the absolute diameter itself. Nevertheless, it has been shown that dilated and tortuous vessels insufficient to be determined as plus disease have a predictive value for the later pathology of ROP (Wallace et al., 2000). In that regard, the mild vascular abnormalities detected in this study may have prognostic significance for the later course of retinal vascular and even neurodevelopmental outcome.

The vessel abnormalities seen in this study are more subtle than in other studies. For example, Holmes and Duffner (1995) found reduced retinal vascularization in large compared to small litters at P6. Further, they showed severe neovascularization at P13 after exposure to hy-

peroxia/hypoxia for seven days and six days of room air recovery (Holmes and Duffner, 1996). Dhaliwal et al. (2011) applied an oxygen profile that was recorded from a preterm baby to neonatal rats for the first 14 days of life and subsequently dissected their retinas. In these three studies, larger avascular areas were found in IHH exposed animals compared to controls.

That the vessel abnormalities were more subtle in this study is due to two facts. First, the oxygen paradigm was less severe than the ones used by other groups (Holmes and Duffner, 1995, 1996). Second, in this study the retinas were dissected at P28, that is relatively late. Consequently, both the inner and outer plexus were fully vascularized, and no avascular areas could be seen. Hence, possible pathological vascular alterations may have regressed. Our study thus allows valuable insights on the subtle vessel anomalies appearing in subjects exposed to fluctuating oxygen levels early in life.

Finally, it has to be kept in mind that even in infants born before 27 weeks of gestation more than half of the ROP cases are mild (stage 1 and 2) and less than 30 % need treatment (Austeng et al., 2009). Therefore, it is likely that abnormalities of retinal vasculature that are detected early are reversible and do not lead to visual impairment. The vessel anomalies that were found at P28 however, are most likely irreversible and thus reflect the long-term influence of IHH exposure on retinal vasculature.

Interestingly, weight was not significantly correlated with vessel diameter ratio. This is in contrast to the clinical setting, where early postnatal weight gain is used to predict the occurrence of ROP (Hellström et al., 2009). However, it has to be kept in mind that only about half of the dissected and stained retinas were suitable for analysis. A larger sample size may have given further insight on subtle abnormalities of retinal vasculature, or effects potentiating these, such as poor postnatal weight gain.

6.6 Is there a Link between Altered Brain Microstructure and Retinal Vasculature?

From statistical analyses of preterm born infants, it can be inferred that there is an association between patients suffering from PVL and ROP (Rose et al., 2014). Further, it has been shown that the severity of ROP in the neonate has predictive value for the neurodevelopmental functional

outcome at 5 years of age (Msall et al., 2000). This suggests a common underlying mechanisms of impaired brain development and abnormal retinal vasculature.

Conversely, in our study, fractional anisotropy, mean, axial and radial diffusivity were not correlated with tortuosity or vessel diameter in any region of interest at any time. This may indicate that additional factors are involved in the pathology of impaired white and grey matter development and/or retinal vascular abnormalities. One possible factor in addition to IHH exposure in our two-hits hypothesis may be inflammation, as prenatal inflammation is associated with preterm birth (Manuck et al., 2015; Stolp et al., 2012). Furthermore, in neonatal rats it has been shown that the vulnerability to hypoxic exposure is potentiated by prenatal inflammation caused by administration of LPS (Brehmer et al., 2012).

Chapter 7

Conclusions and Future Perspectives

A major aim of this study was to investigate the effect of IHH exposure on the microstructural development in white and grey matter as measured by DTI. We observed that white matter was differentially affected by exposure to IHH, dependent on the maturational status of the structures. Since differences in DTI parameters between IHH and room air group occurred mainly at P28 and not P15, the withdrawal of the IHH profile might be the noxious stimulus affecting the brain microstructural development. Regional differences in the effect of IHH exposure on white matter structures might have been due to regional heterogeneity in maturation. Association fibers such as the external capsule were especially vulnerable to oxygen fluctuations. They develop and mature relatively late and thus were more immature by the time of exposure. To further investigate this theory, histological studies could be conducted on the brains that were dissected in this study. One possible staining is luxol-staining, which visualizes myelin, and hence may provide solid evidence to how IHH exposure affects myelination. Furthermore, specific stainings for oligodendrocyte precursors could be used to support or negate our theory of regional differences in maturation.

Furthermore, we suspected that poor postnatal weight gain leads to impaired or retarded white and grey matter maturation. In our experiments, weight gain from birth to P15 seemed to influence white and grey matter maturation, as seen in a strong positive correlation with fractional anisotropy at P15. In contrast, we conclude that the positive correlation of mean, axial and radial diffusivity with weight (gain) at P28 did not indicate a correlation between weight and maturation, but rather reflects a higher water content since body weight correlated positively

with brain volume, and thus most likely also brain water content. This leads to the conclusion, that mean, axial and radial diffusivity are poor measures of brain maturation *per se* as their value is highly dependent on weight. To confirm the association between body weight, brain volume, water content and DTI parameters further analysis of the T_2 relaxation time from our MRI data. Additionally, histological analysis should be carried out. It will give valuable insight on the brain tissue composition, thereby adding information to the differences in mean diffusivity between groups of IHH and room air exposure.

Exposure to IHH lead to subtle changes in retinal vasculature. Blood vessel, particularly veins, were dilated in the mid-periphery. However, vessel tortuosity was not affected by IHH exposure. Furthermore, none of the measures of abnormal retinal vascularization was correlated with weight (gain). To get further insight on the processes leading to ROP, the blood serum sample taken at P28 should be investigated for IGF-1 levels. These are used in the clinic to predict the incidence and severity of ROP. Thus it would be intriguing to know if these levels correlate with the dilation and tortuosity of retinal blood vessels measured in this study. In addition, it would be interesting to investigate the retinal vasculature directly after IHH exposure at P14. At this time point, possibly more severe pathology in the retinal vasculature could be observed, which may have regressed until P28 through recovery in room air.

Finally, we hypothesized that there might be a connection between the microstructural development in the brain and the retinal vasculature. A common underlying mechanism due to susceptibility to oxygen exposure can be assumed from these experiments, albeit the severity of abnormal vasculature did not correlate with DTI parameters. This lack of a direct association leads to the assumption that secondary factors are involved the pathological brain maturation and retinal vascularization. Investigation of the blood serum samples according to pro-inflammatory cytokines such as $TNF-\alpha$ could give insight into a potential role of inflammation regarding pathological development.

In this translational research project it has been shown that subtle alterations in brain microstructural development and retinal vasculature can be caused by fluctuating oxygen levels. Consequently, caution is needed when giving supplemental oxygen to a preterm born infant to avoid both hyperoxic and hypoxic exposure to the immature brain and vasculature.

Appendix A

Acronyms

AD	axial diffusivity
AKM	Avdeling for komparative medisins (comparative medicine core facility)
AMPA	α -amino-3-hydroxy-5-methyl-4-isoxazole-propionic acid
DTI	diffusion tensor (magnetic resonance) imaging
E	embryonic day
<i>E. coli</i>	<i>Escherichia coli</i>
FA	fractional anisotropy
FSL	FMRIB software library
HIF-1	hypoxia inducible factor-1
IGF-1	insulin-like growth factor-1
IQR	interquartile range
IHH	intermittent hyperoxia-hypoxia
LPS	lipopolysaccharide
MD	mean diffusivity
MRI	magnetic resonance imaging
NMDA	<i>N</i> -methyl-D-aspartate
P	postnatal day
PBS	phosphate buffered saline
PFA	paraformaldehyde
PGC-1 α	peroxisome proliferator activated receptor gamma coactivator-1 α
PVL	periventricular leukomalacia
RA	room air
RD	radial diffusivity
RF pulse	radio frequency pulse
ROP	retinopathy of prematurity
T	Tesla
TNF- α	tumor necrosis factor- α
VEGF	vascular endothelial growth factor

Appendix B

Regions of Interest on FA Maps

Regions of interest were drawn manually on FA maps, as shown in figure B.1 for one slice. However, the white matter structures were drawn on several slices, and the striatum on two. Following table B.1 shows which slices the regions of interest were drawn on.

Table B.1: Slices of FA maps on which regions of interest were drawn

	P15	P28
corpus callosum	3/4 - 7/8	3/4 - 9/10
internal capsule	6 - 8	6 - 8
hippocampal fimbria	5/6 - 7/8	6 - 8
external capsule	3/4 - 8/9	3/4 - 9/10
hippocampus	7/8	8
cortex	7/8	8
thalamus	7/8	8
striatum	3/4 - 4/5	4 - 5

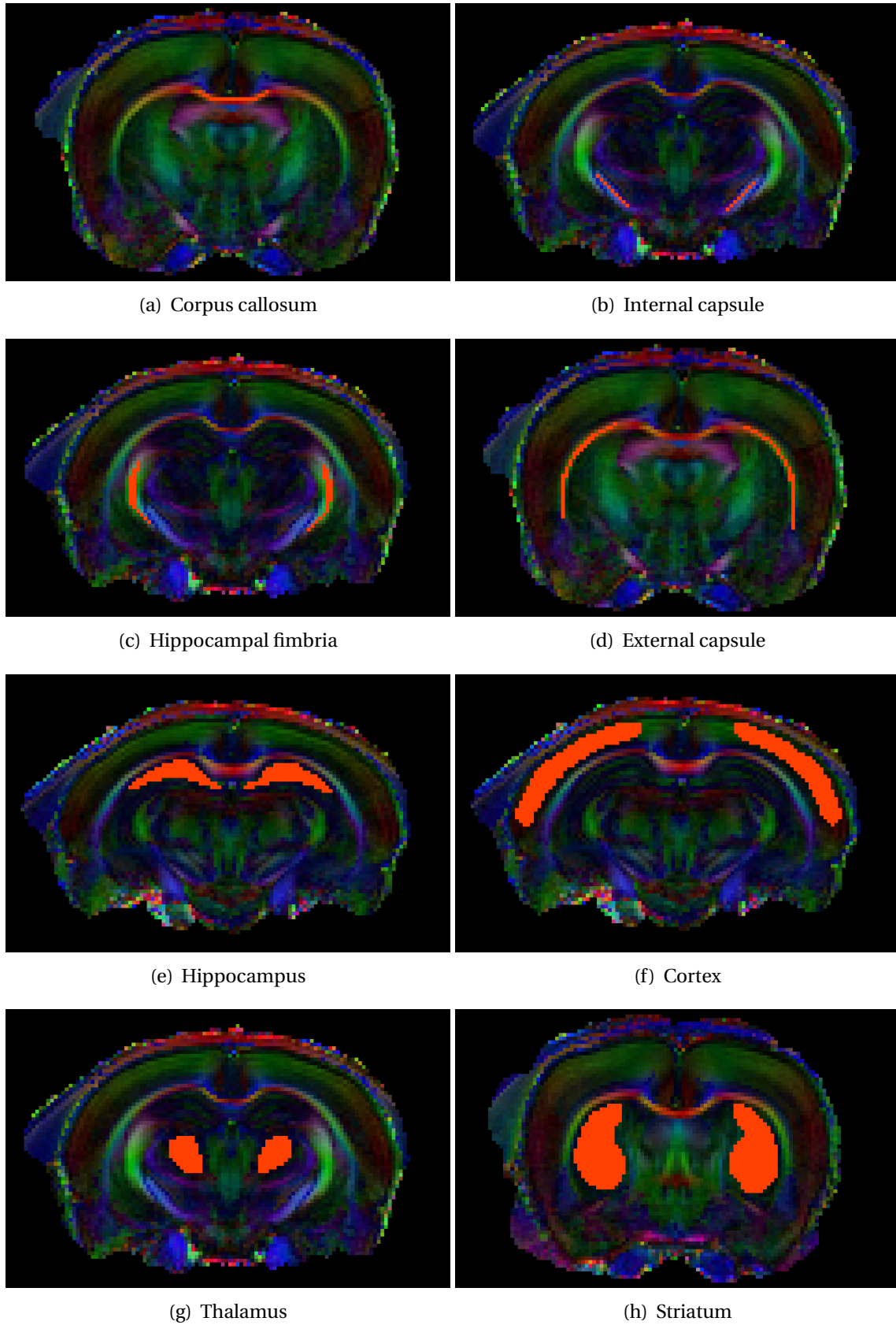


Figure B.1: Regions of interest on FA maps

Appendix C

Raw Data

Table C.1: DTI parameters by structure and oxygen condition at P15 displayed as mean \pm standard error.

RA	Fract. anisotropy		Mean diffusivity		Axial diffusivity		Radial diffusivity	
	mean	SE	mean	SE	mean	SE	mean	SE
cc	0.5330	\pm 0.0067	0.9242	\pm 0.0103	1.5397	\pm 0.0180	0.6164	\pm 0.0092
ric	0.5565	\pm 0.0064	0.9377	\pm 0.0109	1.6246	\pm 0.0223	0.5943	\pm 0.0076
lic	0.5650	\pm 0.0056	0.8345	\pm 0.0109	1.4487	\pm 0.0209	0.5275	\pm 0.0085
rhf	0.5423	\pm 0.0072	0.8850	\pm 0.0081	1.2875	\pm 0.0146	0.6837	\pm 0.0061
lhf	0.5615	\pm 0.0057	0.9382	\pm 0.0128	1.5937	\pm 0.0220	0.6104	\pm 0.0110
rec	0.4157	\pm 0.0046	0.9292	\pm 0.0101	1.5530	\pm 0.0187	0.6173	\pm 0.0088
lec	0.4076	\pm 0.0046	0.8904	\pm 0.0114	1.3013	\pm 0.0155	0.6849	\pm 0.0101
rh	0.1259	\pm 0.0032	0.8181	\pm 0.0078	1.4318	\pm 0.0173	0.5111	\pm 0.0057
lh	0.1198	\pm 0.0037	0.8845	\pm 0.0106	0.9972	\pm 0.0128	0.8281	\pm 0.0098
rc	0.1904	\pm 0.0035	0.8755	\pm 0.0094	0.9824	\pm 0.0124	0.8219	\pm 0.0084
lc	0.1949	\pm 0.0027	0.8127	\pm 0.0112	0.9828	\pm 0.0128	0.7277	\pm 0.0110
rt	0.1342	\pm 0.0043	0.8107	\pm 0.0086	0.9843	\pm 0.0094	0.7239	\pm 0.0085
lt	0.1438	\pm 0.0045	0.8465	\pm 0.0100	0.9636	\pm 0.0121	0.7880	\pm 0.0096
rst	0.1566	\pm 0.0050	0.8355	\pm 0.0086	0.9517	\pm 0.0115	0.7773	\pm 0.0077
lst	0.1444	\pm 0.0041	0.8370	\pm 0.0124	0.9731	\pm 0.0145	0.7688	\pm 0.0119
IHH	Fract. anisotropy		Mean diffusivity		Axial diffusivity		Radial diffusivity	
	mean	SE	mean	SE	mean	SE	mean	SE
cc	0.5512	\pm 0.0041	0.9339	\pm 0.0070	1.5661	\pm 0.0150	0.6177	\pm 0.0062
ric	0.5684	\pm 0.0052	0.9272	\pm 0.0068	1.6034	\pm 0.0167	0.5892	\pm 0.0059
lic	0.5782	\pm 0.0052	0.8307	\pm 0.0067	1.4586	\pm 0.0126	0.5165	\pm 0.0064
rhf	0.5388	\pm 0.0058	0.8944	\pm 0.0058	1.3107	\pm 0.0106	0.6861	\pm 0.0044
lhf	0.5591	\pm 0.0062	0.9316	\pm 0.0085	1.5789	\pm 0.0194	0.6079	\pm 0.0063
rec	0.4190	\pm 0.0044	0.9453	\pm 0.0072	1.6067	\pm 0.0128	0.6144	\pm 0.0075
lec	0.4161	\pm 0.0034	0.9022	\pm 0.0081	1.3250	\pm 0.0135	0.6909	\pm 0.0067
rh	0.1249	\pm 0.0035	0.8243	\pm 0.0048	1.4607	\pm 0.0121	0.5062	\pm 0.0043
lh	0.1253	\pm 0.0029	0.8878	\pm 0.0078	1.0017	\pm 0.0099	0.8309	\pm 0.0072
rc	0.1931	\pm 0.0024	0.8804	\pm 0.0066	0.9939	\pm 0.0083	0.8235	\pm 0.0062
lc	0.1943	\pm 0.0025	0.8177	\pm 0.0079	0.9886	\pm 0.0096	0.7323	\pm 0.0073
rt	0.1412	\pm 0.0046	0.8123	\pm 0.0060	0.9867	\pm 0.0062	0.7250	\pm 0.0062
lt	0.1445	\pm 0.0036	0.8502	\pm 0.0067	0.9745	\pm 0.0076	0.7881	\pm 0.0073
rst	0.1564	\pm 0.0042	0.8436	\pm 0.0059	0.9627	\pm 0.0081	0.7838	\pm 0.0054
lst	0.1497	\pm 0.0030	0.8469	\pm 0.0087	0.9836	\pm 0.0105	0.7787	\pm 0.0085

Table C.2: DTI parameters by structure and oxygen condition at P28 displayed as mean \pm standard error.

RA	Fract. anisotropy		Mean diffusivity		Axial diffusivity		Radial diffusivity	
	mean	SE	mean	SE	mean	SE	mean	SE
cc	0.6830	\pm 0.0042	0.8259	\pm 0.0084	1.5662	\pm 0.0222	0.4558	\pm 0.0053
ric	0.6781	\pm 0.0072	0.8503	\pm 0.0088	1.6985	\pm 0.0215	0.4260	\pm 0.0056
lic	0.6799	\pm 0.0058	0.7605	\pm 0.0089	1.4890	\pm 0.0149	0.3962	\pm 0.0089
rhf	0.6706	\pm 0.0054	0.7900	\pm 0.0064	1.2872	\pm 0.0116	0.5408	\pm 0.0051
lhf	0.6949	\pm 0.0057	0.8530	\pm 0.0072	1.6599	\pm 0.0175	0.4496	\pm 0.0053
rec	0.5322	\pm 0.0034	0.8330	\pm 0.0077	1.6300	\pm 0.0209	0.4344	\pm 0.0039
lec	0.5208	\pm 0.0035	0.8007	\pm 0.0081	1.3188	\pm 0.0162	0.5416	\pm 0.0050
rh	0.1523	\pm 0.0032	0.7590	\pm 0.0072	1.4899	\pm 0.0153	0.3933	\pm 0.0062
lh	0.1553	\pm 0.0031	0.7802	\pm 0.0087	0.9040	\pm 0.0089	0.7181	\pm 0.0088
rc	0.2103	\pm 0.0022	0.7756	\pm 0.0079	0.8996	\pm 0.0080	0.7136	\pm 0.0080
lc	0.2129	\pm 0.0036	0.7255	\pm 0.0092	0.8943	\pm 0.0115	0.6411	\pm 0.0083
rt	0.1660	\pm 0.0050	0.7168	\pm 0.0080	0.8852	\pm 0.0113	0.6324	\pm 0.0068
lt	0.1774	\pm 0.0056	0.7483	\pm 0.0079	0.8761	\pm 0.0079	0.6845	\pm 0.0086
rst	0.1912	\pm 0.0045	0.7218	\pm 0.0071	0.8598	\pm 0.0101	0.6527	\pm 0.0064
lst	0.1891	\pm 0.0044	0.7324	\pm 0.0078	0.8873	\pm 0.0119	0.6548	\pm 0.0064
IHH	Fract. anisotropy		Mean diffusivity		Axial diffusivity		Radial diffusivity	
	mean	SE	mean	SE	mean	SE	mean	SE
cc	0.6896	\pm 0.0035	0.8622	\pm 0.0038	1.6432	\pm 0.0093	0.4715	\pm 0.0056
ric	0.6856	\pm 0.0051	0.8874	\pm 0.0049	1.7842	\pm 0.0124	0.4390	\pm 0.0046
lic	0.6847	\pm 0.0050	0.7882	\pm 0.0034	1.5571	\pm 0.0110	0.4037	\pm 0.0043
rhf	0.6853	\pm 0.0042	0.8250	\pm 0.0039	1.3460	\pm 0.0061	0.5645	\pm 0.0042
lhf	0.7029	\pm 0.0045	0.8940	\pm 0.0051	1.7655	\pm 0.0124	0.4583	\pm 0.0046
rec	0.5211	\pm 0.0027	0.8699	\pm 0.0037	1.7155	\pm 0.0064	0.4472	\pm 0.0048
lec	0.5199	\pm 0.0031	0.8348	\pm 0.0039	1.3632	\pm 0.0065	0.5706	\pm 0.0038
rh	0.1488	\pm 0.0022	0.7790	\pm 0.0044	1.5373	\pm 0.0110	0.3998	\pm 0.0048
lh	0.1496	\pm 0.0026	0.8168	\pm 0.0035	0.9411	\pm 0.0050	0.7546	\pm 0.0029
rc	0.2005	\pm 0.0030	0.8142	\pm 0.0035	0.9390	\pm 0.0053	0.7520	\pm 0.0030
lc	0.2106	\pm 0.0034	0.7600	\pm 0.0034	0.9268	\pm 0.0040	0.6767	\pm 0.0040
rt	0.1571	\pm 0.0047	0.7528	\pm 0.0038	0.9278	\pm 0.0056	0.6654	\pm 0.0039
lt	0.1592	\pm 0.0044	0.7815	\pm 0.0035	0.9110	\pm 0.0072	0.7168	\pm 0.0031
rst	0.1884	\pm 0.0032	0.7568	\pm 0.0037	0.8995	\pm 0.0069	0.6856	\pm 0.0028
lst	0.1853	\pm 0.0032	0.7668	\pm 0.0035	0.9246	\pm 0.0063	0.6879	\pm 0.0026

Table C.3: Comparison of correlations coefficient between fractional anisotropy and weight. Pearson's r and Spearman's ρ with respective p-values are displayed. 0 in the p-value column indicates a p-value of < 0.0005 .

FA P15	Weight at P15				Abs wg P0 - P15				Rel wg P0 - P15			
	Pearson		Spearman		Pearson		Spearman		Pearson		Spearman	
	r	p	ρ	p	r	p	ρ	p	r	p	ρ	p
cc	.545	0	.523	0	.538	0	.513	0	.507	0	.438	0
ric	.383	.001	.339	.003	.374	.001	.34	.003	.34	.003	.283	.015
lic	.52	0	.48	0	.513	0	.478	0	.487	0	.446	0
rhf	.242	.039	.255	.03	.237	.043	.257	.028	.221	.06	.231	.049
lhf	.346	.003	.335	.004	.337	.004	.336	.004	.304	.009	.294	.012
rec	.475	0	.479	0	.467	0	.475	0	.44	0	.427	0
lec	.629	0	.607	0	.621	0	.607	0	.59	0	.551	0
rh	.237	.044	.242	.039	.238	.042	.245	.037	.246	.036	.207	.078
lh	.412	0	.493	0	.409	0	.498	0	.397	.001	.475	0
rc	-.249	.034	-.237	.044	-.239	.042	-.23	.05	-.195	.097	-.193	.102
lc	-.286	.014	-.343	.003	-.28	.017	-.322	.005	-.255	.029	-.255	.029
rt	.299	.01	.289	.013	.302	.009	.299	.01	.31	.008	.32	.006
lt	.29	.013	.264	.024	.29	.013	.27	.021	.283	.015	.275	.019
rst	.26	.026	.307	.008	.262	.025	.309	.008	.267	.022	.287	.014
lst	.513	0	.589	0	.508	0	.58	0	.483	0	.532	0
FA P28	Weight at P28				Abs wg P15 - P28				Rel wg P15 - P28			
	Pearson		Spearman		Pearson		Spearman		Pearson		Spearman	
	r	p	ρ	p	r	p	ρ	p	r	p	ρ	p
cc	.363	.001	.287	.013	.383	.001	.333	.003	.114	.329	.093	.426
ric	.054	.645	-.042	.721	.084	.473	.034	.773	.141	.229	.089	.447
lic	.038	.747	-.034	.775	.071	.547	.032	.786	.13	.268	.126	.28
rhf	.326	.004	.315	.006	.313	.006	.324	.005	-.024	.84	.015	.901
lhf	.421	0	.424	0	.421	0	.443	0	.05	.671	.062	.598
rec	.029	.808	.014	.906	.12	.307	.106	.365	.387	.001	.408	0
lec	.043	.716	.026	.823	.096	.413	.115	.327	.184	.113	.247	.033
rh	-.113	.335	-.061	.606	-.109	.351	-.068	.56	-.026	.828	.103	.379
lh	-.173	.137	-.126	.283	-.167	.152	-.15	.199	-.002	.987	.026	.825
rc	-.189	.105	-.194	.095	-.117	.318	-.122	.296	.243	.035	.276	.016
lc	-.066	.573	-.189	.104	-.014	.907	-.113	.334	.174	.135	.153	.191
rt	-.144	.219	-.105	.371	-.18	.123	-.163	.163	-.143	.221	-.187	.108
lt	-.159	.174	-.08	.495	-.156	.18	-.133	.257	.01	.934	-.052	.66
rst	.352	.002	.33	.004	.364	.001	.303	.008	.072	.542	-.011	.927
lst	.28	.015	.323	.005	.31	.007	.306	.008	.136	.246	.128	.274

Table C.4: Comparison of correlations coefficient between mean diffusivity and weight. Pearson's r and Spearman's ρ with respective p-values are displayed. 0 in the p-value column indicates a p-value of <0.0005 .

MD P15	Weight at P15				Abs wg P0 - P15				Rel wg P0 - P15			
	Pearson		Spearman		Pearson		Spearman		Pearson		Spearman	
	r	p	ρ	p	r	p	ρ	p	r	p	ρ	p
cc	.385	.001	.391	.001	.382	.001	.383	.001	.371	.001	.352	.002
ric	.322	.005	.281	.016	.313	.007	.268	.022	.28	.017	.194	.1
lic	.115	.332	.11	.355	.112	.347	.104	.383	.098	.408	.071	.551
rhf	.441	0	.436	0	.434	0	.426	0	.408	0	.38	.001
lhf	.155	.191	.177	.133	.154	.194	.179	.129	.151	.202	.167	.158
rec	.413	0	.397	0	.41	0	.392	.001	.399	0	.37	.001
lec	.255	.03	.277	.018	.254	.03	.271	.02	.253	.031	.241	.04
rh	.194	.101	.153	.197	.188	.111	.145	.22	.166	.16	.105	.377
lh	.334	.004	.362	.002	.331	.004	.353	.002	.318	.006	.314	.007
rc	.424	0	.436	0	.418	0	.424	0	.392	.001	.374	.001
lc	.343	.003	.387	.001	.341	.003	.377	.001	.33	.004	.339	.003
rt	.487	0	.502	0	.48	0	.488	0	.448	0	.43	0
lt	.205	.082	.199	.092	.199	.091	.19	.108	.179	.129	.156	.187
rst	.407	0	.407	0	.403	0	.399	0	.384	.001	.358	.002
lst	.232	.048	.253	.031	.232	.049	.249	.033	.233	.047	.22	.062
MD P28	Weight at P28				Abs wg P15 - P28				Rel wg P15 - P28			
	Pearson		Spearman		Pearson		Spearman		Pearson		Spearman	
	r	p	ρ	p	r	p	ρ	p	r	p	ρ	p
cc	.636	0	.512	0	.59	0	.52	0	-.111	.344	-.15	.198
ric	.669	0	.579	0	.609	0	.557	0	-.144	.219	-.206	.076
lic	.491	0	.383	.001	.42	0	.331	.004	-.256	.027	-.278	.016
rhf	.581	0	.532	0	.507	0	.49	0	-.198	.088	-.31	.007
lhf	.604	0	.57	0	.555	0	.55	0	-.109	.354	-.168	.15
rec	.612	0	.498	0	.554	0	.49	0	-.156	.181	-.216	.062
lec	.656	0	.56	0	.592	0	.541	0	-.151	.195	-.247	.033
rh	.541	0	.476	0	.5	0	.433	0	-.088	.455	-.173	.137
lh	.647	0	.535	0	.586	0	.512	0	-.149	.203	-.251	.03
rc	.637	0	.534	0	.571	0	.496	0	-.173	.137	-.271	.019
lc	.687	0	.58	0	.634	0	.568	0	-.104	.374	-.204	.079
rt	.652	0	.549	0	.592	0	.523	0	-.143	.222	-.253	.029
lt	.601	0	.505	0	.531	0	.462	0	-.184	.113	-.304	.008
rst	.632	0	.549	0	.566	0	.529	0	-.164	.16	-.278	.016
lst	.641	0	.542	0	.582	0	.541	0	-.127	.277	-.229	.048

Table C.5: Comparison of correlations coefficient between axial diffusivity and weight. Pearson's r and Spearman's ρ with respective p-values are displayed. 0 in the p-value column indicates a p-value of <0.0005 .

AD P15	Weight at P15				Abs wg P0 - P15				Rel wg P0 - P15			
	Pearson		Spearman		Pearson		Spearman		Pearson		Spearman	
	r	p	ρ	p	r	p	ρ	p	r	p	ρ	p
cc	.517	0	.517	0	.512	0	.505	0	.491	0	.439	0
ric	.43	0	.408	0	.419	0	.394	.001	.377	.001	.299	.01
lic	.321	.006	.333	.004	.313	.007	.325	.005	.282	.016	.262	.025
rhf	.589	0	.608	0	.58	0	.599	0	.546	0	.529	0
lhf	.258	.027	.23	.051	.255	.03	.23	.051	.244	.037	.197	.095
rec	.623	0	.586	0	.616	0	.577	0	.591	0	.517	0
lec	.421	0	.355	.002	.417	0	.349	.002	.406	0	.307	.008
rh	.43	0	.38	.001	.422	0	.377	.001	.394	.001	.335	.004
lh	.382	.001	.419	0	.38	.001	.413	0	.372	.001	.373	.001
rc	.493	0	.526	0	.487	0	.517	0	.461	0	.47	0
lc	.258	.027	.32	.006	.259	.027	.312	.007	.258	.028	.281	.016
rt	.425	0	.419	0	.419	0	.413	0	.393	.001	.374	.001
lt	.33	.004	.309	.008	.326	.005	.309	.008	.309	.008	.295	.011
rst	.485	0	.522	0	.479	0	.515	0	.452	0	.469	0
lst	.286	.014	.282	.016	.287	.014	.282	.016	.291	.013	.261	.025
AD P28	Weight at P28				Abs wg P15 - P28				Rel wg P15 - P28			
	Pearson		Spearman		Pearson		Spearman		Pearson		Spearman	
	r	p	ρ	p	r	p	ρ	p	r	p	ρ	p
cc	.683	0	.555	0	.658	0	.577	0	-.032	.782	-.086	.464
ric	.718	0	.656	0	.673	0	.65	0	-.082	.486	-.123	.295
lic	.42	0	.318	.005	.372	.001	.305	.008	-.163	.161	-.193	.097
rhf	.62	0	.506	0	.578	0	.531	0	-.08	.495	-.118	.312
lhf	.615	0	.593	0	.57	0	.592	0	-.101	.389	-.097	.408
rec	.703	0	.572	0	.668	0	.601	0	-.056	.63	-.065	.582
lec	.655	0	.561	0	.631	0	.591	0	.016	.889	-.069	.557
rh	.453	0	.384	.001	.435	0	.401	0	-.013	.914	-.015	.899
lh	.61	0	.527	0	.552	0	.506	0	-.146	.211	-.222	.056
rc	.559	0	.507	0	.496	0	.467	0	-.176	.131	-.262	.023
lc	.65	0	.528	0	.624	0	.557	0	-.007	.954	-.07	.55
rt	.574	0	.459	0	.543	0	.472	0	-.049	.674	-.156	.182
lt	.459	0	.441	0	.369	.001	.383	.001	-.269	.019	-.36	.002
rst	.63	0	.627	0	.586	0	.609	0	-.08	.497	-.2	.086
lst	.638	0	.577	0	.601	0	.568	0	-.052	.656	-.18	.121

Table C.6: Comparison of correlations coefficient between radial diffusivity and weight. Pearson's r and Spearman's ρ with respective p-values are displayed. 0 in the p-value column indicates a p-value of <0.0005 .

RD P15	Weight at P15				Abs wg P0 - P15				Rel wg P0 - P15			
	Pearson		Spearman		Pearson		Spearman		Pearson		Spearman	
	r	p	ρ	p	r	p	ρ	p	r	p	ρ	p
cc	.08	.5	.097	.413	.081	.494	.099	.407	.085	.476	.113	.34
ric	.005	.964	-.079	.506	.004	.971	-.087	.466	-.001	.996	-.092	.437
lic	-.155	.19	-.152	.199	-.152	.199	-.157	.185	-.141	.233	-.145	.221
rhf	.168	.154	.163	.168	.166	.16	.152	.2	.155	.189	.128	.28
lhf	-.036	.765	-.066	.581	-.034	.776	-.064	.591	-.026	.829	-.054	.652
rec	.045	.707	.061	.605	.047	.693	.063	.596	.055	.641	.089	.453
lec	.07	.554	.106	.371	.073	.541	.103	.387	.081	.495	.096	.421
rh	-.273	.019	-.286	.014	-.272	.02	-.289	.013	-.27	.021	-.298	.011
lh	.286	.014	.304	.009	.282	.016	.294	.011	.266	.023	.258	.027
rc	.35	.002	.35	.002	.344	.003	.337	.004	.319	.006	.288	.013
lc	.38	.001	.426	0	.376	.001	.417	0	.359	.002	.375	.001
rt	.5	0	.516	0	.492	0	.499	0	.459	0	.431	0
lt	.109	.36	.099	.405	.102	.388	.088	.461	.083	.486	.049	.681
rst	.315	.007	.315	.007	.312	.007	.309	.008	.301	.01	.276	.018
lst	.182	.123	.213	.071	.182	.124	.208	.078	.182	.123	.177	.135
RD P28	Weight at P28				Abs wg P15 - P28				Rel wg P15 - P28			
	Pearson		Spearman		Pearson		Spearman		Pearson		Spearman	
	r	p	ρ	p	r	p	ρ	p	r	p	ρ	p
cc	.112	.339	.133	.254	.068	.56	.124	.289	-.142	.226	-.132	.257
ric	.167	.152	.104	.373	.119	.308	.081	.491	-.162	.164	-.196	.091
lic	.272	.018	.265	.022	.219	.059	.186	.111	-.204	.079	-.225	.052
rhf	.401	0	.372	.001	.315	.006	.286	.013	-.262	.023	-.357	.002
lhf	.202	.082	.129	.27	.177	.128	.115	.324	-.052	.655	-.083	.479
rec	.098	.404	.112	.337	.039	.741	.068	.56	-.216	.062	-.223	.055
lec	.511	0	.433	0	.415	0	.38	.001	-.31	.007	-.383	.001
rh	.302	.008	.286	.013	.259	.025	.219	.059	-.124	.288	-.214	.065
lh	.647	0	.532	0	.585	0	.511	0	-.146	.212	-.261	.024
rc	.654	0	.548	0	.59	0	.51	0	-.164	.159	-.272	.018
lc	.661	0	.573	0	.596	0	.539	0	-.156	.183	-.274	.017
rt	.631	0	.554	0	.557	0	.504	0	-.199	.087	-.309	.007
lt	.581	0	.458	0	.538	0	.454	0	-.093	.429	-.13	.268
rst	.543	0	.388	.001	.467	0	.386	.001	-.214	.065	-.332	.004
lst	.572	0	.458	0	.498	0	.459	0	-.182	.119	-.309	.007

List of Figures

1.1	Vicious cycle of breathing disorder, oxygen fluctuations and respiratory instability	2
2.1	Research question of this thesis	18
3.1	Diffusion tensor for isotropic and anisotropic diffusion	23
4.1	Testing subjects by litter	26
4.2	IHH profile and oxycycler	31
4.3	White matter regions of interest	32
4.4	Measures for retinal vasculature	32
5.1	Fractional anisotropy by oxygen condition	35
5.2	Mean diffusivity by oxygen condition	36
5.3	Axial diffusivity increased in white matter and decreased in grey matter	37
5.4	Axial diffusivity by oxygen condition	38
5.5	Radial diffusivity by oxygen condition	39
5.6	Highlight table of correlation coefficients between fractional anisotropy and weight (gain)	41
5.7	Highlight table of correlation coefficients between mean diffusivity and weight (gain)	42
5.8	Mean diffusivity against weight at P15 and P28	43
5.9	Highlight table of correlation coefficients between axial diffusivity and weight (gain)	44
5.10	Highlight table of correlation coefficients between radial diffusivity and weight (gain)	45

5.11	Weight at P0, P15 and P28 by litter size and gender	46
5.12	Absolute and relative weight gain by litter size	47
5.13	Weight at P0 (birth), P15 and P28 by litter size and oxygen condition	47
5.14	Absolute and relative weight gain by oxygen condition	48
5.15	Scatterplot of mean diffusivity against weight at P28	49
5.16	Tortuosity and diameter ratio in arteries and veins by oxygen condition	50
6.1	Time line of white matter development and maturation	58
B.1	Regions of interest on FA maps	72

List of Tables

1.1	Comparative time schedule for brain development in animals and humans	3
1.2	Comparative time schedule for axonal maturation in humans and rats	5
4.1	Scan parameters of DTI sequences at P15 and P28	28
5.1	Acronyms for brain structures	33
6.1	Summary of longitudinal development of DTI parameters by oxygen condition . .	51
B.1	Slices of FA maps on which regions of interest were drawn	71
C.1	DTI parameters by structure and oxygen condition at P15	74
C.2	DTI parameters by structure and oxygen condition at P28	75
C.3	Comparison of correlation coefficients between fractional anisotropy and weight .	76
C.4	Comparison of correlation coefficients between mean diffusivity and weight	77
C.5	Comparison of correlation coefficients between axial diffusivity and weight	78
C.6	Comparison of correlation coefficients between radial diffusivity and weight	79

Bibliography

Abbott, N. J., Rönnbäck, L., and Hansson, E. (2006). Astrocyte–endothelial interactions at the blood–brain barrier. *Nature Reviews Neuroscience*, 7(1):41–53.

Allin, M., Walshe, M., Fern, A., Nosarti, C., Cuddy, M., Rifkin, L., Murray, R., Rushe, T., and Wyatt, J. (2008). Cognitive maturation in preterm and term born adolescents. *Journal of Neurology, Neurosurgery & Psychiatry*, 79(4):381–386.

Armstrong, E., Schleicher, A., Omran, H., Curtis, M., and Zilles, K. (1995). The ontogeny of human gyrification. *Cerebral Cortex*, 5(1):56–63.

Asikainen, T. M., Ahmad, A., Schneider, B. K., and White, C. W. (2005). Effect of preterm birth on hypoxia-inducible factors and vascular endothelial growth factor in primate lungs. *Pediatric pulmonology*, 40(6):538–546.

Austeng, D., Källén, K. B., Ewald, U. W., Jakobsson, P. G., and Holmström, G. E. (2009). Incidence of retinopathy of prematurity in infants born before 27 weeks' gestation in sweden. *Archives of ophthalmology*, 127(10):1315–1319.

Axer, H., Klingner, C. M., and Prescher, A. (2013). Fiber anatomy of dorsal and ventral language streams. *Brain and language*, 127(2):192–204.

Babikian, T., Prins, M. L., Cai, Y., Barkhoudarian, G., Hartonian, I., Hovda, D. A., and Giza, C. C. (2010). Molecular and physiological responses to juvenile traumatic brain injury: focus on growth and metabolism. *Developmental neuroscience*, 32(5-6):431–441.

Baburamani, A. A., Ek, C. J., Walker, D. W., and Castillo-Melendez, M. (2012). Vulnerability of

- the developing brain to hypoxic-ischemic damage: contribution of the cerebral vasculature to injury and repair. *Front Physiol*, 3(424):10–3389.
- Bache, M., Rot, S., Keßler, J., Güttler, A., Wichmann, H., Greither, T., Wach, S., Taubert, H., Söling, A., Bilkenroth, U., et al. (2015). mRNA expression levels of hypoxia-induced and stem cell-associated genes in human glioblastoma. *Oncology reports*, 33(6):3155–3161.
- Back, S. A., Luo, N. L., Borenstein, N. S., Levine, J. M., Volpe, J. J., and Kinney, H. C. (2001). Late oligodendrocyte progenitors coincide with the developmental window of vulnerability for human perinatal white matter injury. *The Journal of Neuroscience*, 21(4):1302–1312.
- Back, S. A., Riddle, A., Dean, J., and Hohimer, A. R. (2012). The instrumented fetal sheep as a model of cerebral white matter injury in the premature infant. *Neurotherapeutics*, 9(2):359–370.
- Back, S. A., Riddle, A., and McClure, M. M. (2007). Maturation-dependent vulnerability of perinatal white matter in premature birth. *Stroke*, 38(2):724–730.
- Ballabh, P., Braun, A., and Nedergaard, M. (2004). Anatomic analysis of blood vessels in germinal matrix, cerebral cortex, and white matter in developing infants. *Pediatric research*, 56(1):117–124.
- Balleine, B. W., Delgado, M. R., and Hikosaka, O. (2007). The role of the dorsal striatum in reward and decision-making. *The Journal of Neuroscience*, 27(31):8161–8165.
- Banker, B. Q. and Larroche, J.-C. (1962). Periventricular leukomalacia of infancy: a form of neonatal anoxic encephalopathy. *Archives of Neurology*, 7(5):386–410.
- Banks, M. S. and Bennett, P. J. (1988). Optical and photoreceptor immaturities limit the spatial and chromatic vision of human neonates. *JOSA A*, 5(12):2059–2079.
- Barnett, J. M., Yanni, S. E., and Penn, J. S. (2010). The development of the rat model of retinopathy of prematurity. *Documenta ophthalmologica*, 120(1):3–12.
- Barrick, T. R., Lawes, I. N., Mackay, C. E., and Clark, C. A. (2007). White matter pathway asymmetry underlies functional lateralization. *Cerebral Cortex*, 17(3):591–598.

- Basser, P. and Pierpaoli, C. (1996). Microstructural features measured using diffusion tensor imaging. *J Magn Reson B*, 111(3):209–219.
- Bell, M. J. and Hallenbeck, J. M. (2002). Effects of intrauterine inflammation on developing rat brain. *Journal of neuroscience research*, 70(4):570–579.
- Billiards, S. S., Haynes, R. L., Folkerth, R. D., Borenstein, N. S., Trachtenberg, F. L., Rowitch, D. H., Ligon, K. L., Volpe, J. J., and Kinney, H. C. (2008). Myelin abnormalities without oligodendrocyte loss in periventricular leukomalacia. *Brain Pathology*, 18(2):153–163.
- BioSpherix (2013). Oxycycler a84xov: Dynamix O₂ controller for animal modeling. *User Manual*.
- Blencowe, H., Cousens, S., Oestergaard, M. Z., Chou, D., Moller, A.-B., Narwal, R., Adler, A., Garcia, C. V., Rohde, S., Say, L., et al. (2012). National, regional, and worldwide estimates of preterm birth rates in the year 2010 with time trends since 1990 for selected countries: a systematic analysis and implications. *The Lancet*, 379(9832):2162–2172.
- Bockhorst, K., Narayana, P., Liu, R., Ahobila-Vijjula, P., Ramu, J., Kamel, M., Wosik, J., Bockhorst, T., Hahn, K., Hasan, K., et al. (2008). Early postnatal development of rat brain: in vivo diffusion tensor imaging. *Journal of neuroscience research*, 86(7):1520–1528.
- Bolzenius, J. D., Laidlaw, D. H., Cabeen, R. P., Conturo, T. E., McMichael, A. R., Lane, E. M., Heaps, J. M., Salminen, L. E., Baker, L. M., Gunstad, J., et al. (2013). Impact of body mass index on neuronal fiber bundle lengths among healthy older adults. *Brain imaging and behavior*, 7(3):300–306.
- Børch, K., Lou, H. C., and Greisen, G. (2010). Cerebral white matter blood flow and arterial blood pressure in preterm infants. *Acta Paediatrica*, 99(10):1489–1492.
- Boylan, G. B., Young, K., Panerai, R. B., Rennie, J. M., and Evans, D. H. (2000). Dynamic cerebral autoregulation in sick newborn infants. *Pediatric research*, 48(1):12–17.
- Brands, K., Hofmann, H., and Klees, E. (1958). Die retrolentale fibroplasie. *Geburtshilfe Frauenheilkd*, 18:805–814.

- Brehmer, F., Bendix, I., Prager, S., Van De Looij, Y., Reinboth, B. S., Zimmermanns, J., Schlager, G. W., Brait, D., Sifringer, M., Endesfelder, S., et al. (2012). Interaction of inflammation and hyperoxia in a rat model of neonatal white matter damage. *PloS one*, 7(11):e49023.
- Brew, N., Walker, D., and Wong, F. Y. (2014). Cerebral vascular regulation and brain injury in preterm infants. *American Journal of Physiology-Regulatory, Integrative and Comparative Physiology*, 306(11):R773–R786.
- Bucher, F., Stahl, A., Agostini, H. T., and Martin, G. (2013). Hyperoxia causes reduced density of retinal astrocytes in the central avascular zone in the mouse model of oxygen-induced retinopathy. *Molecular and Cellular Neuroscience*, 56:225–233.
- Bystron, I., Blakemore, C., and Rakic, P. (2008). Development of the human cerebral cortex: Boulder committee revisited. *Nature Reviews Neuroscience*, 9(2):110–122.
- Campbell, K. (1951). Intensive oxygen therapy as a possible cause of retrolental fibroplasia; a clinical approach. *The Medical journal of Australia*, 2(2):48–50.
- Carmeliet, P. and de Almodovar, C. R. (2013). Vegf ligands and receptors: implications in neurodevelopment and neurodegeneration. *Cellular and Molecular Life Sciences*, 70(10):1763–1778.
- Catalani, A., Sabbatini, M., Consoli, C., Cinque, C., Tomassoni, D., Azmitia, E., Angelucci, L., and Amenta, F. (2002). Glial fibrillary acidic protein immunoreactive astrocytes in developing rat hippocampus. *Mechanisms of ageing and development*, 123(5):481–490.
- Chang, H. H., Larson, J., Blencowe, H., Spong, C. Y., Howson, C. P., Cairns-Smith, S., Lackritz, E. M., Lee, S. K., Mason, E., Serazin, A. C., et al. (2013). Preventing preterm births: analysis of trends and potential reductions with interventions in 39 countries with very high human development index. *The Lancet*, 381(9862):223–234.
- Chen, J., Stahl, A., Hellstrom, A., and Smith, L. E. (2011). Current update on retinopathy of prematurity: screening and treatment. *Current opinion in pediatrics*, 23(2):173.

- Cheng, Y., Chou, K.-H., Chen, I.-Y., Fan, Y.-T., Decety, J., and Lin, C.-P. (2010). Atypical development of white matter microstructure in adolescents with autism spectrum disorders. *Neuroimage*, 50(3):873–882.
- Choi, J. Y., Rha, D.-w., and Park, E. S. (2015). The effects of the severity of periventricular leukomalacia on the neuropsychological outcomes of preterm children. *Journal of child neurology*, page 0883073815604229.
- Coleman, R. J., Beharry, K. D., Brock, R. S., Abad-Santos, P., Abad-Santos, M., and Modanlou, H. D. (2008). Effects of brief, clustered versus dispersed hypoxic episodes on systemic and ocular growth factors in a rat model of oxygen-induced retinopathy. *Pediatric research*, 64(1):50–55.
- Cooke, R., Ainsworth, S., and Fenton, A. (2004). Postnatal growth retardation: a universal problem in preterm infants. *Archives of Disease in Childhood-Fetal and Neonatal Edition*, 89(5):F428–F430.
- Crain, B., Cotman, C., Taylor, D., and Lynch, G. (1973). A quantitative electron microscopic study of synaptogenesis in the dentate gyrus of the rat. *Brain Research*, 63:195–204.
- Cuzner, L., Davison, A., and Gregson, N. (1965). Chemical and metabolic studies of rat myelin of the central nervous system*. *Annals of the New York Academy of Sciences*, 122(1):86–94.
- Danbolt, N. C. (2001). Glutamate uptake. *Progress in neurobiology*, 65(1):1–105.
- Danilov, C. A. and Fiskum, G. (2008). Hyperoxia promotes astrocyte cell death after oxygen and glucose deprivation. *Glia*, 56(7):801–808.
- Davis, J. M. and Auten, R. L. (2010). Maturation of the antioxidant system and the effects on preterm birth. In *Seminars in Fetal and Neonatal Medicine*, volume 15, pages 191–195. Elsevier.
- Dhaliwal, C., Wade, J., Gillespie, T., Aspinall, P., McIntosh, N., and Fleck, B. (2011). Early retinal blood vessel growth in normal and growth restricted rat pups raised in oxygen and room air. *British Journal of Ophthalmology*, 95(11):1592–1596.

- Dixon, S. J. and Stockwell, B. R. (2014). The role of iron and reactive oxygen species in cell death. *Nature chemical biology*, 10(1):9–17.
- Dubois, J., Benders, M., Cachia, A., Lazeyras, F., Leuchter, R. H.-V., Sizonenko, S., Borradori-Tolsa, C., Mangin, J., and Hüppi, P. S. (2008). Mapping the early cortical folding process in the preterm newborn brain. *Cerebral Cortex*, 18(6):1444–1454.
- Dubois, J., Dehaene-Lambertz, G., Kulikova, S., Poupon, C., Hüppi, P. S., and Hertz-Pannier, L. (2014). The early development of brain white matter: a review of imaging studies in fetuses, newborns and infants. *Neuroscience*, 276:48–71.
- Dyett, L. E., Kennea, N., Counsell, S. J., Maalouf, E. F., Ajayi-Obe, M., Duggan, P. J., Harrison, M., Allsop, J. M., Hajnal, J., Herlihy, A. H., et al. (2006). Natural history of brain lesions in extremely preterm infants studied with serial magnetic resonance imaging from birth and neurodevelopmental assessment. *Pediatrics*, 118(2):536–548.
- Eikenes, L., Løhaugen, G. C., Brubakk, A.-M., Skranes, J., and Håberg, A. K. (2011). Young adults born preterm with very low birth weight demonstrate widespread white matter alterations on brain dti. *Neuroimage*, 54(3):1774–1785.
- Esplin, M. S., Manuck, T. A., Varner, M. W., Christensen, B., Biggio, J., Bukowski, R., Parry, S., Zhang, H., Huang, H., Andrews, W., et al. (2015). Cluster analysis of spontaneous preterm birth phenotypes identifies potential associations among preterm birth mechanisms. *American journal of obstetrics and gynecology*, 213(3):429–e1.
- Fairchild, K., Mohr, M., Paget-Brown, A., Tabacaru, C., Lake, D., Delos, J., Moorman, J. R., and Kattwinkel, J. (2016). Clinical associations of immature breathing in preterm infants. part 1: Central apnea. *Pediatric research*.
- Floyd, B., Leske, D. A., Wren, S., Mookadam, M., Fautsch, M. P., and Holmes, J. M. (2005). Differences between rat strains in models of retinopathy of prematurity. *Mol Vis*, 11:524–530.
- Frey, H. A. and Klebanoff, M. A. (2016). The epidemiology, etiology, and costs of preterm birth. In *Seminars in Fetal and Neonatal Medicine*. Elsevier.

- Fruttiger, M. (2002). Development of the mouse retinal vasculature: angiogenesis versus vasculogenesis. *Investigative ophthalmology & visual science*, 43(2):522–527.
- Fyfe, K. L., Yiallourou, S. R., Wong, F. Y., and Horne, R. S. (2014). The development of cardiovascular and cerebral vascular control in preterm infants. *Sleep medicine reviews*, 18(4):299–310.
- Georgeson, G. D., Szőny, B. J., Streitman, K., Varga, I. S., Kovács, A., Kovács, L., and László, A. (2002). Antioxidant enzyme activities are decreased in preterm infants and in neonates born via caesarean section. *European Journal of Obstetrics & Gynecology and Reproductive Biology*, 103(2):136–139.
- Gerstner, B., Bühner, C., Rheinländer, C., Polley, O., Schüller, A., Berns, M., Obladen, M., and Felderhoff-Mueser, U. (2006). Maturation-dependent oligodendrocyte apoptosis caused by hyperoxia. *Journal of neuroscience research*, 84(2):306–315.
- Gerstner, B., DeSilva, T. M., Genz, K., Armstrong, A., Brehmer, F., Neve, R. L., Felderhoff-Mueser, U., Volpe, J. J., and Rosenberg, P. A. (2008). Hyperoxia causes maturation-dependent cell death in the developing white matter. *The Journal of Neuroscience*, 28(5):1236–1245.
- Giedd, J. N., Blumenthal, J., Jeffries, N. O., Castellanos, F. X., Liu, H., Zijdenbos, A., Paus, T., Evans, A. C., and Rapoport, J. L. (1999). Brain development during childhood and adolescence: a longitudinal mri study. *Nature neuroscience*, 2(10):861–863.
- Gilbert, S. F. (2014). *Developmental Biology*. Sinauer, Andrew D., 10th edition.
- Ginhoux, E., Lim, S., Hoeffel, G., Low, D., and Huber, T. (2015). Origin and differentiation of microglia. *Never-resting microglia: physiological roles in the healthy brain and pathological implications*, page 6.
- Girolamo, F., Strippoli, M., Errede, M., Benagiano, V., Roncali, L., Ambrosi, G., and Virgintino, D. (2010). Characterization of oligodendrocyte lineage precursor cells in the mouse cerebral cortex: a confocal microscopy approach to demyelinating diseases. *Italian Journal of Anatomy and Embryology*, 115(1/2):95.

- Gole, G. A., Ells, A. L., Katz, X., Holmstrom, G., Fielder, A. R., Capone Jr, A., Flynn, J. T., Good, W. G., Holmes, J. M., McNamara, J., et al. (2005). The international classification of retinopathy of prematurity revisited. *JAMA Ophthalmology*, 123(7):991–999.
- Görlach, A., Bertram, K., Hudecova, S., and Krizanova, O. (2015). Calcium and ros: A mutual interplay. *Redox biology*, 6:260–271.
- Groenendaal, F. and de Vries, L. (2005). Watershed infarcts in the full term neonatal brain. *Archives of disease in childhood. Fetal and neonatal edition*, 90(6):F488.
- Hagberg, H., Peebles, D., and Mallard, C. (2002). Models of white matter injury: Comparison of infectious, hypoxic-ischemic, and excitotoxic insults. *Mental retardation and developmental disabilities research reviews*, 8(1):30–38.
- Harris, A. L. (2002). Hypoxia—a key regulatory factor in tumour growth. *Nature Reviews Cancer*, 2(1):38–47.
- Hatfield, E. M. (1972). Blindness in infants and young children. *Sight-Saving Review*.
- Hellström, A., Hård, A.-L., Engström, E., Niklasson, A., Andersson, E., Smith, L., and Löfqvist, C. (2009). Early weight gain predicts retinopathy in preterm infants: new, simple, efficient approach to screening. *Pediatrics*, 123(4):e638–e645.
- Heneghan, C., Flynn, J., O’Keefe, M., and Cahill, M. (2002). Characterization of changes in blood vessel width and tortuosity in retinopathy of prematurity using image analysis. *Medical image analysis*, 6(4):407–429.
- Hoefl, F., Barnea-Goraly, N., Haas, B. W., Golarai, G., Ng, D., Mills, D., Korenberg, J., Bellugi, U., Galaburda, A., and Reiss, A. L. (2007). More is not always better: increased fractional anisotropy of superior longitudinal fasciculus associated with poor visuospatial abilities in williams syndrome. *The Journal of Neuroscience*, 27(44):11960–11965.
- Holmes, J. M. and Duffner, L. A. (1995). The effect of litter size on normal retinal vascular development in the neonatal rat. *Current eye research*, 14(8):737–740.

- Holmes, J. M. and Duffner, L. A. (1996). The effect of postnatal growth retardation on abnormal neovascularization in the oxygen exposed neonatal rat. *Current eye research*, 15(4):403–409.
- Hong, S., Dissing-Olesen, L., and Stevens, B. (2016). New insights on the role of microglia in synaptic pruning in health and disease. *Current opinion in neurobiology*, 36:128–134.
- Huang, H., Zhang, J., Wakana, S., Zhang, W., Ren, T., Richards, L. J., Yarowsky, P., Donohue, P., Graham, E., van Zijl, P. C., et al. (2006). White and gray matter development in human fetal, newborn and pediatric brains. *Neuroimage*, 33(1):27–38.
- Jantzie, L. L., Talos, D. M., Jackson, M. C., Park, H.-K., Graham, D. A., Lechpammer, M., Folkerth, R. D., Volpe, J. J., and Jensen, F. E. (2015). Developmental expression of n-methyl-d-aspartate (nmda) receptor subunits in human white and gray matter: potential mechanism of increased vulnerability in the immature brain. *Cerebral Cortex*, 25(2):482–495.
- Jenkinson, M., Beckmann, C. F., Behrens, T. E., Woolrich, M. W., and Smith, S. M. (2012). Fsl. *Neuroimage*, 62(2):782–790.
- Johansen-Berg, H. and Behrens, T. E. (2013). *Diffusion MRI: from quantitative measurement to in vivo neuroanatomy*. Academic Press.
- Johnston, M. V. (2005). Excitotoxicity in perinatal brain injury. *metabolism*, 7:61.
- Jones, E. G. (2012). *The thalamus*. Springer Science & Business Media.
- Joyal, J.-S., Omri, S., Sitaras, N., Rivera, J.-C., Sapieha, P., and Chemtob, S. (2012). Neovascularization in retinopathy of prematurity: opposing actions of neuronal factors gpr91 and semaphorins 3a. *Acta Paediatrica*, 101(8):819–826.
- Judaš, M., Radoš, M., Jovanov-Milošević, N., Hrabac, P., Kostović, I., et al. (2005). Structural, immunocytochemical, and mr imaging properties of periventricular crossroads of growing cortical pathways in preterm infants. *American journal of neuroradiology*, 26(10):2671–2684.
- Juergenson, I., Mazzucco, S., and Tinazzi, M. (2011). A typical example of cerebral watershed infarct. *Clinics and practice*, 1(4).

- Kajdaniuk, D., Marek, B., Foltyn, W., and Kos-Kudła, B. (2011). Vascular endothelial growth factor (vegf)-part 1: in physiology and pathophysiology. *Endokrynol Pol*, 62(5):444–455.
- Kandel, E. R., Schwartz, J. H., Jessell, T. M., et al. (2013). *Principles of neural science*, volume 5. McGraw-hill New York.
- Kaufman, J. S., Dole, N., Savitz, D. A., and Herring, A. H. (2003). Modeling community-level effects on preterm birth. *Annals of epidemiology*, 13(5):377–384.
- Khwaja, O. and Volpe, J. (2008). Pathogenesis of cerebral white matter injury of prematurity. *Archives of Disease in Childhood-Fetal and Neonatal Edition*, 93(2):F153–F161.
- Korzhevskii, D. and Otellin, V. (2000). Initial stage of vascular bed development in telencephalon of human embryo. *Bulletin of experimental biology and medicine*, 129(5):508–510.
- Kostović, I. and Jovanov-Milošević, N. (2006). The development of cerebral connections during the first 20–45 weeks' gestation. In *Seminars in Fetal and Neonatal Medicine*, volume 11, pages 415–422. Elsevier.
- Kurihara, T., Westenskow, P. D., and Friedlander, M. (2014). Hypoxia-inducible factor (hif)/vascular endothelial growth factor (vegf) signaling in the retina. In *Retinal Degenerative Diseases*, pages 275–281. Springer.
- Larroque, B., Ancel, P.-Y., Marret, S., Marchand, L., André, M., Arnaud, C., Pierrat, V., Rozé, J.-C., Messer, J., Thiriez, G., et al. (2008). Neurodevelopmental disabilities and special care of 5-year-old children born before 33 weeks of gestation (the epipage study): a longitudinal cohort study. *The Lancet*, 371(9615):813–820.
- Latal-Hajnal, B., von Siebenthal, K., Kovari, H., Bucher, H. U., and Largo, R. H. (2003). Postnatal growth in vlbw infants: significant association with neurodevelopmental outcome. *The Journal of pediatrics*, 143(2):163–170.
- Lebel, C. and Beaulieu, C. (2009). Lateralization of the arcuate fasciculus from childhood to adulthood and its relation to cognitive abilities in children. *Human brain mapping*, 30(11):3563–3573.

- Lehmenkühler, A., Syková, E., Svoboda, J., Zilles, K., and Nicholson, C. (1993). Extracellular space parameters in the rat neocortex and subcortical white matter during postnatal development determined by diffusion analysis. *Neuroscience*, 55(2):339–351.
- Levine, D. and Barnes, P. D. (1999). Cortical maturation in normal and abnormal fetuses as assessed with prenatal mr imaging. *Radiology*, 210(3):751–758.
- Lövblad, K.-O., Schaller, K., and Vargas, M. I. (2014). The fornix and limbic system. *Seminars in Ultrasound, CT and MRI*, 35(5):459–473.
- Manikandan, S. and Devi, R. S. (2005). Antioxidant property of α -asarone against noise-stress-induced changes in different regions of rat brain. *Pharmacological research*, 52(6):467–474.
- Manuck, T. A., Esplin, M. S., Biggio, J., Bukowski, R., Parry, S., Zhang, H., Huang, H., Varner, M. W., Andrews, W., Saade, G., et al. (2015). The phenotype of spontaneous preterm birth: application of a clinical phenotyping tool. *American journal of obstetrics and gynecology*, 212(4):487–e1.
- Marret, S., Mukendi, R., Gadiisseux, J.-F., Gressens, P., and Evrard, P. (1995). Effect of ibotenate on brain development: an excitotoxic mouse model of microgyria and posthypoxic-like lesions. *Journal of Neuropathology & Experimental Neurology*, 54(3):358–370.
- Martin, R. J., Di Fiore, J. M., and Walsh, M. C. (2015). Hypoxic episodes in bronchopulmonary dysplasia. *Clinics in perinatology*, 42(4):825–838.
- Mathai, S., Booth, L. C., Davidson, J. O., Drury, P. P., Fraser, M., Jensen, E. C., George, S., Naylor, A., Gunn, A. J., and Bennet, L. (2013). Acute on chronic exposure to endotoxin in preterm fetal sheep. *American Journal of Physiology-Regulatory, Integrative and Comparative Physiology*, 304(3):R189–R197.
- McCloskey, M., Wang, H., Jiang, Y., Smith, G. W., Strange, J., and Hartnett, M. E. (2013). Anti-vegf antibody leads to later atypical intravitreal neovascularization and activation of angiogenic pathways in a rat model of retinopathy of prematurityanti-vegf antibody in rop model. *Investigative ophthalmology & visual science*, 54(3):2020–2026.

- McDonald, J. W., Silverstein, F. S., and Johnston, M. V. (1988). Neurotoxicity of n-methyl-d-aspartate is markedly enhanced in developing rat central nervous system. *Brain research*, 459(1):200–203.
- McQuillen, P. S. and Ferriero, D. M. (2004). Selective vulnerability in the developing central nervous system. *Pediatric neurology*, 30(4):227–235.
- McQuillen, P. S., Sheldon, R. A., Shatz, C. J., and Ferriero, D. M. (2003). Selective vulnerability of subplate neurons after early neonatal hypoxia-ischemia. *The Journal of neuroscience*, 23(8):3308–3315.
- Mendi, M. (1988). The effects of litter size variation on mother-offspring relationships and behavioural and physical development in several mammalian species (principally rodents). *Journal of Zoology*, 215(1):15–34.
- Michell-Robinson, M. A., Touil, H., Healy, L. M., Owen, D. R., Durafourt, B. A., Bar-Or, A., Antel, J. P., and Moore, C. S. (2015). Roles of microglia in brain development, tissue maintenance and repair. *Brain*, 138(5):1138–1159.
- Miyawaki, T., Matsui, K., and Takashima, S. (1998). Developmental characteristics of vessel density in the human fetal and infant brains. *Early human development*, 53(1):65–72.
- Moeller, K., Willmes, K., and Klein, E. (2015). A review on functional and structural brain connectivity in numerical cognition. *Frontiers in human neuroscience*, 9.
- Momjian-Mayor, I. and Baron, J.-C. (2005). The pathophysiology of watershed infarction in internal carotid artery disease review of cerebral perfusion studies. *Stroke*, 36(3):567–577.
- Monier, A., Adle-Biassette, H., Delezoide, A.-L., Evrard, P., Gressens, P., and Verney, C. (2007). Entry and distribution of microglial cells in human embryonic and fetal cerebral cortex. *Journal of Neuropathology & Experimental Neurology*, 66(5):372–382.
- Monier, A., Evrard, P., Gressens, P., and Verney, C. (2006). Distribution and differentiation of microglia in the human encephalon during the first two trimesters of gestation. *Journal of Comparative Neurology*, 499(4):565–582.

- Mori, S. and Zhang, J. (2006). Principles of diffusion tensor imaging and its applications to basic neuroscience research. *Neuron*, 51(5):527–539.
- Morken, T. S., Widerøe, M., Vogt, C., Lydersen, S., Havnes, M., Skranes, J., Goa, P. E., and Brubakk, A.-M. (2013). Longitudinal diffusion tensor and manganese-enhanced MRI detect delayed cerebral grey and white matter injury after hypoxia-ischemia and hyperoxia in the immature rat. *Pediatric Research*, 73:171–179.
- Msall, M. E., Phelps, D. L., DiGaudio, K. M., Dobson, V., Tung, B., McClead, R. E., Quinn, G. E., Reynolds, J. D., Hardy, R. J., Palmer, E. A., et al. (2000). Severity of neonatal retinopathy of prematurity is predictive of neurodevelopmental functional outcome at age 5.5 years. *Pediatrics*, 106(5):998–1005.
- Munro, M. J., Walker, A. M., and Barfield, C. P. (2004). Hypotensive extremely low birth weight infants have reduced cerebral blood flow. *Pediatrics*, 114(6):1591–1596.
- NEI (2014). National eye institute: Facts about retinopathy of prematurity. <https://nei.nih.gov/health/rop/rop>, last accessed 05/12/2016.
- Neil, J. J., Shiran, S. I., McKinstry, R. C., Schefft, G. L., Snyder, A. Z., Almlí, C. R., Akbudak, E., Aronovitz, J. A., Miller, J. P., Lee, B., et al. (1998). Normal brain in human newborns: apparent diffusion coefficient and diffusion anisotropy measured by using diffusion tensor mr imaging. *Radiology*, 209(1):57–66.
- Netzer, N. C. and Breitenbach, M. (2010). Metabolic changes through hypoxia in humans and in yeast as a comparable cell model. *Sleep and Breathing*, 14(3):221–225.
- Nossin-Manor, R., Card, D., Morris, D., Noormohamed, S., Shroff, M. M., Whyte, H. E., Taylor, M. J., and Sled, J. G. (2013). Quantitative mri in the very preterm brain: assessing tissue organization and myelination using magnetization transfer, diffusion tensor and t 1 imaging. *Neuroimage*, 64:505–516.
- O’Campo, P., Burke, J. G., Culhane, J., Elo, I. T., Eyster, J., Holzman, C., Messer, L. C., Kaufman, J. S., and Laraia, B. A. (2008). Neighborhood deprivation and preterm birth among non-

- hispanic black and white women in eight geographic areas in the united states. *American journal of epidemiology*, 167(2):155–163.
- Ogunshola, O. O., Stewart, W. B., Mihalcik, V., Solli, T., Madri, J. A., and Ment, L. R. (2000). Neuronal vegf expression correlates with angiogenesis in postnatal developing rat brain. *Developmental brain research*, 119(1):139–153.
- Padilla, N., Junqué, C., Figueras, F., Sanz-Cortes, M., Bargalló, N., Arranz, A., Donaire, A., Figueras, J., and Gratacos, E. (2014). Differential vulnerability of gray matter and white matter to intrauterine growth restriction in preterm infants at 12 months corrected age. *Brain research*, 1545:1–11.
- Patel-Hett, S. and D'Amore, P. A. (2011). Signal transduction in vasculogenesis and developmental angiogenesis. *The International journal of developmental biology*, 55:353.
- Patz, A. (1954). Oxygen studies in retrolental fibroplasia: Iv. clinical and experimental observations the first edward l. holmes memorial lecture. *American journal of ophthalmology*, 38(3):291–308.
- Penn, J. S., Henry, M. M., and Tolman, B. L. (1994). Exposure to alternating hypoxia and hyperoxia causes severe proliferative retinopathy in the newborn rat. *Pediatric research*, 36(6):724–731.
- Penn, J. S., Henry, M. M., Wall, P., and Tolman, B. L. (1995). The range of pao₂ variation determines the severity of oxygen-induced retinopathy in newborn rats. *Investigative ophthalmology & visual science*, 36(10):2063–2070.
- Penn, J. S., Tolman, B. L., and Lowery, L. A. (1993). Variable oxygen exposure causes preretinal neovascularization in the newborn rat. *Investigative ophthalmology & visual science*, 34(3):576–585.
- Perrone, S., Tataranno, L. M., Stazzoni, G., Ramenghi, L., and Buonocore, G. (2015). Brain susceptibility to oxidative stress in the perinatal period. *The Journal of Maternal-Fetal & Neonatal Medicine*, 28(sup1):2291–2295.

- Peters, A. and Jones, E. G. (2013). *Cerebral Cortex: Normal and Altered States of Function*, volume 9. Springer Science & Business Media.
- Pierson, C. R., Folkerth, R. D., Billiards, S. S., Trachtenberg, F. L., Drinkwater, M. E., Volpe, J. J., and Kinney, H. C. (2007). Gray matter injury associated with periventricular leukomalacia in the premature infant. *Acta neuropathologica*, 114(6):619–631.
- Platt, M. J., Cans, C., Johnson, A., Surman, G., Topp, M., Torrioli, M. G., and Krageloh-Mann, I. (2007). Trends in cerebral palsy among infants of very low birthweight (< 1500 g) or born prematurely (< 32 weeks) in 16 european centres: a database study. *The Lancet*, 369(9555):43–50.
- Pogledic, I., Kostovic, I., Fallet-Bianco, C., Adle-Biassette, H., Gressens, P., and Verney, C. (2014). Involvement of the subplate zone in preterm infants with periventricular white matter injury. *Brain pathology*, 24(2):128–141.
- Portera-Cailliau, C., Price, D. L., and Martin, L. J. (1997). Excitotoxic neuronal death in the immature brain is an apoptosis-necrosis morphological continuum. *Journal of Comparative Neurology*, 378(1):10–87.
- Prins, M. L. and Hovda, D. A. (2003). Developing experimental models to address traumatic brain injury in children. *Journal of neurotrauma*, 20(2):123–137.
- Provis, J. M. (2001). Development of the primate retinal vasculature. *Progress in retinal and eye research*, 20(6):799–821.
- Qiu, A., Mori, S., and Miller, M. I. (2015). Diffusion tensor imaging for understanding brain development in early life. *Annual review of psychology*, 66:853–876.
- Quintero, P., Milagro, F., Campion, J., and Martinez, J. (2010). Impact of oxygen availability on body weight management. *Medical hypotheses*, 74(5):901–907.
- Ramani, M., van Groen, T., Kadish, I., Bulger, A., and Ambalavanan, N. (2013). Neurodevelopmental impairment following neonatal hyperoxia in the mouse. *Neurobiology of disease*, 50:69–75.

- Raymond, M., Li, P., Mangin, J.-M., Huntsman, M., and Gallo, V. (2011). Chronic perinatal hypoxia reduces glutamate–aspartate transporter function in astrocytes through the janus kinase/signal transducer and activator of transcription pathway. *The Journal of Neuroscience*, 31(49):17864–17871.
- Rea, P. (2015). *Chapter 2 - Essential Anatomy and Function of the Brain*. Academic Press, San Diego.
- Recoquillon, S., Carusio, N., Lagrue-Lakhal, A.-H., Tual-Chalot, S., Filippelli, A., Martinez, M. C., and Andriantsitohaina, R. (2015). Non muscular myosin light chain kinase (nmmlck) and nf- κ b pathway interaction in endothelium is critical for lipopolysaccharide-induced vascular hyporeactivity. *Archives of Cardiovascular Diseases Supplements*, 7(2):136.
- Rezzola, S., Belleri, M., Gariano, G., Ribatti, D., Costagliola, C., Semeraro, F., and Presta, M. (2014). In vitro and ex vivo retina angiogenesis assays. *Angiogenesis*, 17(3):429–442.
- Rice, D. and Barone, S. (2000). Critical periods of vulnerability for the developing nervous system: evidence from humans and animal models. *Environmental health perspectives*, 108(Suppl 3):511.
- Rice, J. E., Vannucci, R. C., and Brierley, J. B. (1981). The influence of immaturity on hypoxic-ischemic brain damage in the rat. *Annals of neurology*, 9(2):131–141.
- Ringelstein, E. B., Dittrich, R., and Stögbauer, F. (2001). Borderzone infarcts. *Stroke syndromes*, pages 564–582.
- Rose, J., Vassar, R., Cahill-Rowley, K., Guzman, X. S., Stevenson, D. K., and Barnea-Goraly, N. (2014). Brain microstructural development at near-term age in very-low-birth-weight preterm infants: an atlas-based diffusion imaging study. *Neuroimage*, 86:244–256.
- Ruhrberg, C. and Bautch, V. L. (2013). Neurovascular development and links to disease. *Cellular and Molecular Life Sciences*, 70(10):1675–1684.
- Russel, W. M. and Burch, R. L. (1959). The principles of humane experimental technique. *Methuen, London*, pages 54–66.

- Salmaso, N., Jablonska, B., Scafidi, J., Vaccarino, F. M., and Gallo, V. (2014). Neurobiology of premature brain injury. *Nature neuroscience*, 17(3):341.
- Sanai, N., Nguyen, T., Ihrie, R. A., Mirzadeh, Z., Tsai, H.-H., Wong, M., Gupta, N., Berger, M. S., Huang, E., Garcia-Verdugo, J.-M., et al. (2011). Corridors of migrating neurons in the human brain and their decline during infancy. *Nature*, 478(7369):382–386.
- Sarnat, H. B. (2004). Watershed infarcts in the fetal and neonatal brainstem. an aetiology of central hypoventilation, dysphagia, möbius syndrome and micrognathia. *European Journal of Paediatric Neurology*, 8(2):71–87.
- Schindelin, J., Arganda-Carreras, I., Frise, E., Kaynig, V., Longair, M., Pietzsch, T., Preibisch, S., Rueden, C., Saalfeld, S., Schmid, B., et al. (2012). Fiji: an open-source platform for biological-image analysis. *Nature methods*, 9(7):676–682.
- Scott, A., Powner, M. B., Gandhi, P., Clarkin, C., Gutmann, D. H., Johnson, R. S., Ferrara, N., and Fruttiger, M. (2010). Astrocyte-derived vascular endothelial growth factor stabilizes vessels in the developing retinal vasculature. *PLoS One*, 5(7):e11863.
- Seetho, I. W. and Wilding, J. P. (2014). Sleep-disordered breathing, type 2 diabetes and the metabolic syndrome. *Chronic respiratory disease*, page 1479972314552806.
- Semple, B. D., Blomgren, K., Gimlin, K., Ferriero, D. M., and Noble-Haeusslein, L. J. (2013). Brain development in rodents and humans: Identifying benchmarks of maturation and vulnerability to injury across species. *Progress in neurobiology*, 106:1–16.
- Shah, P. K., Prabhu, V., Karandikar, S. S., Ranjan, R., Narendran, V., and Kalpana, N. (2016). Retinopathy of prematurity: Past, present and future. *World journal of clinical pediatrics*, 5(1):35.
- Shen, Y., Yu, H.-M., Yuan, T.-M., Gu, W.-Z., and Wu, Y.-D. (2009). Erythropoietin attenuates white matter damage, proinflammatory cytokine and chemokine induction in developing rat brain after intra-uterine infection. *Neuropathology*, 29(5):528–535.

- Shukla, V., Singh, S. N., Vats, P., Singh, V. K., Singh, S. B., and Banerjee, P. (2005). Ghrelin and leptin levels of sojourners and acclimatized lowlanders at high altitude. *Nutritional neuroscience*, 8(3):161–165.
- Silverstein, F. S., Barks, J. D., Hagan, P., Xiao-Hong, L., Ivacko, J., and Szaflarsky, J. (1997). Cytokines and perinatal brain injury. *Neurochemistry international*, 30(4):375–383.
- Sola, A., Rogido, M. R., and Deulofeut, R. (2007). Oxygen as a neonatal health hazard: call for detente in clinical practice. *Acta Paediatrica*, 96(6):801–812.
- Soul, J. S., Hammer, P. E., Tsuji, M., Saul, J. P., Bassan, H., Limperopoulos, C., Disalvo, D. N., Moore, M., Akins, P., Ringer, S., et al. (2007). Fluctuating pressure-passivity is common in the cerebral circulation of sick premature infants. *Pediatric Research*, 61(4):467–473.
- Squarzoni, P., Thion, M. S., and Garel, S. (2015). Neuronal and microglial regulators of cortical wiring: usual and novel guideposts. *Frontiers in neuroscience*, 9.
- Steck, J., Blueml, C., Kampmann, S., Greene, B., Maier, R. F., Arnhold, S., Gerstner, B., Stieger, K., and Lorenz, B. (2015). Retinal vessel pathologies in a rat model of periventricular leukomalacia: A new model for retinopathy of prematurity? retinal vessel pathology in rat pvl model. *Investigative ophthalmology & visual science*, 56(3):1830–1841.
- Stolp, H., Neuhaus, A., Sundramoorthi, R., and Molnár, Z. (2012). The long and the short of it: gene and environment interactions during early cortical development and consequences for long-term neurological disease. *New mechanisms and therapeutics in neurodevelopmental disorders*, page 87.
- Stone, J., Itin, A., Alon, T., Pe'Er, J., Gnessin, H., Chan-Ling, T., and Keshet, E. (1995). Development of retinal vasculature is mediated by hypoxia-induced vascular endothelial growth factor (vegf) expression by neuroglia. *The Journal of neuroscience*, 15(7):4738–4747.
- Strange, B. A., Witter, M. P., Lein, E. S., and Moser, E. I. (2014). Functional organization of the hippocampal longitudinal axis. *Nature Reviews Neuroscience*, 15(10):655–669.
- Stubbs, D., DeProto, J., Nie, K., Englund, C., Mahmud, I., Hevner, R., and Molnár, Z. (2009). Neurovascular congruence during cerebral cortical development. *Cerebral cortex*, page bhp040.

- Szydłowska, K. and Tymianski, M. (2010). Calcium, ischemia and excitotoxicity. *Cell calcium*, 47(2):122–129.
- Talos, D. M., Follett, P. L., Folkerth, R. D., Fishman, R. E., Trachtenberg, F. L., Volpe, J. J., and Jensen, F. E. (2006). Developmental regulation of ampa receptor subunit expression in fore-brain and relationship to regional susceptibility to hypoxic/ischemic injury: part i. rodent cerebral white matter and cortex, part ii. human cerebral white matter and cortex. *The Journal of comparative neurology*, 497(1):61.
- Terry, T. L. (1942). Extreme prematurity and fibroblastic overgrowth of persistent vascular sheath behind each crystalline lens: I. preliminary report. *American Journal of Ophthalmology*, 25(2):203–204.
- Thau-Zuchman, O., Shohami, E., Alexandrovich, A. G., and Leker, R. R. (2012). Combination of vascular endothelial and fibroblast growth factor 2 for induction of neurogenesis and angiogenesis after traumatic brain injury. *Journal of Molecular Neuroscience*, 47(1):166–172.
- Thom, R., Rowe, G. C., Jang, C., Safdar, A., and Arany, Z. (2014). Hypoxic induction of vascular endothelial growth factor (vegf) and angiogenesis in muscle by truncated peroxisome proliferator-activated receptor γ coactivator (pgc)-1 α . *Journal of Biological Chemistry*, 289(13):8810–8817.
- Thornton, J., Amess, P., Penrice, J., Chong, W., Wyatt, J., and Ordidge, R. (1999). Cerebral tissue water spin-spin relaxation times in human neonates at 2.4 tesla: methodology and the effects of maturation. *Magnetic resonance imaging*, 17(9):1289–1295.
- Topçu, Y., Bayram, E., Özbal, S., Yiş, U., Tuğyan, K., Karaoğlu, P., Kumral, A., Yılmaz, O., and Kurul, S. H. (2014). Zonisamide attenuates hyperoxia-induced apoptosis in the developing rat brain. *Neurological Sciences*, 35(11):1769–1775.
- Traynelis, S. F., Wollmuth, L. P., McBain, C. J., Menniti, F. S., Vance, K. M., Ogden, K. K., Hansen, K. B., Yuan, H., Myers, S. J., and Dingledine, R. (2010). Glutamate receptor ion channels: structure, regulation, and function. *Pharmacological reviews*, 62(3):405–496.

- Tsuji, M., Saul, J. P., du Plessis, A., Eichenwald, E., Sobh, J., Crocker, R., and Volpe, J. J. (2000). Cerebral intravascular oxygenation correlates with mean arterial pressure in critically ill premature infants. *Pediatrics*, 106(4):625–632.
- Tual-Chalot, S., Allinson, K. R., Fruttiger, M., and Arthur, H. M. (2013). Whole mount immunofluorescent staining of the neonatal mouse retina to investigate angiogenesis in vivo. *JoVE (Journal of Visualized Experiments)*, (77):e50546–e50546.
- Vailhé, B., Vittet, D., Feige, J.-J., et al. (2001). In vitro models of vasculogenesis and angiogenesis. *Laboratory investigation*, 81(4):439–452.
- Vallon, M., Chang, J., Zhang, H., and Kuo, C. J. (2014). Developmental and pathological angiogenesis in the central nervous system. *Cellular and Molecular Life Sciences*, 71(18):3489–3506.
- van der Knaap, L. J. and van der Ham, I. J. (2011). How does the corpus callosum mediate inter-hemispheric transfer? a review. *Behavioural brain research*, 223(1):211–221.
- Van Os, S., Klaessens, J., Hopman, J., Liem, D., and Van De Bor, M. (2006). Cerebral oxygen supply during hypotension in near-term lambs: A near-infrared spectroscopy study. *Brain and Development*, 28(2):115–121.
- van Wijngaarden, P., Coster, D. J., Brereton, H. M., Gibbins, I. L., and Williams, K. A. (2005). Strain-dependent differences in oxygen-induced retinopathy in the inbred rat. *Investigative ophthalmology & visual science*, 46(4):1445–1452.
- Verney, C., Monier, A., Fallet-Bianco, C., and Gressens, P. (2010). Early microglial colonization of the human forebrain and possible involvement in periventricular white-matter injury of preterm infants. *Journal of anatomy*, 217(4):436–448.
- Verney, C., Pogledic, I., Biran, V., Adle-Biassette, H., Fallet-Bianco, C., and Gressens, P. (2012). Microglial reaction in axonal crossroads is a hallmark of noncystic periventricular white matter injury in very preterm infants. *Journal of Neuropathology & Experimental Neurology*, 71(3):251–264.

- Verstynen, T. D., Weinstein, A. M., Schneider, W. W., Jakicic, J. M., Rofey, D. L., and Erickson, K. I. (2012). Increased body mass index is associated with a global and distributed decrease in white matter microstructural integrity. *Psychosomatic medicine*, 74(7):682.
- Volpe, J. J. (2003). Cerebral white matter injury of the premature infant—more common than you think. *Pediatrics*, 112(1):176–180.
- Volpe, J. J. (2005). Encephalopathy of prematurity includes neuronal abnormalities. *Pediatrics*, 116(1):221–225.
- Volpe, J. J. (2008). *Neurology of the newborn*. Elsevier Health Sciences.
- Volpe, J. J. (2009). Brain injury in premature infants: a complex amalgam of destructive and developmental disturbances. *The Lancet Neurology*, 8(1):110–124.
- Vottier, G., Pham, H., Pansiot, J., Biran, V., Gressens, P., Charriaut-Marlangue, C., and Baud, O. (2011). Deleterious effect of hyperoxia at birth on white matter damage in the newborn rat. *Developmental neuroscience*, 33(3-4):261–269.
- Wake, H., Moorhouse, A. J., and Nabekura, J. (2011). Functions of microglia in the central nervous system—beyond the immune response. *Neuron glia biology*, 7(01):47–53.
- Wallace, D. K., Kylstra, J. A., and Chesnutt, D. A. (2000). Prognostic significance of vascular dilation and tortuosity insufficient for plus disease in retinopathy of prematurity. *Journal of American Association for Pediatric Ophthalmology and Strabismus*, 4(4):224–229.
- Wang, H., Smith, G. W., Yang, Z., Jiang, Y., McCloskey, M., Greenberg, K., Geisen, P., Culp, W. D., Flannery, J., Kafri, T., et al. (2013). Short hairpin rna-mediated knockdown of vegfa in müller cells reduces intravitreal neovascularization in a rat model of retinopathy of prematurity. *The American journal of pathology*, 183(3):964–974.
- Watkins, W. M., McCollum, G. W., Savage, S. R., Capozzi, M. E., Penn, J. S., and Morrison, D. G. (2013). Hypoxia-induced expression of vegf splice variants and protein in four retinal cell types. *Experimental eye research*, 116:240–246.

- Werdich, X. Q., McCollum, G. W., Rajaratnam, V. S., and Penn, J. S. (2004). Variable oxygen and retinal vegf levels: correlation with incidence and severity of pathology in a rat model of oxygen-induced retinopathy. *Experimental eye research*, 79(5):623–630.
- Westbrook, C. and Roth, C. K. (2011). *MRI in Practice*. John Wiley & Sons.
- Westerterp, K. R., Kayser, B., Wouters, L., Le Trong, J.-L., and Richalet, J.-P. (1994). Energy balance at high altitude of 6,542 m. *Journal of Applied Physiology*, 77(2):862–866.
- Westerterp-Plantenga, M. S., Westerterp, K. R., Rubbens, M., Verwegen, C. R., Richelet, J.-P., and Gardette, B. (1999). Appetite at “high altitude” [operation everest iii (comex-'97)]: a simulated ascent of mount everest. *Journal of Applied Physiology*, 87(1):391–399.
- Widerøe, M., Olsen, Ø., Pedersen, T. B., Goa, P. E., Kavelaars, A., Heijnen, C., Skranes, J., Brubakk, A.-M., and Brekken, C. (2008). Manganese-enhanced magnetic resonance imaging of hypoxic-ischemic brain injury in the neonatal rat. *Neuroimage*, 45:880–890.
- Wimberger, D. M., Roberts, T. P., Barkovich, A. J., Prayer, L. M., Moseley, M. E., and Kucharczyk, J. (1995). Identification of “premyelination” by diffusion-weighted mri. *Journal of computer assisted tomography*, 19(1):28–33.
- Wolke, D., Samara, M., Bracewell, M., Marlow, N., Group, E. S., et al. (2008). Specific language difficulties and school achievement in children born at 25 weeks of gestation or less. *The Journal of pediatrics*, 152(2):256–262.
- Xu, G., Broadbelt, K. G., Haynes, R. L., Folkerth, R. D., Borenstein, N. S., Belliveau, R. A., Trachtenberg, F. L., Volpe, J. J., and Kinney, H. C. (2011). Late development of the gabaergic system in the human cerebral cortex and white matter. *Journal of neuropathology and experimental neurology*, 70(10):841.
- Yao, D., Zhang, W., He, X., Wang, J., Jiang, K., and Zhao, Z. (2016). Establishment and identification of a hypoxia-ischemia brain damage model in neonatal rats. *Biomedical Reports*, 4(4):437–443.

- Yilmaz, M. S., Goktalay, G., Millington, W. R., Myer, B. S., Cutrera, R. A., and Feleder, C. (2008). Lipopolysaccharide-induced hypotension is mediated by a neural pathway involving the vagus nerve, the nucleus tractus solitarius and alpha-adrenergic receptors in the preoptic anterior hypothalamic area. *Journal of neuroimmunology*, 203(1):39–49.
- York, J. R., Landers, S., Kirby, R. S., Arbogast, P. G., and Penn, J. S. (2004). Arterial oxygen fluctuation and retinopathy of prematurity in very-low-birth-weight infants. *Journal of perinatology*, 24(2):82–87.
- Young RS, Hernandez MJ, Y. S. (1982). Selective reduction of blood flow to white matter during hypotension in newborn dogs: a possible mechanism of periventricular leukomalacia. *Annals of Neurology*, (12):445–448.
- Yuan, T.-M., Yu, H.-M., Gu, W.-Z., and Li, J.-P. (2005). White matter damage and chemokine induction in developing rat brain after intrauterine infection. *Journal of perinatal medicine*, 33(5):415–422.
- Yuodelis, C. and Hendrickson, A. (1986). A qualitative and quantitative analysis of the human fovea during development. *Vision research*, 26(6):847–855.
- Zanin, E., Ranjeva, J.-P., Confort-Gouny, S., Guye, M., Denis, D., Cozzone, P. J., and Girard, N. (2011). White matter maturation of normal human fetal brain. an in vivo diffusion tensor tractography study. *Brain and behavior*, 1(2):95–108.
- Zhang, Z.-w. (2006). Canadian association of neurosciences review: postnatal development of the mammalian neocortex: role of activity revisited. *Canadian Journal of Neurological Sciences/Journal Canadien des Sciences Neurologiques*, 33(02):158–169.
- Zhou, M., Schools, G. P., and Kimelberg, H. K. (2006). Development of glast (+) astrocytes and ng2 (+) glia in rat hippocampus ca1: mature astrocytes are electrophysiologically passive. *Journal of neurophysiology*, 95(1):134–143.
- Zilles, K. (2012). *The cortex of the rat: a stereotaxic atlas*. Springer Science & Business Media.